THE VULCANIZATION TRANSITION AND THE AMORPHOUS SOLID STATE IT YIELDS: A STATISTICAL MECHANICAL PERSPECTIVE

BY

WEIQUN PENG

B.A., Peking University, 1992
M.S., Peking University, 1995

THESIS

Submitted in partial fulfillment of the requirements
for the degree of Doctor of Philosophy in Physics
in the Graduate College of the
University of Illinois at Urbana-Champaign, 2001

Urbana, Illinois

Abstract

The vulcanization transition is a crosslink-density-controlled equilibrium phase transition from the liquid to the amorphous solid state. In order to understand the origins and consequences of the universal aspects of this transition and the emergent solid state, we construct a minimal model in the spirit of the Landau approach to continuous phase transitions. At the mean-field level this model produces the essential features of the liquid state and, especially, the amorphous solid state, such as the fraction of randomly localized particles and the scaling function that describes the statistical distribution of localization lengths. Our investigation of the vulcanization transition beyond the mean-field level, via both a perturbative renormalization group approach and a diagrammatic analysis of the two- and three-point vertex functions to all orders in perturbation theory, shows that percolation theory correctly captures the critical phenomenology of the vulcanization transition associated with percolative aspects of the liquid and critical states. In addition, we study certain density correlators associated with the vulcanization transition, which are accessible via various experimental techniques. These correlators turns out to contain essential information about both the vulcanization transition and the emergent amorphous solid state.

Acknowledgments

This thesis would not have been possible without the guidance and encouragement of Prof. Paul Goldbart. I have had the privilege to work with him in his research group for nearly six years, and it has been six wonderful years of my life. Being an expert in many areas of theoretical physics, Paul is full of deep insights and fresh ideas. That, together with his infectious passion for physics, makes talking with him always fun and helpful. What is more, his door has always been open to me, both during the working day and in the evenings and weekends. He has interacted constantly with me and been involved deeply with my research. This has helped me tremendously in every stage of my life as a graduate student, especially during the first couple of years when I, as a layman, sometimes felt lost. Innumerable discussions with him have taught me to think carefully and critically. As a mentor, he cares for his students and prompts us to grow professionally. He always goes out of his way to help us in things such as finding conferences to attend, looking for potential collaborations and even helping prepare talks and postdoc applications. Along with ensuring our professional development, he cares deeply about us personally, and he has served as a role model to me as a human being with his strong sense of i ntegrity and responsibility ... To him, I express my deepest gratitude.

Special thanks are given to Dr. Horacio Castillo, who was a senior graduate student in our research group and one of the main contributor to the semi-microscopic model theory of the vulcanization transition. In the years that we shared the same office, he not only helped guide me through his works but also gave me a lot of very sincere and precious advice on the many facets of a student's academic growth. Special thanks are also given to Dr. Alan McKane, who patiently taught me the field-theoretic renormalization-group technique while we were working together on the renormalization-group analysis of vulcanization transition. Collaboration with him has always been enjoyable and exciting, and I am constantly amazed by his ability to see through technical

mazes and land right on target; and also to Prof. Paul Selvin, who is the first experimentalist with whom I have worked closely. Interaction with him has opened up my mind and taught me a lot of things that I would never have thought of were I not in touch with an experimentalist. He has a straightforward and physically intuitive way of looking at problems. From him, I learned to appreciate this kind of thinking, which is particularly powerful when the problem is not well defined and has a lot of possible causes. Special thanks are also due to Prof. Nigel Goldenfeld, whose two wonderful courses shaped my viewpoint in the statistical mechanics and critical phenomena; to Prof. Michael Plischke, who has always been enthusiastic about our works on the vulcanization transition and has given me a lot of encouragements. I would like to acknowledge their tremendous help in various stages, especially during the past several months while I was on the market for a job. Furthermore,I would also like to thank Profs. Annette Zippelius, Eduardo Fradkin, Michael Stone and Ian Robinson, and Drs. José María Román and Vincent Liu for stimulating discussions.

At last, I would like to thank my parents and my wife, Ye Zang, for their whole-hearted support all these years. In the rainy days, they helped me through frustrations, and when the sunshine comes out, they share my joy. I would extend thanks to my friends, Chang Lin, Gang Zou, Fenghua Zong, Feng Liu and others for their valuable help.

The work presented in this thesis was supported by the National Science Foundation through grants DMR91-20000, DMR94-24511, DMR99-75187 and by the Campus Research Board of the University of Illinois.

Table of Contents

List of Figures

List of Abbreviations

RCMS Randomly Crosslinked Macromolecular System

RG Renormalization Group

HRW Houghton, Reeve and Wallace [25]

HRS Higher Replica Sector

LRS Lower Replica Sector

1RS One Replica Sector

GFP Gaussian Fixed Point

WFFP Wilson-Fisher Fixed Point

Chapter 1

Introduction

1.1 Vulcanized matter—rubber and the vulcanization transition

Natural rubber is derived from the sap of a number of tropical trees, most commonly the tree known as *Hevea braziliensis*. The sap is a milky-looking liquid which consists of rubber (see Fig. 1.1), suspended in the form of microscopic globules, together with other substances including fats and proteins. The word *rubber* is derived from the fact that this material can remove marks from paper, as discovered by the chemist Priestley in 1770.

In the early nineteenth century, the American Charles Goodyear spent many years studying natural rubber, trying to improve its properties for technological use. In 1839, He discovered the vulcanization process, a chemical reaction in which natural rubber is mixed with sulphur under heat. The sulphur particles act as crosslinkers to join together, at certain points along their length, the long chain macromolecules in the natural rubber, so that the whole assembly of chains becomes effectively a single giant random structure. The resulting *vulcanized* rubber overcomes many technological defects of the natural rubber, among which are the permanent loss of shape due to the inherent tendency to flow and the stiffening or loss of elasticity occurring at low temperatures [1].

1.2 Building block: Linear polymers

The constituents of the vulcanization transition are most commonly linear polymers. Linear polymers [1, 2] are very long, covalently bonded molecules made up of many small group of atoms, chemically combined in a particular manner. Each repeating small group is called a monomer. A

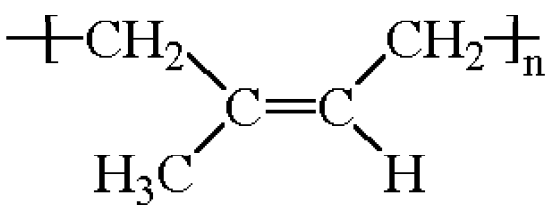

Figure 1.1: Structural formula of natural rubber, i.e., polyisoprene

typical polymer may contain thousands of monomers.

In a polymer chain with a backbone of carbon-carbon covalent bond, the length of each C-C bond and the valance angle between successive bonds are essentially fixed, but the angle between successive units around the axis of the bond is not fixed. It is the multiplicity of each of this angle between successive units (available when the energetic difference between different choices of the angle is less than or comparable to the thermal energy kT) that produces the various conformations of a linear polymer. When the energy barrier between different choices is comparable to or smaller than thermal energy kT, the chain conformation is able to fluctuate temporally.

A minimal model that describes the large length-scale polymer properties views the polymer configurations as the trajectories of a random walk. The short-range spatial correlation of the monomers along the chain is abstracted into a parameter called the persistence length ℓ (also called the effective bond-length). The random-walk idealization works best when the chain length is much much longer than the persistence length ℓ and details of the chain structure are not the object of investigation. In three spatial dimensions the conformational distribution function function of such a chain, usually called a Gaussian chain, is given by the Wiener distribution [3], i.e.,

$$\Phi\left\{\mathbf{R}(\cdot)\right\} = \text{const.} \times \exp\left(-\frac{3}{2\ell}\int_0^L d\sigma \left|\frac{d}{d\sigma}\mathbf{R}(\sigma)\right|^2\right) \ . \tag{1.1}$$

Here, L is the arclength of the chain and $\mathbf{R}(\sigma)$ is the position vector of the monomer an arclength distance σ from a specific end of the chain. According to the Wiener distribution, the end-to-end distance of the chain $\mathbf{R}(L)-\mathbf{R}(0)$ has a Gaussian distribution with mean value $\langle \mathbf{R}(L)-\mathbf{R}(0)\rangle = \mathbf{0}$ and mean square value $\langle |\mathbf{R}(L)-\mathbf{R}(0)|^2\rangle = (L/\ell)\ell^2 = L\ell$.

A more refined model takes into account the fact that distinct monomers cannot occupy the same

region of space by inclusion of a short-range repulsive interaction between monomers approaching each other closely enough spatially. This is called the Edwards model of a linear polymer [4, 5], and its distribution function is given by

$$\Phi\{\mathbf{R}(\cdot)\} = \text{const.} \times \exp\left(-\frac{3}{2\ell}\int_0^L d\sigma \left|\frac{d}{d\sigma}\mathbf{R}(\sigma)\right|^2 - \frac{u_0}{2\ell^2}\int_0^L d\sigma \int_0^L d\sigma' \delta(\mathbf{R}(\sigma) - \mathbf{R}(\sigma'))\right), \quad (1.2)$$

where u_0 is an interaction-strength parameter having the dimension of volume and referred to as the excluded volume. As we are only interested in the *global* (i.e. large length-scale) physical properties of ensembles of polymers, we shall adopt the Edwards model for linear polymers in our work.

1.3 Gelation and vulcanization

In a polymerization process, polyfunctional units form larger and larger macromolecules when more and more bonds are formed between the original molecules. Gelation is said to have occurred when a single macromolecule is formed that spans the polymerization vessel. The fraction of monomers that constitute this infinite macromolecule is called the *gel* fraction (here denoted by q), and the remaining fraction (whose constituents are the finite macromolecules) is called the *sol* fraction.

In general, there are two kinds of gelation processes, *strong* gelation and *weak* gelation. The difference between the two cases lies in the strength of the bonding. In a *weak* gel (i.e. a *reversible gel*), bonds form and break in thermal equilibrium, whereas in a *strong* gel (i.e. an *irreversible* gel) the bonds, once made, are completely stable (at least on the timescales of the experiments). The two kinds of gelation process have substantially different physical features. Whereas the strong gelation process causes a continuous equilibrium continuous phase transition, the transition caused by weak gelation is believed to be a non-equilibrium transition and similar to glass transition [6]. From here on, unless specifically noted, we shall confine ourselves to the discussion of *strong* gelation.

The vulcanization transition is a particular example of *strong* gelation. In the case of the vulcanization transition for randomly crosslinked macromolecular systems (henceforth denoted RCMSs), the polyfunctional unit is the long, linear polymer chain whose functionality is equal to the number of monomers on the chain L/ℓ ($\gg 1$). The bonding is achieved via crosslinkers (such as sulfur) that join randomly chosen pairs of monomers (see Fig. 1.2). In the case of endlinked macromolecular

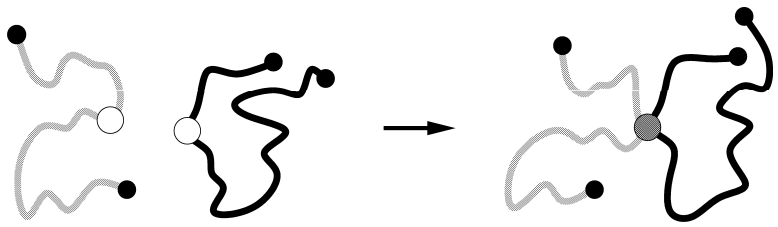

Figure 1.2: A pair of macromolecules before and after crosslinking. The two empty circles represents the pair of monomers that are to be crosslinked, and the shaded circle represents the pair of monomers already crosslinked together.

systems, the reactive monomers are located only at the ends of the linear macromolecules, and these end monomers are able to link with one another so as to form permanent junctions between some specified number of ends of macromolecules (see Fig. 1.3).

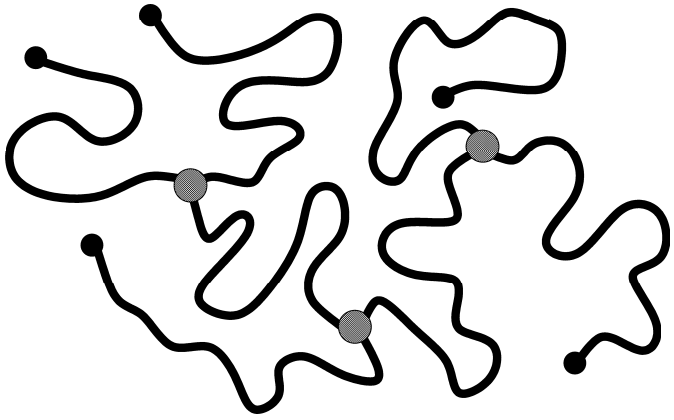

Figure 1.3: Semi-microscopic configuration of 7 macromolecules that are connected by 3 endlinks (shaded circles), corresponding to the case of 3-type endlinking.

The presence of crosslinks between macromolecules changes the properties of these systems in many ways. Structurally, upon increasing the crosslink density, the average size of macromolecules grows and eventually a single random macromolecule spanning the whole system comes into existence. In the mean time, a liquid state of matter is transformed into an amorphous solid state of matter. As to dynamical responses, as the system approaches the transition from the liquid side, its viscosity grows and ultimately diverges at the vulcanization transition. Into the amorphous solid state, the material develops a zero-frequency shear elasticity. There are also differences in the chemical behavior between uncrosslinked and crosslinked polymers, such as the way in which they respond to heat [7]. In this thesis, we put our focus on the structures and structural changes of the

vulcanized systems.

1.4 Percolation approach to the gelation/vulcanization transition

There has been a great deal of work on the theory of the gelation/vulcanization transition [6, 8, 9]. The primary approach has been via an identification of the vulcanization transition with the percolation transition. In this section we present a brief overview of the percolation approach [10].

1.4.1 Classical theory

The classical theory of gelation was pioneered by Flory [11] and Stockmayer [12]. They approximated the gelation phenomena as a branching process without the presence of closed loops. Their approach, in the language of modern statistical mechanics, is in fact the mean-field theory of the percolation transition, i.e., the percolation transition on a Cayley tree. To build a Cayley tree,

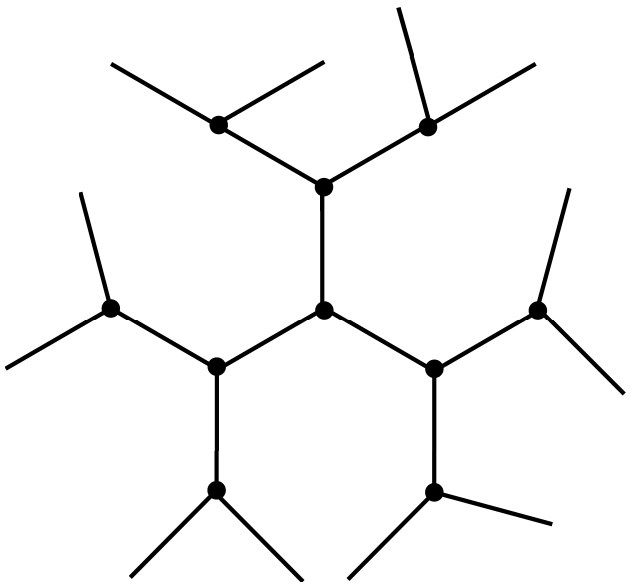

Figure 1.4: A small Cayley tree, where each unit has functionality $z = 3$

one starts with a central point ("origin") having z bonds. Each bond leads to another site from which again z bonds emanate; one of these z bonds connects with the origin, the other $z-1$ bonds lead to new sites. The branching process is continued again and again to build a Cayley tree as

large as one wishes. Figure 1.4 shows a small Cayley tree, having $z = 3$. On the Cayley tree, each bond has a probability p to be occupied. Two sites are in the same cluster if there exists a path of occupied bonds between them. Percolation is said to have happened when an infinite cluster appears (with probability unity). The percolation language can be readily translated into the gelation/vulcanization language. In the case of gelation/vulcanization each site represents a polyfunctional unit with functionality z. If two neighboring units react to form a chemical bond, the corresponding bond is said to be occupied. A cluster of sites is, therefore, a molecule consisting of monomer units bonded together.

The percolation threshold on the Cayley tree can be found by the following observation. Pick one site downstream from the origin, assuming there already exists a path with occupied bonds from the origin to this site. Aside from the bond through which we arrive at this site from the origin, there are $z-1$ bonds emanating from it. Each of these $z-1$ bonds leads to a new neighbor. Thus, for this particular site there are, on average, $(z-1)p$ occupied bonds on which we can continue our path. If this number $(z-1)p$ is smaller (larger) than unity, on average the number of different paths continuing to infinity will decrease (increase) at each generation by a factor $(z-1)p < 1$ $[(z-1)p > 1]$. Therefore we find that the percolation threshold p_c is given by

$$p = p_c \equiv \frac{1}{z-1} \ . \tag{1.3}$$

Other quantities of interest can also be found exactly in this model. For example, near the transition, the gel fraction q grows linearly with $p - p_c$ [10].

The classical theory of gelation is in fact the mean-field theory of percolation, and it has the significance and limitations of a mean-field theory. It turns out that it does give good estimate of the gelation threshold p_c [6]. On the other hand, it necessarily breaks down if the system is sufficiently near the transition (i.e. in the critical region).

1.4.2 Percolation model

The mathematical theory of percolation, together with its name, was introduced by Broadbent and Hammersley in 1957. In order to improve on the understanding of the gelation transition, de Gennes [13] and Stauffer [14] proposed to identify strong gelation with percolation on a regular

lattice. As is mentioned above, each lattice site represents a polyfunctional unit, with the number

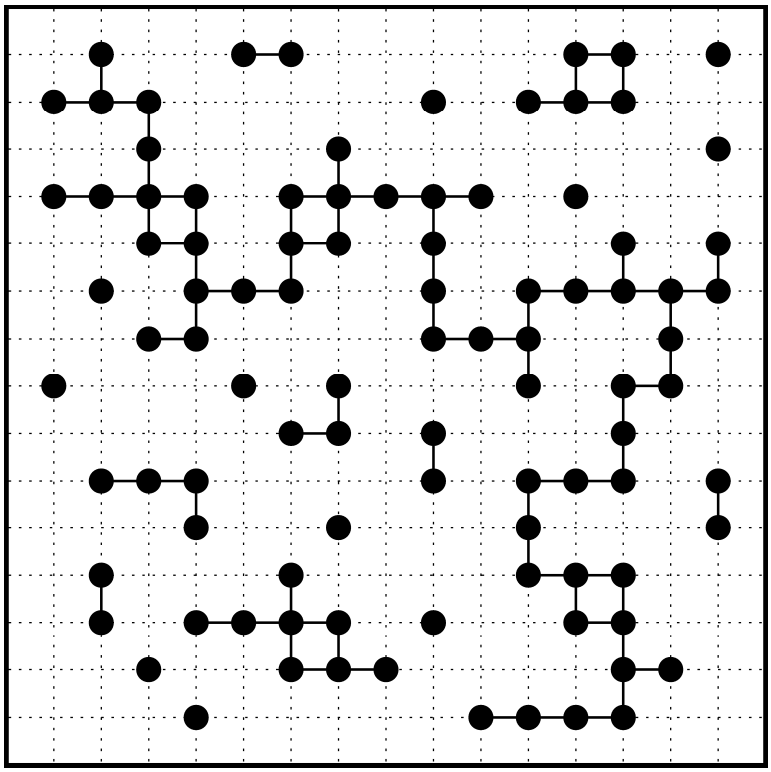

Figure 1.5: Gelation of 4-functional monomers identified as bond percolation on a square lattice

of reactive arms equal to the number of nearest neighbors. Two neighboring monomers can react, and a reacted bond is represented by a solid line, as shown in Fig. 1.5. The probability p of a bond being formed is identified with the reacted fraction of the theory of gelation. In this manner, the gelation transition is identified with the percolation transition. With this identification, one is able to investigate the structural characteristics both around the gelation transition and in the gel state by making use of results obtained from the study of the percolation transition.

1.4.3 Field-theoretic approaches to the percolation transition

The percolation transition has been investigated with various experimental, computational and analytical techniques. In this section we introduce some of the field-theoretic formulations of the percolation transition, among which we focus on the Potts field theory in its one-state limit. The purpose of this introduction is to facilitate understanding of and comparison with the statistical

field theory of the vulcanization transition, which we shall discuss in details in Chap. 3. The present section is organized as follows. First, we introduce the lattice Potts model and its relationship with the percolation transition [15, 16, 17, 18]. Second, we present the correspond Potts field theory and its percolation limit [20, 21, 22, 23, 24]. Third, we describe the Houghton, Reeve and Wallace representation of percolation field theory [25]. Then, we briefly discuss the Lubensky and Isaacson approach [26].

The Potts model [15, 16] is a natural generalization of Ising model. Instead of two states, as in Ising model, there is an arbitrary number $Q(=1,2,\ldots)$ of discrete states at any given site $\mathbf{x}$ of a d-dimensional lattice: $s(\mathbf{x}) = 1, 2, \ldots, Q$. Two neighboring Potts "spins" $s(\mathbf{x})$ and $s(\mathbf{x}')$ have energy $-J$ if they are in the same state and energy 0 if they are in different states, i.e., the Hamiltonian is given by

$$\mathcal{H} = -J \sum_{\langle \mathbf{x},\mathbf{x}' \rangle} \delta_{s(\mathbf{x}),s(\mathbf{x}')} \ , \tag{1.4}$$

where $\langle \mathbf{x}, \mathbf{x}' \rangle$ means that $\mathbf{x}$ and $\mathbf{x}'$ are nearest neighbor sites. The Potts model is ferromagnetic if $J > 0$ and antiferromagnetic if $J < 0$. Evidently, the Ising model is the $Q = 2$ case of the Potts model. Kastelyn and Fortuin [17] proved that the statistics of bond percolation can be exactly recovered from the Potts model in the limit that the number of Potts states Q tends to unity. (For a clear and concise derivation, see Ref. [18].) By choosing the energy J such that $e^{J/kT} - 1 = p/(1-p)$, where p is the bond occupation probability, one sees that as Q approaches 1 the partition function for the Q-state Potts model indeed becomes the generating function for bond percolation statistics. Furthermore, one can establish that quantities of physical significance in percolation can also be formulated in terms of the Potts model. Central among these is the mean number $\langle N_{\rm c} \rangle$ of clusters $N_{\rm c}$ in the percolation problem, the correspondence with the Potts model being given by

$$\langle N_{\rm c} \rangle = \lim_{Q \to 1} \frac{\partial \ln Z}{\partial Q}. \tag{1.5}$$

In addition, the correlation function for percolation $G(\mathbf{x}_1, \mathbf{x}_2)$, defined as the probability that $\mathbf{x}_1$ and $\mathbf{x}_2$ are in the same cluster, is connected to the Potts model via

$$G(\mathbf{x}_1, \mathbf{x}_2) = \lim_{Q \to 1} \frac{\partial}{\partial Q} \left\langle (\delta_{s(\mathbf{x}_1),1} - Q^{-1})(\delta_{s(\mathbf{x}_2),1} - Q^{-1}) \right\rangle , \tag{1.6}$$

where $\left\langle (\delta_{s(\mathbf{x}_1),1} - Q^{-1})(\delta_{s(\mathbf{x}_2),1} - Q^{-1}) \right\rangle$ is a certain correlation function for the Potts model.

The merit of the mapping between bond percolation and the Potts model lies in the fact that when $Q \leq 2$ the Q-state Potts model has a continuous phase transition. Therefore, one can make use of the renormalization group (RG) approach and scaling arguments to study the critical properties of this transition, and in return one obtains the characteristics of the critical properties of the purely geometrical transition, the percolation transition. In general, the critical exponents of percolation are those of the Q-state Potts model evaluated at $Q = 1$ [18].

To facilitate the analytical investigation of the critical properties the percolation transition, it is convenient to convert the lattice Potts model into a field theory. To do this, it is useful to formulate the Hamiltonian (1.4) alternatively in a $Q-1$ dimensional internal space to reflect its full symmetry. This is achieved by introducing a set of Q vectors $\{\mathbf{e}^\sigma\}_{\sigma=1}^{Q}$ $(\sigma = 1, 2, \ldots, Q)$, each of length $\sqrt{Q-1}$. This is the set of vectors defining the Q vertices of a hypertetrahedron placed at the origin in $Q-1$ dimensional space. It is easy to see that

$$\mathbf{e}^\sigma \cdot \mathbf{e}^{\sigma'} = Q\delta^{\sigma,\sigma'} - 1\,. \tag{1.7}$$

With the help of Eq. (1.7) one can rewrite the Hamiltonian, i.e., Eq. (1.4), as (up to a constant additional term)

$$\mathcal{H} = -J \sum_{\langle \mathbf{x},\mathbf{x}' \rangle} \mathbf{e}^{\sigma(\mathbf{x})} \cdot \mathbf{e}^{\sigma(\mathbf{x}')}\,. \tag{1.8}$$

Then, following a standard procedure of statistical mechanics, one arrives at a $Q-1$ component field theory of the Potts model [20], the Landau-Wilson effective Hamiltonian is given by

$$\int_V d^d x \Big(\sum_{\alpha=1}^{Q-1} \Big(\frac{1}{2} r\, \psi_\alpha^2 + \frac{1}{2} |\nabla \psi_\alpha|^2 \Big) - w^{(3)} \sum_{\alpha,\beta,\gamma=1}^{Q-1} \lambda^{(3)}_{\alpha\beta\gamma}\, \psi_\alpha\, \psi_\beta\, \psi_\gamma \Big)\,. \tag{1.9}$$

Here, r controls the bond-occupation probability (and hence the percolation transition), $w^{(3)}$ is the nonlinear coupling strength, $\lambda^{(3)}$ is the "Potts tensor," defined via

$$\lambda^{(3)}_{\alpha\beta\gamma} = \sum_{\sigma=1}^{Q} e^\sigma_\alpha e^\sigma_\beta e^\sigma_\gamma\ , \tag{1.10}$$

which controls the internal symmetry of the theory, i.e., Q-fold permutation symmetry of field components [which can be easily seen in the lattice version, Eq. (1.8)]. The mean-field and critical properties of this effective Hamiltonian have been investigated extensively [20, 21, 22, 23, 24]. It has a continuous phase transition in the limit of $Q \to 1$. Due to the cubic nonlinear term, its upper critical dimension is six. In the vicinity of and below six dimensions, the Gaussian fixed-point bifurcates, and the critical properties of the emergent Wilson-Fisher fixed point can be calculated using ε ($\equiv 6 - d$) expansion RG techniques. The critical exponents for the percolation transition have been calculated to third order in ε, and good agreement has been found with the results of other approaches [24].

While investigating the higher-order (in ε) behaviors of ϕ^3 field theories, Houghton, Reeve and Wallace (whom we shall henceforth refer to as HRW) developed another field-theoretic representation for the percolation problem [25], the Landau-Wilson Hamiltonian for which is given by

$$\mathcal{H} = \int d^d x \left\{ \frac{1}{2}(\nabla\phi)^2 - \frac{1}{2}(\nabla\psi)^2 + \frac{1}{2} r_0 (\phi^2 - \psi^2) + \frac{g}{3!}(\phi + \psi)^3 \right\}, \tag{1.11}$$

where ϕ is an ordinary field but ψ is a so-called ghost field. As HRW have shown [25], via an analysis of the Feynman diagrams of this theory, provided one enforces the rule that *only graphs that are connected by ϕ-lines be included*, the two- and three-point ϕ vertex functions are identical (order-by-order in perturbation theory in the coupling constant g) to those of the one-state (i.e. percolation) limit of the Potts model. (Figure 1.6 gives an example of the HRW rule.) We mention, in passing, that this HRW representation consists of fields residing on d-dimensional space, and does not necessitate the taking of a replica (or Potts) limit. However, it does require the additional rule by which certain diagrams are excluded by hand. Note that due to this extra by-hand rule, the HRW representation is not a Lagrangian field theory in the strict sense. In Chap. 4 we shall make use of this HRW representation of the percolation transition (but only as a convenient intermediate, and not mandatory, step) to establish the connection between the critical properties of the vulcanization transition and those of the percolation transition.

We mention that other field-theoretic approaches have been developed to study the percolation transition. Among these is the approach of Lubensky and Isaacson [26], who developed a field theory that describes the statistics of branched polymers. Their approach extends the connection between

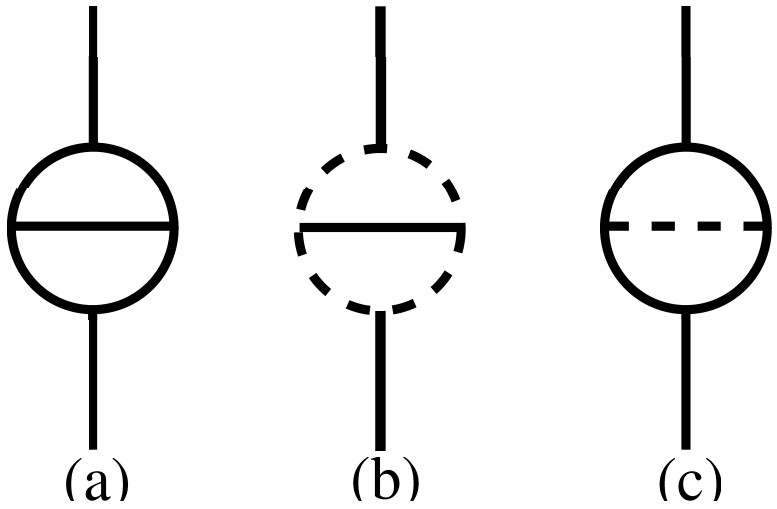

Figure 1.6: An example of the HRW rule for diagrams generated by the Hamiltonian defined in Eq. (1.11). Shown are three two-loop diagrams that contribute to two-point ϕ vertex function. Solid lines represent ϕ propagators and dashed lines represent ψ propagators. Graph (b) is not ϕ connected and gives no contribution.

the statistics of linear macromolecules and the zero-component limit of a spin system [27, 28]. Treating the Boltzmann weight as a generating function for different cluster configurations of the system of monomer units, Lubensky and Isaacson add to the Hamiltonian higher powers of field variables that incorporate the effects of polyfunctional units, and configurations of branched polymers are therefore generated in the Feynman-diagrammatic expansion. They concluded that in the usual experimental settings (which means the fugacities for the number of different polyfunctional units, number of end points and polymers are set to certain values), their field theory reduces to that of the one-state limit of Potts model.

1.4.4 Comments on the percolation approach to the vulcanization transition

The percolation approach to the vulcanization transition appeals to the intimate relation between the connectivity of the system of the crosslinked macromolecules and percolation theory. Nevertheless, the percolation transition is purely a geometrical transition, and thus in its own right is not a *statistical mechanical* theory. In the percolation approach, what is under study is the *statistics* of the clusters formed due to the crosslinking of the underlying macromolecules (i.e. the ensemble of the configurations of quenched randomness). Hence, the thermal fluctuation of individual

monomers (i.e. the annealed degrees of freedom) are not addressed, and neither is the interplay between the quenched randomness produced by random crosslinking and the thermal motion of the remaining degrees of freedom in the system. As we shall see, in the approach that we shall adopt, both the quenched degrees of freedom and the annealed degrees of freedom are naturally present, and the interplay between the two ensembles of degrees of freedom enables us to find the appropriate order parameter for diagnosing the vulcanization transition, and produces rich physics in the description of the amorphous solid state. We will discuss the relationship of the percolation approach to our approach in more detail in the context of the RG analysis of the vulcanization transition field theory (see Chapter 3).

1.5 Semi-microscopic theory of the vulcanization transition

During the last decade there has been an ongoing effort to obtain a detailed understanding of the behavior of RCMSs near the vulcanization transition via an approach that is based on a microscopic theory [29, 30, 31, 32, 2] (In addition to the technical reports just cited, we refer the reader to some informal accounts of the physics of the vulcanization transition [33, 35, 36].) . This approach is rooted in the pioneering work of Edwards and co-workers on the semi-microscopic formulation of the statistical mechanics of RCMSs [37, 38] and the Edwards-Anderson theory of spin glasses [39]. These works provide the technical foundation and physical intuition for the establishment of a minimal Landau-Wilson Hamiltonian for the vulcanization transition. The purpose of the present section is to collect together the basic ingredients of the semi-microscopic approach to the vulcanization transition, including the order parameter, underlying semi-microscopic model, and replica field theory. As the reader will see, although its construction follows a quite conventional path, the theory does possess some intricacies. We shall therefore take various opportunities to shed some light on the physical meaning of its various ingredients. We shall follow closely the notation of Ref. [32] and, accordingly, we shall adopt units of length in which the characteristic size of the underlying macromolecules is unity.

We remind the reader that the vulcanization transition is an equilibrium phase transition from a liquid state of matter to an amorphous solid state. The transition occurs when a sufficient density of permanent random constraints (e.g. chemical crosslinks)—the quenched randomness—

are introduced to connect the constituents (e.g. macromolecules), whose locations are the thermally fluctuating variables. In the resulting amorphous solid state, the thermal motion of (at least a fraction of) the constituents of the liquid undergo a qualitative change: no longer wandering throughout the container, they are instead localized in space at random positions about which they execute thermal (i.e. Brownian) motion characterized by random r.m.s. displacements.

1.5.1 Order parameter for the vulcanization transition

The simple idea of using the monomer density as the order parameter does not work, because in the amorphous solid state, due to the randomness of the mean positions of the localized monomers, the system's density (after averaging over the quenched randomness) remains uniform upon entering the amorphous state, just as it is in the liquid state. As we need a more delicate construction, the order parameter constructed for spin glass transition [40] gives us some hints. To motivate this construction of an order parameter, we observe that the basic difference between the liquid state and amorphous solid states is the emergence of *static* random density fluctuations in the solid state, which leads us to consider the autocorrelation for the position $\mathbf{c}_j(s)$ of monomer (j,s)'s (i.e. the monomer at fractional arclength s along the j^{th} macromolecule) between time t and 0: $\langle \exp i\mathbf{k}\cdot(\mathbf{c}_j(s;t)-\mathbf{c}_j(s;0))\rangle_\chi$. The bracket $\langle\cdots\rangle_\chi$ denotes a thermal average for a specific realization of the random constraints (indicated by χ). In the liquid state, correlation decays to zero as the time-difference t increases, whereas in the solid state, if particle j is localized, its position remains correlated with itself even in the limit $t\to\infty$. Therefore, the quantity $\langle \exp i\mathbf{k}\cdot\mathbf{c}_j(s)\rangle\langle\exp -i\mathbf{k}\cdot\mathbf{c}_j(s)\rangle$, which is the $t\to\infty$ limit of the autocorrelation function, can tell the difference between the two states, and this difference survives averaging over the particles and the quenched randomness.

The appropriate order parameter for the vulcanization transition is a generalization of the above intuitive suggestion, being the following function of A wave vectors $\{\mathbf{k}^1,\mathbf{k}^2,\cdots,\mathbf{k}^A\}$ [29, 32]:

$$\Big[\frac{1}{N}\sum_{j=1}^{N}\int_0^1 ds\,\langle\exp i\mathbf{k}^1\cdot\mathbf{c}_j(s)\rangle_\chi\langle\exp i\mathbf{k}^2\cdot\mathbf{c}_j(s)\rangle_\chi\cdots\langle\exp i\mathbf{k}^A\cdot\mathbf{c}_j(s)\rangle_\chi\Big]\,. \tag{1.12}$$

Here N is the total number of macromolecules, as above, $\langle\cdots\rangle_\chi$ denotes a thermal average for a particular realization χ of the quenched disorder (i.e. the crosslinking), and $[\cdots]$ represents a suit-

able averaging over this quenched disorder. It is worth emphasizing that the disorder resides in the specification of what monomers are crosslinked together: the resulting constraints *do not* explicitly break the translational symmetry of the system. In the liquid state, for each monomer (j, s) the thermal average $\langle \exp i\mathbf{k} \cdot \mathbf{c}_j(s) \rangle_\chi$ takes the value $\delta^{(d)}_{\mathbf{k},\mathbf{0}}$ (i.e. a Kronecker δ) and thus the order parameter is simply $\prod_{a=1}^{A} \delta^{(d)}_{\mathbf{k}^a,\mathbf{0}}$. On the other hand, in the amorphous solid state we expect a nonzero fraction of the monomers to be localized, and for such monomers $\langle \exp i\mathbf{k} \cdot \mathbf{c}_j(s) \rangle_\chi$ takes the form $\wp_{(j,s)}(\mathbf{k}) \exp i\mathbf{k} \cdot \mathbf{b}_j(s)$, i.e., a random phase-factor determined by the random mean position $\mathbf{b}_j(s)$ of the monomer (j, s) multiplied by a random Debye-Waller factor $\wp_{(j,s)}(\mathbf{k})$ describing the random extent to which the monomer is localized. Using an isotropic Gaussian distribution characterized by a localization length to approximate the random Debye-Waller factor $\wp_{(j,s)}(\mathbf{k})$, one arrive at the following *Ansatz* for the order-parameter value in the amorphous solid state [31, 32]:

$$(1-q) \prod_{a=1}^{A} \delta^{(d)}_{\mathbf{0},\mathbf{k}^a} + q\, \delta^{(d)}_{\mathbf{0},\sum_{a=1}^{A} \mathbf{k}^a} \int_0^\infty dt\, p(t) \exp\Big(-\sum_{a=1}^{A} |\mathbf{k}^a|^2/2t \Big). \tag{1.13}$$

The first term accounts for the delocalized monomers, and the second term accounts for the localized monomers. The number q is the fraction of the localized monomers, i.e., gel fraction. The Kronecker δ factor in the second term is a reflection of the fact that the summation over monomers will add up destructively (due to random phase factors $\exp i\mathbf{k} \cdot \mathbf{b}_j(s)$ as mentioned above) unless the wave vectors happen to sum to zero. The integral represents the fact that there is a statistical distribution of localization lengths. This Ansatz turns out to solve the mean-field theory of the vulcanization transition exactly. Note that, unlike in the more common settings such as the Ising model, the order parameter for the amorphous solidification transition and its value in the amorphous solid state is a *function* of the set of wave vectors $\{\mathbf{k}^1, \mathbf{k}^2, \cdots, \mathbf{k}^A\}$, and hence encodes a rich physical content.

1.5.2 The underlying unconstrained macromolecular liquid

The underlying unconstrained liquid is a melt or solution of identical macromolecules subject to short-range repulsive interactions. The Hamiltonian that accounts for these physical ingredients is the Edwards measure, a multi-chain generalization of (1.2), the effective Hamiltonian for which is

given by [41]

$$H^{\mathrm{E}} = \frac{1}{2}\sum_{i=1}^{N}\int_0^1 ds \Big|\frac{d}{ds}\mathbf{c}_i(s)\Big|^2 + \frac{\lambda^2}{2}\sum_{i,i'=1}^{N}\int_0^1 ds\int_0^1 ds'\,\delta^{(d)}(\mathbf{c}_i(s)-\mathbf{c}_{i'}(s')). \tag{1.14}$$

Here, the dimensionless (real, positive) parameter λ^2 characterizes the strength of the suppression of statistical weight due to the (repulsive) excluded-volume interaction between monomers [4, 5]. The system can be regarded as a melt of macromolecules, in which case the interaction parameter λ^2 is intended to account for the monomer-monomer interaction. Alternatively, it can be regarded as a solution of macromolecules dissolved in a good solvent, in which case λ^2 is intended to represent the effective monomer-monomer interaction (i.e. the bare interaction renormalized by the monomer-solvent and solvent-solvent interactions, the solvent degrees of freedom having been integrated out).

1.5.3 Replicated semi-microscopic model of vulcanized macromolecular systems

On top of the semi-microscopic Hamiltonian describing a system of macromolecules interacting via an excluded-volume interaction, Eq. (1.14), random crosslinks are introduced as permanent constraints [37, 38]. Suppose there are M random crosslinks,

$$\mathbf{c}_{i_e}(s_e) = \mathbf{c}_{i'_e}(s'_e) \qquad (\text{with } e = 1,\ldots,M)\,. \tag{1.15}$$

Then the partition function under the specific configuration of crosslinks is given by

$$\tilde{Z}(\{j_e, s_e; j'_e, s'_e\}_{e=1}^{M}) \propto \Big\langle \prod_{e=1}^{M}\delta\Big(\mathbf{c}_{j_e}(s_e) - \mathbf{c}_{j'_e}(s'_e)\Big)\Big\rangle^{\mathrm{E}}, \tag{1.16}$$

where the product of Dirac δ-functions serves to remove all configurations that fail to satisfy the constraints (1.15). The statistical average $\langle\cdots\rangle^{\mathrm{E}}$ is taken relative the underlying unlinked liquid, Eq. (1.14). In other words, $\tilde{Z}$ is a quotient of partition functions, the numerator for a system with crosslinks, the denominator for a system without. This quotient of partition functions furnishes the change in the free energy that crosslinking causes, and this is the quantity of central concern

to us.

As it is impossible to keep track of all the random constraints in the theory, we resort to averaging the physical observables over some suitable distribution of quenched randomness, armed with the expectations that the fluctuations of physical observables across different configurations of the quenched randomness is negligible (in the thermodynamic limit). In order to perform the quenched randomness average indicated by $[\cdots]$, we adopt the elegant and physical choice of the Deam-Edwards distribution [37]:

$$P_M(\{j_e, s_e; j'_e, s'_e\}_{e=1}^M) \propto \frac{(\mu^2)^M}{M!} \tilde{Z}(\{j_e, s_e; j'_e, s'_e\}_{e=1}^M) \ , \tag{1.17}$$

where μ^2 is the parameter that controls the average constraint density, and thus the transition. This distribution can be understood as a product of two probabilities: the partition function $\tilde{Z}$ represents the probability that the specified m pairs of monomers happen to be near each other (pairwise) in the unlinked liquid; the Poisson-like factor $(\mu^2)^M/M!$ is the probability that those M pairs of monomers do indeed get crosslinked, given that they are already near each other. Therefore, this distribution assumes that the constraints are established instantaneously and simultaneously into the uncrosslinked fluid in equilibrium and, hence, reflects the correlations of the uncrosslinked liquid.

The physical observable of central importance is $\mathcal{F}$, the quenched-randomness-average of the free energy, which is proportional to the quenched-randomness average of the logarithm of the partition function for fixed quenched-randomness $[\ln Z]$. This average can be done using the replica trick, i.e., by invoking the mathematical identity

$$\mathcal{F} \propto [\ln Z(\{\cdots\})] = \lim_{n\to 0} \frac{[Z(\{\cdots\})^n] - 1}{n} \ , \tag{1.18}$$

where $\{\cdots\}$ specifies the precise realization of the random constraints. Thus, we have transformed the problem into the consideration of $[Z^n]$, which can be carried out for general integer n almost as simply as for $[Z]$, followed by the more subtle step involving the $n \to 0$ limit.

By making use of Eqs. (1.16) and (1.17), we see that the disorder average of Z^n is a disorder-free but $(n+1)$-fold-replicated effective Hamiltonian with a disorder-induced interaction coupling the

replicas, not only n replicas arising from Z^n, but also the additional "zeroth" one arising from the Deam-Edwards distribution:

$$[Z^n] \propto \langle \exp(-\mathcal{H}^{\rm P}_{n+1}) \rangle^{\rm W}_{n+1} , \tag{1.19}$$

$$\mathcal{H}^{\rm P}_{n+1} \equiv \frac{\lambda^2}{2} \sum_{j,j'=1}^{N} \int_0^1 ds \int_0^1 ds' \sum_{\alpha=0}^{n} \delta^{(d)}(\mathbf{c}_j^\alpha(s) - \mathbf{c}_{j'}^\alpha(s')) - \frac{\mu^2 V}{2N} \sum_{j,j'=1}^{N} \int_0^1 ds \int_0^1 ds' \prod_{\alpha=0}^{n} \delta^{(d)}(\mathbf{c}_j^\alpha(s) - \mathbf{c}_{j'}^\alpha(s')). \tag{1.20}$$

Here, $\langle \cdots \rangle^{\rm W}_{n+1}$ denotes a thermal average taken with respect to the Hamiltonian for $n+1$ replicas of the noninteracting uncrosslinked system of macromolecules [i.e. the replicated and multi-chain version of Eq. (1.1)]. The parameter λ^2 measures the strength of the excluded-volume interaction; the parameter μ^2 measures the density of the constraints and serves as the control parameter for the vulcanization transition. As a result of there being random *constraints* rather than, say, *fields* or *pairwise interactions*, the coupling between the replicas takes the form of *product* over all replicas rather than, say, a *pairwise sum*. Let us pause to mention the symmetry content of this replica theory: $\mathcal{H}^{\rm P}_{n+1}$ is invariant under arbitrary independent translations and rotations of the replicas, as well as their arbitrary permutation.

The natural collective coordinates for the vulcanization transition are

$$Q(\hat{k}) \equiv \frac{1}{N} \sum_{j=1}^{N} \int_0^1 ds \, \exp i\hat{k} \cdot \hat{c}_j(s), \tag{1.21}$$

which emerge upon introducing Fourier representations of the two types of delta function in Eq. (1.20), as discussed in detail in see Sec. 5.1 of Ref. [32]. (Such collective coordinates were first introduced in the context of crosslinked macromolecular melts by Ball and Edwards [38].) We use the symbol $\hat{k}$ to denote the replicated wave vector $\{\mathbf{k}^0, \mathbf{k}^1, \ldots, \mathbf{k}^n\}$, and define the extended scalar product $\hat{k} \cdot \hat{c}$ by $\mathbf{k}^0 \cdot \mathbf{c}^0 + \mathbf{k}^1 \cdot \mathbf{c}^1 + \cdots + \mathbf{k}^n \cdot \mathbf{c}^n$ (and hence, $\hat{k}^2 \equiv \hat{k} \cdot \hat{k} \equiv \mathbf{k}^0 \cdot \mathbf{k}^0 + \mathbf{k}^1 \cdot \mathbf{k}^1 + \cdots + \mathbf{k}^n \cdot \mathbf{k}^n$). The collective coordinates $Q(\hat{k})$ are the microscopic prototype of the order parameter (1.12), i.e.,

for $\hat{k} = (\mathbf{0}, \mathbf{k}^1, \mathbf{k}^2, \ldots, \mathbf{k}^A, \ldots, \mathbf{0})$, and we have that

$$\begin{aligned} \lim_{n\to 0} \langle Q(\hat{k}) \rangle_{n+1}^{\mathrm{P}} &= \Big[\frac{1}{N} \sum_{j=1}^{N} \int_0^1 ds \, \langle \exp i\mathbf{k}^1 \cdot \mathbf{c}_j(s) \rangle_\chi \langle \exp i\mathbf{k}^2 \cdot \mathbf{c}_j(s) \rangle_\chi \cdots \langle \exp i\mathbf{k}^A \cdot \mathbf{c}_j(s) \rangle_\chi \Big], \\ \langle \cdots \rangle_{n+1}^{\mathrm{P}} &\equiv \frac{\langle \cdots \exp(-\mathcal{H}_{n+1}^{\mathrm{P}}) \rangle_{n+1}^{\mathrm{W}}}{\langle \exp(-\mathcal{H}_{n+1}^{\mathrm{P}}) \rangle_{n+1}^{\mathrm{W}}} \, . \end{aligned} \tag{1.22}$$

This formula provides a connection between the physically significant order parameter and a quantity that, as we shall see, can be calculated in a well-controlled manner.

1.5.4 Replica field theory for vulcanized macromolecular systems

As discussed in detail in Sec. 5.3 of Ref. [32], one can put the partition function into a form of a field theory by applying a Hubbard-Stratonovich transformation to the collective coordinates $Q(\hat{k})$; we denote the corresponding auxiliary order-parameter field by $\Omega(\hat{k})$. At this stage one encounters a vital issue, viz., that it is *essential* to draw the distinction between examples of $Q(\hat{k})$ and $\Omega(\hat{k})$ that belong to the *one-replica sector* (1RS) and those that belong to the *higher-replica sector* (HRS).

Consider the space of replicated wave vectors $\hat{k}$. We decompose this space into three disjoint sets:

(i) The *higher replica sector*, HRS, which consists of those $\hat{k}$ containing at least two nonzero component-vectors $\mathbf{k}^\alpha$. For example, if $\hat{k} = (\mathbf{0}, \ldots, \mathbf{0}, \mathbf{k}^\alpha \neq \mathbf{0}, \ldots, \mathbf{k}^\beta \neq \mathbf{0}, \mathbf{0}, \ldots, \mathbf{0})$ then $\hat{k}$ lies in the HRS. (More specifically, in this example $\hat{k}$ lies in the two-replica sector of the HRS).

(ii) The *one replica sector*, 1RS, which consists of those $\hat{k}$ containing exactly one nonzero component-vector $\mathbf{k}^\alpha$ [e.g. $\hat{k} = (\mathbf{0}, \ldots, \mathbf{0}, \mathbf{k}^\alpha \neq \mathbf{0}, \mathbf{0}, \ldots, \mathbf{0})$].

(iii) The *zero replica sector*, 0RS, which consists of the vector $\hat{k} = \hat{0}$. This decomposition is illustrated schematically in Fig. 1.7 for the case of two replicas of one-spatial-dimensional systems. It is especially straightforward to visualize this decomposition if the volume of the system is kept finite (and periodic boundary conditions are imposed) so that replicated plane waves with discrete, equally spaced, replicated wave vectors furnish the natural complete set of functions.

For the wave vector $\hat{k}$ lying in 1RS, we say that the corresponding $Q(\hat{k})$ and $\Omega(\hat{k})$ are 1RS quantities. For the wave vector $\hat{k}$ lying in HRS, we say that the corresponding $Q(\hat{k})$ and $\Omega(\hat{k})$ are HRS quantities. The importance of this distinction between the 1RS and the HRS lies in the

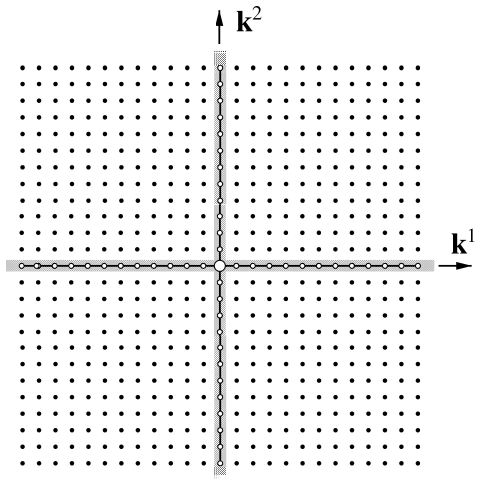

Figure 1.7: Decomposition of the space of replicated wave vectors. Off-axis wave vectors lie in the HRS; on-axis (but off-origin) wave vectors lie in the 1RS; the wave vector at the origin is the 0RS.

fact, evident from the order parameter (1.12), that the vulcanization transition is detected by fields residing in the HRS, whereas the 1RS fields measure the local monomer density and neither exhibit critical fluctuations near the vulcanization transition nor acquire a nonzero expectation value in the amorphous solid state.

Bearing in mind this distinction between the 1RS and HRS fields, the aforementioned Hubbard-Stratonovich transformation leads to the following field-theoretic representation of the disordered-averaged replicated partition function [42]:

$$[Z^n] \propto \int \mathcal{D}_n^\dagger \Omega \int \overline{\mathcal{D}}^\dagger \Omega \, \exp\left(- ndN\mathcal{F}_n \right), \tag{1.23}$$

$$\begin{aligned} ndN\mathcal{F}_n(\{\Omega^\alpha(\mathbf{k}), \Omega(\hat{k})\}) \equiv{}& \tilde{\lambda}_n^2 NV^{-1} \sum_{\alpha=0}^{n} \sum_{\mathbf{k}}^{\dagger} |\Omega^\alpha(\mathbf{k})|^2 + \mu^2 V^{-n} \overline{\sum_{\hat{k}}}^{\dagger} |\Omega(\hat{k})|^2 \\ & - \ln \Big\langle \exp\Big(2i\tilde{\lambda}_n^2 NV^{-1} \sum_{\alpha=0}^{n} \sum_{\mathbf{k}}^{\dagger} \mathrm{Re}\, \Omega^\alpha(\mathbf{k})^* \int_0^1 ds \, \exp\left(i\mathbf{k} \cdot \mathbf{c}^\alpha(s) \right) \Big) \\ & \times \exp\Big(2\mu^2 V^{-n} \overline{\sum_{\hat{k}}}^{\dagger} \mathrm{Re}\, \Omega(\hat{k})^* \int_0^1 ds \, \exp\left(i\hat{k} \cdot \hat{c}(s) \right) \Big) \Big\rangle_{n+1}^{\mathrm{W}}, \end{aligned} \tag{1.24}$$

where $\Omega^\alpha(\mathbf{k})$ [which represents $\Omega(\hat{k})$ when $\hat{k} = (\mathbf{0}, \ldots, \mathbf{0}, \mathbf{k}^\alpha = \mathbf{k} \neq \mathbf{0}, \mathbf{0}, \ldots, \mathbf{0})$] is a 1RS field, $\Omega(\hat{k})$ is a HRS field, and $\tilde{\lambda}_n^2$ is the effective excluded volume after being renormalized by the crosslinking. In this formulation of the statistical mechanics of RCMSs, one can readily establish

exact relationships connecting average values and correlators of $Q(\hat{k})$ with those of $\Omega(\hat{k})$ (by, e.g., adding source terms to the effective Hamiltonian $\mathcal{H}^{\rm P}_{n+1}$ that generate these correlators [43]). (Such relationships between expectation values involving microscopic variables and auxiliary fields are common in the setting of field theories derived via Hubbard-Stratonovich transformations [44].) For example, for wave vectors lying in the HRS one has

$$\langle Q(\hat{k})\rangle^{\rm P}_{n+1} = \langle \Omega(\hat{k})\rangle^{\mathcal{F}}_{n+1} \ , \tag{1.25}$$

$$\langle Q(\hat{k})\, Q(\hat{k}')\rangle^{\rm P}_{n+1,{\rm c}} = \langle \Omega(\hat{k})\, \Omega(\hat{k}')\rangle^{\mathcal{F}}_{n+1,{\rm c}} - \frac{V^n}{\mu^2 N}\, \delta_{\hat{k}+\hat{k}',\hat{0}} \ , \tag{1.26}$$

where $\langle \cdots \rangle^{\mathcal{F}}_{n+1}$ denotes an average over the field theory (1.23), and the subscript c indicates that the correlators are connected. Relationships such as those given in Eqs. (1.25) and (1.26) allow one to relate order-parameter correlators to correlators of the field theory.

As we have discussed, this semi-microscopic approach takes into account both the thermal fluctuations of individual monomers, short-range excluded-volume interactions between the monomers, and permanent random constraints resulting from crosslinking. However, there are a number of limitations of this approach. First, this approach does not take into account the entanglement effect, i.e., the interlocking of closed loops induced by the crosslinking process. In fact, no microscopic approach has managed to take these features into account, except for some heuristic approximation schemes [45]. Secondly, this approach, in it present form, is not suitable for the high crosslinking regime. Other formulations, including the one developed by Edwards and collaborators, and its continuation by Panyukov and collaborators [46], are designed to work in that regime.

1.6 Vulcanization transition in mean-field theory: Brief summary of results

A detailed mean-field study of the effective free energy $\mathcal{F}$ [31, 32] makes the following predictions:
(i) For densities of crosslinks smaller than a certain critical value (on the order of one crosslink per macromolecule) the system exhibits a liquid state in which all particles (in the context of macromolecules, monomers) are delocalized.
(ii) At the critical crosslink density there is a continuous thermodynamic phase transition to an

amorphous solid state, this state being characterized by the emergence of random static density fluctuations. This transition is contained within the HRS. Both the liquid and the amorphous solid states have uniform densities, and therefore the order parameter is zero in the 1RS on both sides of the transition.

(iii) In the amorphous solid state, a nonzero fraction of the particles have become localized around random positions and with random localization lengths (i.e. r.m.s. displacements). As far as symmetry is concerned, translational invariance is spontaneously broken at the microscopic level. However, owing to the randomness of the localization, this symmetry-breaking is hidden. [Hence the need for a subtle order parameter (1.12).] In the language of replicas, the symmetries of independent translations and rotations of the replicas are spontaneously broken, and all that remains are the symmetries of common translations and rotations (corresponding to the macroscopic homogeneity and isotropy of the amorphous solid state). The permutation symmetry amongst the $n+1$ replicas appears to remain intact at the transition.

(iv) The fraction of localized particles grows linearly with the excess crosslink density, as does the characteristic inverse square localization length. Furthermore, when scaled by their mean value, the statistical distribution of localization lengths is universal for all near-critical crosslink densities, the form of this scaled distribution being uniquely determined by a certain integro-differential equation.

Furthermore, the elastic properties of the vulcanized matter have been studied in the mean-field level by Castillo and Goldbart [48], in which they calculate the free-energy change of the system when it is deformed, and find that upon the transition the static shear modulus grows from zero continuously with the third power of excessive crosslink density. In addition to this, Castillo et al. gave a full proof of the local stability (up to the anticipated Goldstone modes) of the mean-field solution in the amorphous solid state [49].

1.7 Outline of this thesis

This thesis is organized as follows. In Chap. 2 we present the construction of the minimal Landau free energy using two different methods, either in terms of the replicated order parameter or in terms of the distribution of local static density fluctuations. We study this Landau free energy at the mean-field level, obtain the value of the order parameter in the liquid and amorphous solid

states, and determine the chief universal characteristics. We then compare the universal predictions of the theory with the results of extensive numerical simulations of randomly crosslinked macromolecular systems, due to Barsky and Plischke, and find excellent agreement. In Chap. 3 we examine the two-field correlation function involving fluctuations of the amorphous solid order parameter, elucidate its physical meaning and construct the associated susceptibility. Then, we center our analysis on the minimal model of the vulcanization transition, derive the Ginzburg criterion for the width (in crosslink density) of the critical region, finding it to be consistent with a prediction due to de Gennes [50]. We develop a renormalization-group procedure within the framework of an expansion around the upper critical dimension. We compute certain universal critical exponents characterizing the vulcanization transition, and find that they are, to lowest nontrivial order, identical to those governing physically analogous quantities in the percolation theory. We explore the relationship between the present approach to vulcanized matter and other approaches, such as those based on percolation ideas, in the light of this connection. In Chap. 4, in order to go beyond the first-order calculation of ε-expansion for the vulcanization-transition field theory, we consider the appropriate long-wave-length behavior of the two- and three-point vertex functions diagrammatically, to all orders in perturbation theory, and identify them with the corresponding quantities in the Houghton-Reeve-Wallace field-theoretic approach to the percolation critical phenomenon. Hence, we show that percolation theory correctly captures the critical phenomenology of the vulcanization transition associated with the liquid and critical states, i.e., they are in the same universality class. In Chap. 5 we consider certain density correlators, measurable via various experimental techniques, in the context of the vulcanization transition. We show that these correlators contain essential information about both the vulcanization transition and the emergent amorphous solid state, and make contact with various physical ingredients that have featured in experimental studies of amorphous colloidal as well as gel systems and in theoretical studies of the glassy state.

We have performed the work presented in Chap. 2 with Dr. Horacio Castillo and Prof. Annette Zippelius. It has been published as *Universality and its origins at the amorphous solidification transition* in Physical Review B **57**, 839-847 (1998) [51]. The work presented in Chaps. 3 has been published as *Renormalization-group approach to the vulcanization transition* in Physical Review

E **61**, 3339-3357 (2000) [52]. We have performed the work presented in Chap. 4 with Prof. Alan McKane and have submitted this work to Physical Review E [53]. The work presented in Chap. 5 has been published as *Density-correlator signatures of the vulcanization transition* in European Physical Journal B **19**, 461-466 (2001) [54].

Chapter 2

Mean-Field Universality at the Vulcanization Transition

2.1 Introduction

In the course of the effort to understand the vulcanization transition for RCMSs, it has become clear that one can employ similar approaches to study randomly *end-linked* macromolecular systems [55], randomly crosslinked *manifolds* (i.e. higher dimensional objects) [56], and chemical gels formed by permanent random covalent bonding of small molecules [57, 58, 59] as well; in each case, a specific semi-microscopic model has been studied. For example, in the original case of RCMSs, the macromolecules were modeled as long, flexible linear chains, with a short-ranged excluded-volume interaction, and the crosslinks were imposed at random arc-length locations. On the other hand, in the case of *end-linked* systems, although the excluded-volume interaction remained the same, the macromolecules were now modeled as either flexible or stiff, and the random linking was restricted to the ends of the macromolecules. Despite the differences between the unlinked systems and the styles of linking, in all cases identical critical behavior has been obtained in mean-field theory, right down to the precise form of the statistical distribution of scaled localization lengths.

Perhaps even more strikingly, in extensive numerical simulations of randomly crosslinked macromolecular systems, Barsky and Plischke [60] have employed an off-lattice model of macromolecules interacting via a Lennard-Jones potential, and, yet again, an essentially identical picture has emerged for the transition to and properties of the amorphous solid state, despite the substantial differences between physical ingredients incorporated in the simulation and in the analytical theory.

In the light of these observations, it is reasonable to ask whether one can find a common theoretical formulation of the amorphous solidification transition (of which the vulcanization transition is a prime example) that brings to the fore those emergent collective properties of all these systems that are model-independent, and therefore provide useful predictions for a broad class of experimentally realizable systems. In this chapter we explain how this is done. In fact, we approach the issue in two distinct (but related) ways, in terms of a replica order parameter and in terms of the distribution of random static density fluctuations, either of which can be invoked to characterize the emergent amorphous solid state.

The outline of this chapter is as follows. In Sec. 2.2 we construct the universal replica Landau free energy of the amorphous solidification transition by employing symmetry considerations along with three further assumptions: (i) that we need only consider order-parameter configurations representing physical situations in which the fraction of constituents localized is at most small; (ii) that the field components responsible for the incipient instability of the liquid phase are those with long wavelengths (i.e. that the emergent localization is weak), and (iii) that fluctuations representing real-space variations in the local density of the constituents are free-energetically very costly, and should therefore be either suppressed energetically or, equivalently (as far as our present aims are concerned), prevented via a kinematic constraint. In Sec. 2.3 we invoke a physical hypothesis to solve the stationarity condition for the replica order parameter, thereby obtaining a mean-field theory of the transition. We exhibit the universal properties of this solution and, in particular, the scaling behavior of certain central physical quantities. In Sec. 2.4 we describe an alternative approach to the amorphous solidification transition, in which we construct and analyze the Landau free energy expressed in terms of the distribution of static density fluctuations. Although we shall invoke the replica approach in the construction of this Landau free energy, its ultimate form does not refer to replicas. As we show, however, the physical content of this Landau theory is identical to that of the replica Landau theory addressed in Secs. 2.2 and 2.3. In Sec. 2.5 we exhibit the predicted universality by examining the results of extensive numerical simulations of randomly crosslinked macromolecular networks, due to Barsky and Plischke. In Sec. 2.6 we give some concluding remarks.

2.2 Universal replica free energy for the amorphous solidification transition

We are concerned, then, with systems of extended objects, such as macromolecules, that undergo a transition to a state characterized by the presence of random static fluctuations in the particle-density when subjected to a sufficient density of permanent random constraints (the character and statistics of which constraints preserve translational and rotational invariance). As we shall see, in such states, translational and rotational symmetry are spontaneously broken, but in a way that is hidden at the macroscopic level. We focus on the long wavelength physics in the vicinity of this transition.

In the spirit of the standard Landau approach, we envisage that the replica technique has been invoked to incorporate the consequences of the permanent random constraints, and propose a phenomenological mean-field replica free energy, the $n \to 0$ limit of which gives the disorder-averaged free energy, in the form of a power series in the replica order parameter. We invoke symmetry arguments, requiring the effective Hamiltonian to remain invariant under translation and rotation of each replica as well as permutation of replicas. The control parameter τ is proportional to the amount by which the constraint density exceeds its value at the transition. As we shall see, the stationarity condition for this general, symmetry-inspired Landau free energy is satisfied by precisely the order-parameter hypothesis that exactly solves the stationarity conditions derived from semi-microscopic models of crosslinked and end-linked macromolecules. From the properties of this solution we recover the primary features of the liquid-amorphous solid transition.

We first study the transformation properties of the order parameter under translations and rotations, and then make use of the resulting information to determine the possible terms appearing in the replica free energy. [A notational issue: to keep in line with work in semi-microscopic models, we use $\Omega(\hat{k})$ as our order parameter field. In the semi-microscopic model of the vulcanization transition, $\Omega(\hat{k})$ is the Hubbard-Stratonovich field conjugate to the microscopically-defined collective coordinate $Q(\hat{k})$, and therefore must have the same transformation properties as $Q(\hat{k})$; see Eqs. (1.21), (1.22) and (1.25). Of course, a merit of the Landau approach is that one can just as well use $Q(\hat{k})$ as the order parameter field, because symmetry consideration would lead to the

same free energy functional as using $\Omega(\hat{k})$.]. Under independent translations of all the replicas, i.e., $\mathbf{c}_i^\alpha \to \mathbf{c}_i^\alpha + \mathbf{a}^\alpha$, the replica order parameter $\Omega(\hat{k})$ transforms as

$$\Omega(\hat{k}) \to \Omega'(\hat{k}) = \mathrm{e}^{i\sum_{\alpha=0}^{n} \mathbf{k}^\alpha \cdot \mathbf{a}^\alpha} \Omega(\hat{k}). \tag{2.1}$$

Under independent rotations of the replicas, defined by $\mathbf{c}_i^\alpha \to R^\alpha \mathbf{c}_i^\alpha$, the order parameter transforms as

$$\Omega(\hat{k}) \to \Omega'(\hat{k}) = \Omega(\hat{R}^{-1}\hat{k}), \tag{2.2}$$

where $\hat{R}\hat{v} \equiv \{R^0\mathbf{v}^0, \cdots, R^n\mathbf{v}^n\}$. As has been shown in the semi-microscopic theories [32], no macroscopically inhomogeneous modes (such as crystalline modes), represented by 1RS order parameters, order or fluctuate critically in the vicinity of the vulcanization transition, such modes being stabilized by the excluded-volume interaction. Therefore, the sought free energy can be expressed in terms of contributions referring to the HRS order parameter alone.

We express the free energy as an expansion in (integral) powers of the replica order parameter $\Omega(\hat{k})$, retaining the two lowest possible powers of $\Omega(\hat{k})$, which in this case are the second and the third (When we go beyond mean-field theory, below, RG arguments will justify our omission of all other symmetry-allowed terms on the grounds that they are irrelevant at the fixed-points of interest.) We consider the case in which no external potential couples to the order parameter. Hence, e.g., there is no term linear in the order parameter. We make explicit use of translational symmetry, Eq. (2.1), and thus obtain the following expression for the effective Hamiltonian [61]

$$\mathcal{S}(\Omega) = N \sum_{\hat{k}\in\mathrm{HRS}} g_2(\hat{k})|\Omega(\hat{k})|^2 - N \sum_{\hat{k}_1,\hat{k}_2,\hat{k}_3\in\mathrm{HRS}} g_3(\hat{k}_1,\hat{k}_2,\hat{k}_3)\Omega(\hat{k}_1)\,\Omega(\hat{k}_2)\,\Omega(\hat{k}_3)\,\delta_{\hat{k}_1+\hat{k}_2+\hat{k}_3,\hat{0}}\,. \tag{2.3}$$

Here, the symbol $\sum_{\hat{k}\in\mathrm{HRS}}$ denotes a summation over replicated wave vectors $\hat{k}$, subject to the restriction that $\hat{k}$ lies in the HRS. In a microscopic approach, the functions $g_2(\hat{k})$ and $g_3(\hat{k}_1,\hat{k}_2,\hat{k}_3)$ would be obtained in terms of the control parameter that represents the crosslink density, together with density correlators of an uncrosslinked liquid having interactions renormalized by the crosslinking. Here, however, we will ignore the microscopic origins of g_2 and g_3, and instead use symmetry considerations and a long-wavelength expansion to determine only their general forms.

The disorder-averaged free-energy density of the system is related to the effective Hamiltonian via [42]

$$f \propto -N^{-1} \lim_{n\to 0} n^{-1} \ln[Z^n] \,, \tag{2.4}$$

$$[Z^n] \propto \int \overline{\mathcal{D}}^{\dagger} \Omega \exp(-\mathcal{S}), \tag{2.5}$$

In the saddle-point approximation, then, the disorder-averaged free energy density f is given by

$$f \propto N^{-1} \lim_{n\to 0} \min_{\Omega} n^{-1} \mathcal{S}(\{\Omega(\cdot)\}). \tag{2.6}$$

Bearing in mind the physical notion that near the transition any localization should occur only on long length-scales, we examine the long wavelength limit by also performing a low-order gradient expansion. In the term quadratic in the order parameter we keep only the leading and next-to-leading order terms in $\hat{k}$; in the cubic term in the order parameter we keep only the leading term in $\hat{k}$. Thus, the function g_3 in Eq. (2.3) is replaced by a constant and the function g_2 is expanded to quadratic order in $\hat{k}$. By analyticity and rotational invariance, g_2 can only depend on $\{\mathbf{k}^0, \ldots, \mathbf{k}^n\}$ via $\{|\mathbf{k}^0|^2, \ldots, |\mathbf{k}^n|^2\}$, and, in particular, terms linear in $\hat{k}$ are excluded. In addition, by the permutation symmetry among the replicas, each term $|\mathbf{k}^\alpha|^2$ must enter the expression for g_2 with a common prefactor, so that the dependence is in fact on $\hat{k}^2$ (which, as we may recall, is defined to be $\mathbf{k}^0 \cdot \mathbf{k}^0 + \mathbf{k}^1 \cdot \mathbf{k}^1 + \cdots + \mathbf{k}^n \cdot \mathbf{k}^n$). Thus, the replica free energy for long-wavelength fluctuations has the general form:

$$\mathcal{S}(\{\Omega(\hat{k})\}) = N \sum_{\hat{k}\in \mathrm{HRS}} \Big(-a\tau + \frac{b}{2}\hat{k}^2 \Big) |\Omega(\hat{k})|^2 - Ng \sum_{\hat{k}_1,\hat{k}_2,\hat{k}_3 \in \mathrm{HRS}} \Omega(\hat{k}_1)\, \Omega(\hat{k}_2)\, \Omega(\hat{k}_3)\, \delta_{\hat{k}_1+\hat{k}_2+\hat{k}_3,\hat{0}} \,, \tag{2.7}$$

where τ is the reduced control-parameter measuring the crosslink density. Coefficients a, b and g are phenomenological parameters that contain microscopic details. Although the semi-microscopic derivation of $\mathcal{S}$ contains n-dependent coefficients a_n, b_n and g_n, it is admissible for us to keep only the $n \to 0$ limit of these coefficients (i.e. a, b and g) at the outset because $\mathcal{S}$ is already proportional to n for pertinent field-configurations.

We wish to emphasize the point that this minimal model *does not contain fields outside the*

HRS. This (linear) constraint on the field embodies the notion that inter-particle interactions give a "mass" in the 1RS (i.e. produce a free-energy penalty for density inhomogeneities) that remains nonzero at the vulcanization transition. From the standpoint of symmetry, this constraint has the effect of ensuring that the only symmetry of the theory (associated with the mixing of the replicas) is the *permutation* symmetry S_{n+1}. Without it, the model would have the larger orthogonal symmetry $\mathrm{O}\left((n+1)d\right)$ of rotations that mix the (Cartesian components of the) replicas; see the term associated with the inter-replica coupling arising from the disorder-averaging of the replicated crosslinking constraints in Eq. (1.20). In addition to permutation symmetry, the model has the symmetry of independent translations and rotations of each replica. The restriction to the HRS (or, equivalently, the energetic suppression of the 1RS) is vital: it entirely changes the content of the theory. Without it, one would be led to completely erroneous results for both the mean-field picture of the amorphous solid state (and, as we shall see later, the critical properties of the vulcanization transition).

For use in Sec. 3.3.2 of Chap. 3 , when we come to examine the physical implications of the Ginzburg criterion, we list values of the dimensionful coefficients in the effective free-energy derived for the case of RCMSs (up to inessential factors of the crosslink density control parameter μ^2):

$$\tau = (\mu^2 - \mu_{\mathrm{c}}^2)/\mu_{\mathrm{c}}^2, \tag{2.8}$$

$$a = 1/2, \tag{2.9}$$

$$b = L\ell/6d, \tag{2.10}$$

$$g = 1/6. \tag{2.11}$$

Here, μ_{c}^2 is the mean-field critical value of μ^2, L is the arclength of each macromolecule, and ℓ is the persistence length of the macromolecules.

By taking the first variation with respect to Ω we obtain the stationarity condition for the replica order parameter:

$$0 = \frac{\delta \mathcal{S}}{\delta \Omega(-\hat{k})} = 2\Big(- a\tau + \frac{b}{2}\hat{k}^2\Big)\Omega(\hat{k}) - 3g \sum_{\hat{k}_1,\hat{k}_2 \in \mathrm{HRS}} \Omega(\hat{k}_1)\,\Omega(\hat{k}_2)\,\delta_{\hat{k}_1+\hat{k}_2,\hat{k}}\,. \tag{2.12}$$

This self-consistency condition applies for all values of $\hat{k}$ lying in the HRS.

2.3 Universal properties of the order parameter in the amorphous solid state

Generalizing what was done for crosslinked and end-linked macromolecular systems, we hypothesize that the particles have a probability q of being localized (also called the "gel fraction" in the context of vulcanization) and $1-q$ of being delocalized, and that the localized particles are characterized by a probability distribution $2\xi^{-3}p(\xi^{-2})$ for their localization lengths ξ. Such a characterization weaves in the physical notion that amorphous systems should show a spectrum of possibilities for the behavior of their constituents, and adopts the perspective that it is this spectrum that one should aim to calculate. This hypothesis translates into the following expression for the form of the stationary value of the HRS order parameter [31, 32]:

$$\overline{\Omega}(\hat{k}) = q\,\delta^{(d)}_{\tilde{\mathbf{k}},\mathbf{0}} \int_0^\infty dt\, p(t)\, \mathrm{e}^{-\hat{k}^2/2t}, \tag{2.13}$$

where we have used the notation $\tilde{\mathbf{k}} \equiv \sum_{\alpha=0}^{n} \mathbf{k}^\alpha$. On the right hand side the term that would represent delocalized particles has been omitted, as it is proportional to $\delta_{\hat{k},\hat{0}}$, due to the fact that not only the average particle density but the individual particle densities are translationally invariant, and thus vanishes for $\hat{k} \in$ HRS. The term representing localized particles survives, and is only invariant under *common* translations (i.e. translations in which $\mathbf{a}^\alpha = \mathbf{a}$ for all α) and common rotations of the replicas. This corresponds to the fact that the individual particle density for localized particles is not translationally invariant, so that translational invariance is broken microscopically, but the average density remains translationally invariant (i.e. the system still is macroscopically translationally invariant).

By inserting the hypothesis (2.13) into the stationarity condition (2.12), and taking the $n \to 0$ limit, we obtain

$$0 \;=\; \delta^{(d)}_{\tilde{\mathbf{k}},\mathbf{0}} \left\{ 2\left(3gq^2 - a\tau q + bq\hat{k}^2/2\right) \int_0^\infty dt\, p(t)\; \mathrm{e}^{-\hat{k}^2/2t} \right.$$

$$- 3gq^2 \int_0^\infty dt_1\, p(t_1) \int_0^\infty dt_2\, p(t_2)\, \mathrm{e}^{-\hat{k}^2/2(t_1+t_2)} \Bigg\} . \tag{2.14}$$

In the limit $\hat{k}^2 \to 0$, this equation reduces to a condition for the localized fraction q, viz.,

$$0 = -2aq\tau + 3gq^2. \tag{2.15}$$

For negative or zero τ, corresponding to a constraint density less than or equal to its critical value, the only physical solution is $q = 0$, corresponding to the liquid state. In this state, all particles are delocalized. For positive τ, corresponding to a constraint density in excess of the critical value, there are two solutions. One, unstable, is the continuation of the liquid state $q = 0$; the other, stable, corresponds to a nonzero localized fraction,

$$q = \frac{2a}{3g}\tau^\beta, \qquad \beta = 1\ . \tag{2.16}$$

We identify this second state as the amorphous solid state. From the dependence of the localized fraction q on the control parameter τ and the form of the order parameter (2.13) we conclude that there is a continuous phase transition between the liquid and the amorphous solid states at $\tau = 0$, with localized fraction exponent $\beta = 1$ (i.e. the classical exponent [12]). It is worth mentioning that microscopic approaches go beyond this linear behavior near the transition, yielding a transcendental equation for $q(\tau)$, valid for all values of the control parameter τ; see Ref. [31, 32]. From Eq. (2.7) it is evident that the liquid state is locally stable (unstable) for negative (positive) τ: the eigenvalues of the resulting quadratic form are given by $\lambda(\hat{k}) = -a\tau + b\hat{k}^2/2$. We note that it has been shown that the stationary solution proposed in Eq. (2.13) is locally stable (up to the usual Goldstone modes) in the amorphous solid state (i.e. for positive τ) [49]. However, there is, in principle, no guarantee that this state is globally stable (i.e. that no states with lower free energy exist).

Now concentrating on the amorphous solid state, by inserting the value of the localized fraction into Eq. (2.14), we obtain the following integro-differential equation for the probability distribution

for the localization lengths:

$$\frac{bt^2}{a}\frac{dp}{dt} = \Big(\tau - \frac{2b}{a}t\Big)p(t) - \tau\int_0^t dt_1\, p(t_1)\, p(t-t_1). \tag{2.17}$$

All parameters can be seen to play an elementary role in this equation by expressing $p(t)$ in terms of a scaling function:

$$p(t) = \frac{2b}{a\tau}\,\pi(\theta); \qquad t = \frac{a\tau}{2b}\,\theta. \tag{2.18}$$

Thus, the universal function $\pi(\theta)$ is seen to obey the nonlinear integro-differential equation

$$\frac{\theta^2}{2}\frac{d\pi}{d\theta} = (1-\theta)\,\pi(\theta) - \int_0^\theta d\theta'\pi(\theta')\pi(\theta-\theta'). \tag{2.19}$$

By solving this equation numerically, together with the normalization condition $1 = \int_0^\infty d\theta\,\pi(\theta)$ [31, 32], one recovers the scaling function derived in the semi-microscopic model for the vulcanization transition [31, 32]. The function $\pi(\theta)$ has a peak at $\theta \simeq 1$ of width of order unity, and decays rapidly both as $\theta \to 0$ and $\theta \to \infty$ (see Fig. 2.1). By combining these features of $\pi(\theta)$ with the scaling transformation (2.18) we conclude that the typical localization length scales as $\tau^{-1/2}$ near the transition. The order parameter also has a scaling form near the transition:

$$\overline{\Omega}(\hat{k}) = \frac{2\tau}{3g}\delta^{(d)}_{\tilde{\mathbf{k}},\mathbf{0}}\,\omega\Big(\sqrt{\frac{2b}{a\tau}\hat{k}^2}\Big), \tag{2.20}$$

$$\omega(k) = \int_0^\infty d\theta\,\pi(\theta)\mathrm{e}^{-k^2/2\theta}\,. \tag{2.21}$$

Equation (2.19) and the normalization condition on $\pi(\theta)$ are precisely the conditions that determine the scaling function for the crosslinked and end-linked cases [31, 32, 55].

It is a very interesting observation that the same scaling function $\pi(\theta)$ also appears as the kernel of the mean-field order parameter value for the system of random resistor network [62].

As discussed in this section, the localized fraction $q(\tau)$ and the scaled distribution of inverse square localization lengths $\pi(\theta)$ are universal near the transition. We now discuss this issue in more detail.

First, let us focus at the mean-field level. Recall the mean-field theory of ferromagnetism [63] and, in particular, the exponent β, which characterizes the vanishing of the magnetization density

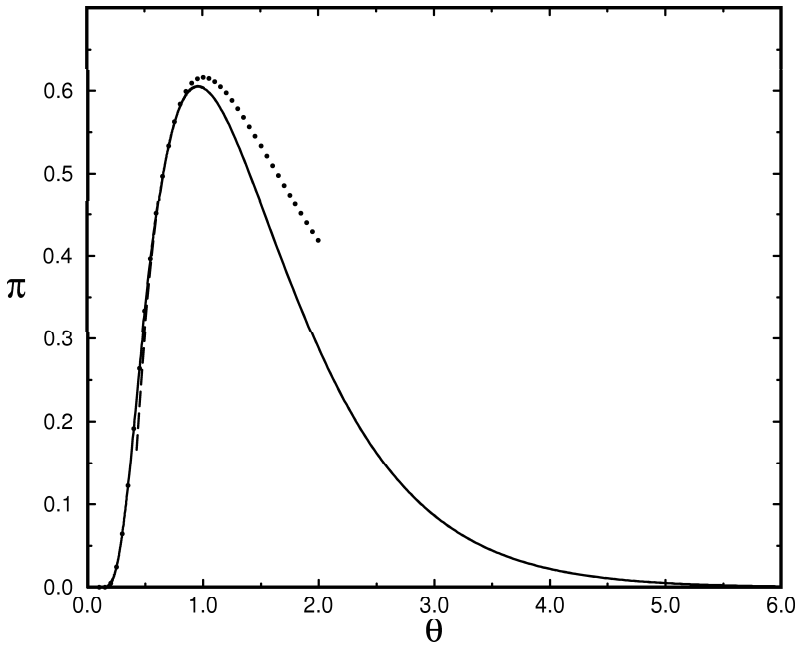

Figure 2.1: Scaling function $\pi(\theta)$ (full line) for the probability distribution of localization lengths; asymptotic form for $\theta \to 0$ (dotted line); asymptotic form for $\theta \to \infty$ (broken line) [32].

order parameter (from the ferromagnetic state) as a function of the temperature at zero applied magnetic field. The exponent β takes on the value of $1/2$, regardless of the details of the mean-field theory used to compute it. The functions $q(\tau)$, $\pi(\theta)$ and $\omega(k)$ are universal in the same sense. The case of $q(\tau)$ is on essentially the same, standard, footing as that of the magnetization density. What is not standard, however, is that describing the (equilibrium) order parameter is a universal scaling *function*, $\omega(k)$ [or, equivalently, $\pi(\theta)$] that is not a simple power law. This feature arises because the usual presence of fields carrying *internal* indices, such as Cartesian vector indices in the case of ferromagnetism, is replaced here by the external continuous replicated wave vector variable $\hat{k}$. There are two facets to this universal scaling behavior of the order parameter. First, for systems differing in their microscopic details and their constraint densities there is the possibility of collapsing the distribution of localization lengths on to a single function, solely by rescaling the independent variable. Second, there is a definite prediction for the dependence of this rescaling on the control parameter τ.

Now, going beyond the mean-field level, in the context of the vulcanization transition de Gennes has argued that the width of the critical region, in which fluctuations dominate and mean-field the-

ory fails, vanishes in the limit of very long macromolecules in space-dimension $d = 3$ or higher [50]. Thus, one may anticipate that for extended objects the mean-field theory discussed here will be valid, except in an narrow region around the transition.

Up to this point we have assumed that the free energy is invariant under interchange of all replicas, including the one representing the constraint distribution ($\alpha = 0$), with any of the remaining n, i.e., that the free energy is symmetric under the group S_{n+1} of permutations of all $n + 1$ replicas. This need not be the case, in general, as the system can be changed, (e.g. by changing the temperature) after the constraints have been imposed. In this latter case, the free energy retains the usual replica-induced S_n symmetry under permutations of replicas $\alpha = 1, \ldots, n$. The argument we have developed here can be reproduced for this more general case with only a minor change: in the free energy, we can no longer invoke S_{n+1} symmetry to argue that all of the $|\mathbf{k}^\alpha|^2$ must enter the expression for g_2 with a common prefactor. Instead, we only have permutation symmetry among replicas $\alpha = 1, \ldots, n$ and, therefore, the prefactor b for all of these replicas must be the same, but now the prefactor b_0 for replica $\alpha = 0$ can be different. This amounts to making the replacement

$$\hat{k}^2 \to \bar{k}^2 \equiv b_0 b^{-1} |\mathbf{k}^\mathbf{0}|^2 + \sum\nolimits_{\alpha=1}^{n} |\mathbf{k}^\alpha|^2 \tag{2.22}$$

in the free energy. Both the rest of the derivation and the results are unchanged, except that $\hat{k}^2$ needs to be replaced by $\bar{k}^2$, throughout.

We mention that no saddle points exhibiting the spontaneous breaking of replica permutation symmetry have been found, to date, either for systems with S_{n+1} or S_n symmetry [31].

2.4 Free energy in terms of the distribution of static density fluctuations

The aim of this section is to construct an expression for the disorder-averaged Landau free energy for the amorphous solidification transition (i.e. the effective Hamiltonian $\mathcal{S}$) in terms of the distribution of static density fluctuations. We present this approach as an alternative to the strategy of constructing a replica free energy $\mathcal{S}$ in terms of the replica order parameter Ω. In the familiar way, the equilibrium state will be determined via a variational principle: $\delta\mathcal{S} = 0$ and $\delta^2\mathcal{S} > 0$.

What may be less familiar, however, is that in the present setting the *independent* variables for the variation (i.e. the distribution of static density fluctuations) themselves constitute a functional.

Our aim, then, is to work not with the replica order parameter $\Omega(\hat{k})$, but instead with the disorder-averaged probability density functional for the random static density fluctuations [32, 64], $\mathcal{N}(\{\rho_{\mathbf{k}}\})$, which is defined via

$$\mathcal{N}(\{\rho_{\mathbf{k}}\}) \equiv \left[\frac{1}{N} \sum_{i=1}^{N} \prod_{\mathbf{k}} \delta_{\mathrm{c}} \Big(\rho_{\mathbf{k}} - \langle \exp\left(i\mathbf{k} \cdot \mathbf{c}_i\right) \rangle_{\chi} \Big) \right]. \tag{2.23}$$

Here, $\prod_{\mathbf{k}}$ denotes the product over all d-vectors $\mathbf{k}$, and the Dirac δ-function of complex argument $\delta_{\mathrm{c}}(z)$ is defined by $\delta_{\mathrm{c}}(z) \equiv \delta(\mathrm{Re}\, z)\, \delta(\mathrm{Im}\, z)$, where $\mathrm{Re}\, z$ and $\mathrm{Im}\, z$ respectively denote the real and imaginary parts of the complex number z. From the definition of $\mathcal{N}(\{\rho_{\mathbf{k}}\})$, we see that $\rho_{-\mathbf{k}} = \rho_{\mathbf{k}}^{*}$ and $\rho_{\mathbf{0}} = 1$. Thus we can take as independent variables $\rho_{\mathbf{k}}$ for all d-vectors $\mathbf{k}$ in the half-space given by the condition $\mathbf{k} \cdot \mathbf{n} > 0$ for a suitable unit d-vector $\mathbf{n}$. In addition, $\mathcal{N}(\{\rho_{\mathbf{k}}\})$ obeys the normalization condition

$$\int \mathcal{D}\rho\, \mathcal{N}(\{\rho_{\mathbf{k}}\}) = 1. \tag{2.24}$$

It is straightforward to check that, for any particular positive integer g, the replica order parameter $\Omega(\hat{k})$ is a g^{th} moment of $\mathcal{N}(\{\rho_{\mathbf{k}}\})$:

$$\int \mathcal{D}\rho\, \mathcal{N}(\{\rho_{\mathbf{k}}\})\, \rho_{\mathbf{k}^1}\, \rho_{\mathbf{k}^2} \cdots \rho_{\mathbf{k}^g} = \Omega(\mathbf{k}^1, \mathbf{k}^2, \ldots, \mathbf{k}^g), \tag{2.25}$$

where we have used $\mathcal{D}\rho$ to denote the measure $\prod_{\mathbf{k}} d\,\mathrm{Re}\,\rho_{\mathbf{k}}\, d\,\mathrm{Im}\,\rho_{\mathbf{k}}$.

The merit of the distribution functional $\mathcal{N}(\{\rho_{\mathbf{k}}\})$ over the replica order parameter $\Omega(\hat{k})$ is that, as we shall soon see, it allows us to formulate a Landau free energy for the amorphous solidification transition, depending on $\mathcal{N}(\{\rho_{\mathbf{k}}\})$, in which replicated quantities do not appear, while maintaining the physical content of the theory. At the present time, this approach is not truly independent of the replica approach, in the following sense: we employ the replica approach to derive the free energy, Eq. (2.7), and only then do we transform from the language of order parameters to the language of the distribution of static density fluctuations. We are not yet in possession of either an analytical scheme or a set of physical arguments that would allow us to construct the Landau

free energy directly. Nevertheless, we are able, by this indirect method, to propose a (replica-free) free energy, and also to hypothesize (and verify the correctness of) a stationary value of $\mathcal{N}(\{\rho_{\mathbf{k}}\})$. It would, however, be very attractive to find a scheme that would allow us to eschew the replica approach and work with the distribution of static density fluctuations from the outset.

To proceed, we take the replica Landau free energy $\mathcal{S}$, Eq. (2.7), in terms of the replica order parameter $\Omega(\hat{k})$, and replace $\Omega(\hat{k})$ by its expression in terms of the $(n+1)^{\text{th}}$ moment of $\mathcal{N}(\{\rho_{\mathbf{k}}\})$. Thus, we arrive at the replica Landau free energy:

$$\begin{aligned}
\mathcal{S}/N &= a\tau - 2g + (3g - a\tau) \int \mathcal{D}\rho_1 \, \mathcal{N}(\{\rho_{1,\mathbf{k}}\}) \, \mathcal{D}\rho_2 \, \mathcal{N}(\{\rho_{2,\mathbf{k}}\}) \, \left(\sum_{\mathbf{k}} \rho_{1,\mathbf{k}} \, \rho_{2,-\mathbf{k}} \right)^{n+1} \\
&\quad + \frac{1}{2} b(n+1) \int \mathcal{D}\rho_1 \, \mathcal{N}(\{\rho_{1,\mathbf{k}}\}) \, \mathcal{D}\rho_2 \, \mathcal{N}(\{\rho_{2,\mathbf{k}}\}) \, \left(\sum_{\mathbf{k}} k^2 \, \rho_{1,\mathbf{k}} \, \rho_{2,-\mathbf{k}} \right) \left(\sum_{\mathbf{k}} \rho_{1,\mathbf{k}} \, \rho_{2,-\mathbf{k}} \right)^{n} \\
&\quad - g \int \mathcal{D}\rho_1 \, \mathcal{N}(\{\rho_{1,\mathbf{k}}\}) \, \mathcal{D}\rho_2 \, \mathcal{N}(\{\rho_{2,\mathbf{k}}\}) \, \mathcal{D}\rho_3 \, \mathcal{N}(\{\rho_{3,\mathbf{k}}\}) \, \left(\sum_{\mathbf{k}_1, \mathbf{k}_2} \rho_{1,\mathbf{k}_1} \rho_{2,\mathbf{k}_2} \rho_{3,-\mathbf{k}_1-\mathbf{k}_2} \right)^{n+1}
\end{aligned} \tag{2.26}$$

In order to obtain the desired (replica-independent) free energy we take the limit $n \to 0$ of Eq. (2.26):

$$\begin{aligned}
f &= N^{-1} \lim_{n \to 0} n^{-1} \mathcal{S} \\
&= (3g - a\tau) \int \mathcal{D}\rho_1 \, \mathcal{N}(\{\rho_{1,\mathbf{k}}\}) \, \mathcal{D}\rho_2 \, \mathcal{N}(\{\rho_{2,\mathbf{k}}\}) \, \left(\sum_{\mathbf{k}} \rho_{1,\mathbf{k}} \, \rho_{2,-\mathbf{k}} \right) \ln \left(\sum_{\mathbf{k}} \rho_{1,\mathbf{k}} \, \rho_{2,-\mathbf{k}} \right) \\
&\quad + \frac{b}{2} \int \mathcal{D}\rho_1 \, \mathcal{N}(\{\rho_{1,\mathbf{k}}\}) \, \mathcal{D}\rho_2 \, \mathcal{N}(\{\rho_{2,\mathbf{k}}\}) \, \left(\sum_{\mathbf{k}} k^2 \rho_{1,\mathbf{k}} \, \rho_{2,-\mathbf{k}} \right) \ln \left(\sum_{\mathbf{k}} \rho_{1,\mathbf{k}} \, \rho_{2,-\mathbf{k}} \right) \\
&\quad - g \int \mathcal{D}\rho_1 \, \mathcal{N}(\{\rho_{1,\mathbf{k}}\}) \, \mathcal{D}\rho_2 \, \mathcal{N}(\{\rho_{2,\mathbf{k}}\}) \, \mathcal{D}\rho_3 \, \mathcal{N}(\{\rho_{3,\mathbf{k}}\}) \, \left(\sum_{\mathbf{k}_1, \mathbf{k}_2} \rho_{1,\mathbf{k}_1} \, \rho_{2,\mathbf{k}_2} \, \rho_{3,-\mathbf{k}_1-\mathbf{k}_2} \right) \\
&\qquad \times \ln \left(\sum_{\mathbf{k}_1, \mathbf{k}_2} \rho_{1,\mathbf{k}_1} \, \rho_{2,\mathbf{k}_2} \, \rho_{3,-\mathbf{k}_1-\mathbf{k}_2} \right) .
\end{aligned} \tag{2.27}$$

In deriving the above free energy we have employed the physical fact that the average particle-density is uniform. In other words, the replica order parameter is zero if all but one of the replicated wave vectors is nonzero which, translated in the language of the distribution of static density fluctuations, means that the first moment of the static density distribution equals $\delta_{\mathbf{k},\mathbf{0}}$. It is worth noting that within this formalism the replica limit can already be taken at the level of the free energy,

prior to the hypothesizing of an explicit form for the stationary value of the order parameter. On the one hand, this is attractive, as it leads to a Landau theory in which replicas play no role. On the other hand, the approach is, at present, restricted to replica-symmetric states.

Next we construct the self-consistency condition that follows from the stationarity of the replica-independent free energy. We then proceed to solve the resulting functional equation exactly, by hypothesizing a solution having precisely the same physical content as the exact solution of the replica self-consistency condition discussed in Sec. 2.3.

To construct the self-consistency condition for $\mathcal{N}(\{\rho_{\mathbf{k}}\})$ it is useful to make two observations. First, $\mathcal{N}(\{\rho_{\mathbf{k}}\})$ obeys the normalization condition (2.24). This introduces a constraint on the variations of $\mathcal{N}(\{\rho_{\mathbf{k}}\})$ which is readily accounted for via Lagrange's method of undetermined multipliers. Second, as mentioned above, not all the variables $\{\rho_{\mathbf{k}}\}$ are independent: we have the relations $\rho_{\mathbf{0}} = 1$ and $\rho_{-\mathbf{k}} = \rho_{\mathbf{k}}^*$. In principle, one could proceed by defining a new distribution that only depends on the independent elements of $\{\rho_{\mathbf{k}}\}$, and re-express the free energy in terms of this new distribution. However, for convenience we will retain $\mathcal{N}(\{\rho_{\mathbf{k}}\})$ as the basic quantity to be varied, and bear in mind the fact that $\rho_{\mathbf{0}} = 1$ and $\rho_{-\mathbf{k}} = \rho_{\mathbf{k}}^*$. By performing the constrained variation of f with respect to the functional $\mathcal{N}(\{\rho_{\mathbf{k}}\})$,

$$0 = \frac{\delta}{\delta \mathcal{N}(\{\rho_{\mathbf{k}}\})} \left(f + \lambda \int \mathcal{D}\rho_1 \, \mathcal{N}(\{\rho_{1,\mathbf{k}}\}) \right), \tag{2.28}$$

where λ is the undetermined multiplier, we obtain the self-consistency condition obeyed by $\mathcal{N}(\{\rho_{\mathbf{k}}\})$:

$$\begin{aligned} 0 \;=\; & \lambda + 2(3g - a\tau) \int \mathcal{D}\rho_1 \, \mathcal{N}(\{\rho_{1,\mathbf{k}}\}) \left(\sum_{\mathbf{k}} \rho_{\mathbf{k}} \, \rho_{1,-\mathbf{k}} \right) \ln \left(\sum_{\mathbf{k}} \rho_{\mathbf{k}} \, \rho_{1,-\mathbf{k}} \right) \\ & + b \int \mathcal{D}\rho_1 \, \mathcal{N}(\{\rho_{1,\mathbf{k}}\}) \left(\sum_{\mathbf{k}} k^2 \rho_{\mathbf{k}} \, \rho_{1,-\mathbf{k}} \right) \ln \left(\sum_{\mathbf{k}} \rho_{\mathbf{k}} \rho_{1,-\mathbf{k}} \right) \\ & - 3g \int \mathcal{D}\rho_1 \, \mathcal{N}(\{\rho_{1,\mathbf{k}}\}) \, \mathcal{D}\rho_2 \, \mathcal{N}(\{\rho_{2,\mathbf{k}}\}) \left(\sum_{\mathbf{k},\mathbf{k}'} \rho_{\mathbf{k}} \, \rho_{1,\mathbf{k}'} \, \rho_{2,-\mathbf{k}-\mathbf{k}'} \right) \\ & \times \ln \left(\sum_{\mathbf{k},\mathbf{k}'} \rho_{\mathbf{k}} \, \rho_{1,\mathbf{k}'} \, \rho_{2,-\mathbf{k}-\mathbf{k}'} \right). \end{aligned} \tag{2.29}$$

To solve this self-consistency condition for $\mathcal{N}(\{\rho_{\mathbf{k}}\})$ we import our experience with the replica

approach, thereby constructing the normalized hypothesis

$$\mathcal{N}(\{\rho_{\mathbf{k}}\}) = (1-q)\,\delta_{\rm c}(\rho_{\mathbf{0}}-1)\prod_{\mathbf{k}\neq\mathbf{0}}\delta_{\rm c}(\rho_{\mathbf{k}}) + q\int\frac{d\mathbf{c}}{V}\int_0^\infty dt\,p(t)\prod_{\mathbf{k}}\delta_{\rm c}(\rho_{\mathbf{k}}-{\rm e}^{i\mathbf{c}\cdot\mathbf{k}-k^2/2t}), \tag{2.30}$$

in which q (which satisfies $0\leq q\leq 1$) is the localized fraction and $p(t)$ (which is regular and normalized to unity) is the distribution of localization lengths of localized particles. It is straightforward to show that by taking the $(n+1)^{\rm th}$ moment of $\mathcal{N}(\{\rho_{\mathbf{k}}\})$ we recover the self-consistent form of the replica order parameter, Eq. (2.13).By inserting the hypothesis (2.30) into Eq. (2.29), making the replacement $\rho_{\mathbf{0}}\to 1$, and performing some algebra, the self-consistency condition is seen to take the form

$$\begin{aligned} 0 \;=\; & \int\frac{d\mathbf{c}}{V}\int_0^\infty dt\,\left(1+\sum_{\mathbf{k}\neq\mathbf{0}}\rho_{\mathbf{k}}\,{\rm e}^{-i\mathbf{c}\cdot\mathbf{k}-k^2/2t}\right)\,\ln\left(1+\sum_{\mathbf{k}\neq\mathbf{0}}\rho_{\mathbf{k}}\,{\rm e}^{-i\mathbf{c}\cdot\mathbf{k}-k^2/2t}\right) \\ & \times\left\{2q(-a\tau+3gq)p(t)-bq\frac{d}{dt}(2t^2p(t))-3gq^2\int_0^t dt_1\,p(t_1)\,p(t-t_1)\right\} \\ & -\frac{3g}{2}dq^2\int_0^\infty dt_1\,p(t_1)\,dt_2\,p(t_2)\,\ln\left\{V^{2/d}\frac{t_1t_2}{2\pi{\rm e}(t_1+t_2)}\right\}+\lambda\,, \end{aligned} \tag{2.31}$$

in terms of the undetermined multiplier λ. To determine λ we insert the choice $\rho_{\mathbf{k}}=\delta_{\mathbf{k},\mathbf{0}}$, which yields

$$\lambda = \frac{3g}{2}dq^2\int_0^\infty dt_1\,p(t_1)\,dt_2\,p(t_2)\,\ln\left\{V^{2/d}\frac{t_1t_2}{2\pi{\rm e}(t_1+t_2)}\right\}. \tag{2.32}$$

By using this result to eliminate λ from the self-consistency condition, and observing that this condition must be satisfied for arbitrary $\{\rho_{\mathbf{k}}\}$, we arrive at a condition on q and $p(t)$, viz.,

$$0 = 2q\,(-a\tau+3gq)\,p(t)-bq\frac{d}{dt}\Big(2t^2p(t)\Big)-3gq^2\int_0^t dt_1\,p(t_1)\,p(t-t_1). \tag{2.33}$$

We integrate this equation over all values of t and use the normalization condition on $p(t)$ to arrive at the same equation relating q and τ as was found in Eq. (2.15) of the previous section, the appropriate solution of which is given by $q=2a\tau/3g$, i.e., Eq. (2.16). Finally, we use this result for q to eliminate it from Eq. (2.33), thus arriving at the same self-consistency condition on $p(t)$ as was found in Eq. (2.17) of the previous section. Thus, we see that these conditions, one for q and one for $p(t)$, are precisely the same as those arrived at by the replica method discussed in Sec. 2.3.

2.5 Comparison with numerical simulations: Universality exhibited

The purpose of the present section is to examine the conclusions of the Landau theory, especially those concerning universality and scaling, in the light of the extensive molecular dynamics simulations, performed by Barsky and Plischke [60]. These simulations address the amorphous solidification transition in the context of RCMSs, doing so by using an off-lattice model of macromolecules interacting via a Lennard-Jones potential. It should be emphasized that there are substantial dif-

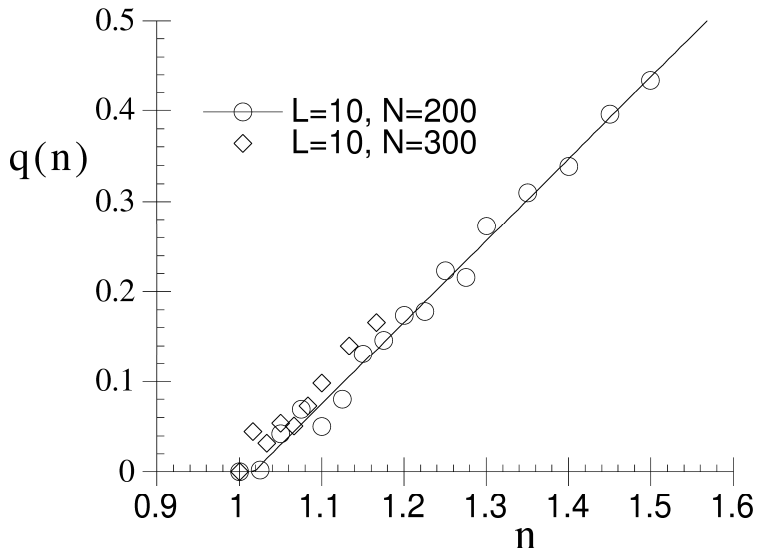

Figure 2.2: Localized fraction q as a function of the number of crosslinks per macromolecule n, as computed in molecular dynamics simulations by Barsky and Plischke (1997, unpublished). L is the number of monomers in each macromolecule; N is the number of macromolecules in the system. The straight line is a linear fit to the $N = 200$ data. Note the apparent existence of a continuous phase transition near $n = 1$, as well as the apparent linear variation of q with n, both features being consistent with the mean-field description.

ferences between the ingredients and calculational schemes used in the analytical and simulational approaches. In particular, the analytical approach: (i) invokes the replica technique; (ii) retains interparticle interactions only to the extent that macroscopically inhomogeneous states are disfavored (i.e. the one-replica sector remains stable at the transition); (iii) neglects order-parameter fluctuations, its conclusions therefore being independent of the space-dimension; and (iv) is solved via an Ansatz, which is not guaranteed to capture the optimal solution. Nevertheless, and rather

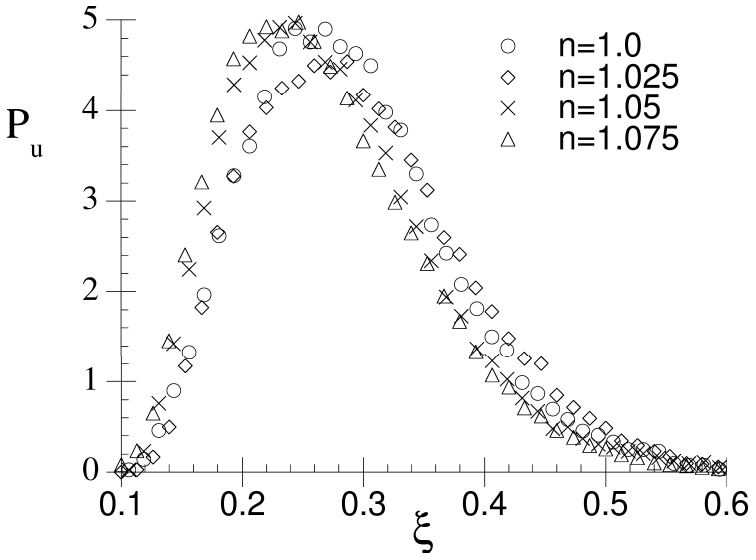

Figure 2.3: Unscaled probability distribution $P_{\rm u}$ of localization lengths ξ (in units of the linear system size), as computed in molecular dynamics simulations by Barsky and Plischke (1997, unpublished). In the simulations the number of segments per macromolecule is 10; and the number of macromolecules is 200.

strikingly, the simulations yield an essentially identical picture for the transition to and properties of the amorphous solid state, inasmuch as they indicate that (i) there exists a (crosslink–density controlled) continuous phase transition from a liquid state to an amorphous solid state; (ii) the critical crosslink density is very close to one crosslink per macromolecule; (iii) the localized fraction q varies linearly with the density of crosslinks, at least in the vicinity of this transition (see Fig. 2.2); (iv) when scaled appropriately (i.e. by the mean localization length), the simulation data for the distribution of localization lengths exhibit very good collapse on to a universal scaling curve for the several (near-critical) crosslink densities and macromolecule lengths considered (see Figs. 2.3 and 2.4); and (v) the form of this universal scaling curve appears to be in remarkably good agreement with the precise form of the analytical prediction for this distribution.

It should not be surprising that by focusing on universal quantities, one finds agreement between the analytical and computational approaches. This indicates that the proposed Landau theory does indeed contain the essential ingredients necessary to describe the amorphous solidification transition.

Let us now look more critically at the comparison between the results of the simulation and

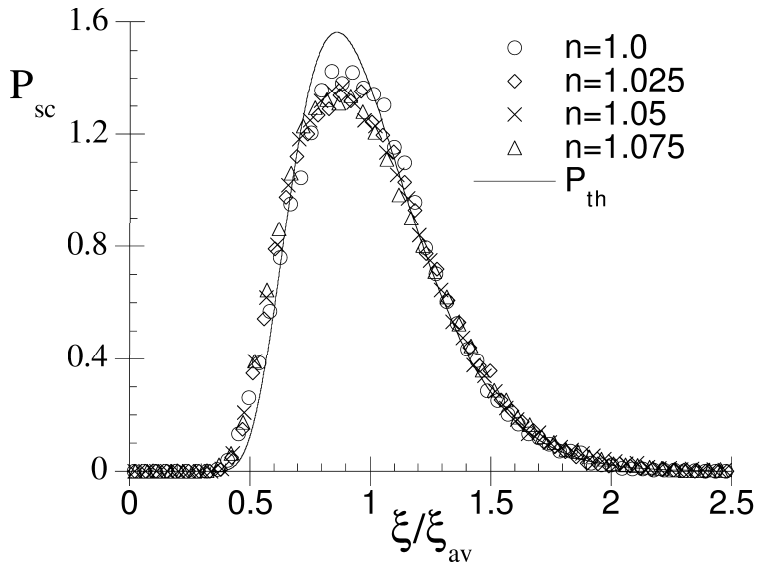

Figure 2.4: Probability distribution (symbols) $P_{\rm s}$ of localization lengths ξ, scaled with the sample-average of the localization lengths $\xi_{\rm av}$, as computed in molecular dynamics simulations by Barsky and Plischke. Note the apparent collapse of the data on to a single universal scaling distribution, as well as the good quantitative agreement with the mean-field prediction for this distribution (solid line). In the simulation the number of segments per macromolecule is 10; the number of macromolecules is 200. The mean-field prediction for $P_{\rm sc}(\xi/\xi_{\rm av})$ is obtained from the universal scaling function $\pi(\theta)$ by $P_{\rm sc}(y) = (2s/y^3)\,\pi(s/y^2)$, where the constant $s \simeq 1.224$ is fixed by demanding that $\int_0^\infty dy\, y\, P_{\rm sc}(y) = 1$.

the mean-field theory. With respect to the localized fraction, the Landau theory is only capable of showing the linearity of the dependence, near the transition, on the excess crosslink density, leaving undetermined the proportionality factor. The simulation results are consistent with this linear dependence, giving, in addition, the amplitude. There are two facets to the universality of the distribution of localization lengths, as mentioned in Sec. 2.3. First, that the distributions can, for different systems and different crosslink densities, be collapsed on to a universal scaling curve, is verified by the simulations, as pointed out above. Second, the question of how the scaling parameter depends on the excess crosslink density is difficult to address in current simulations, because the dynamic range for the mean localization length accessible in them is limited, so that its predicted divergence at the transition is difficult to verify.

2.6 Summary and concluding remarks

To summarize, in this chapter we have proposed a replica Landau free energy for the amorphous solidification transition (of which the vulcanization transition is a primary example). The theory is applicable to systems of extended objects undergoing thermal density fluctuations and subject to quenched random translationally-invariant constraints. The statistics of the quenched randomness are determined by the equilibrium density fluctuations of the unconstrained system. We have shown that there is, generically, a continuous phase transition between a liquid and an amorphous solid state, as a function of the density of random constraints. Both states are described by exact stationary points of this replica free energy, and are replica symmetric and macroscopically translationally invariant. They differ, however, in that the liquid is translationally invariant at the microscopic level, whereas the amorphous solid breaks this symmetry.

We have also shown how all these results may be recovered using an alternative formulation in which we focus less on the replica order parameter and more on the distribution of random static density fluctuations. In particular, we construct a representation of the free energy in terms of this distribution, and solve the resulting stationarity condition.

Lastly, we have examined our results in the light of the extensive molecular dynamics simulations of randomly crosslinked macromolecular systems, due to Barsky and Plischke. Not only do these simulations support the general theoretical scenario of the vulcanization transition, but also they confirm the detailed analytical results for universal quantities, including the localized fraction exponent and the distribution of scaled localization lengths.

The ultimate origin of mean-field universality is not hard to understand, despite the apparent intricacy of the order parameter associated with the amorphous solidification transition. As we saw in Secs. 2.2 and 2.3, there are two small emergent physical quantities, the fraction of localized particles and the characteristic inverse square localization length of localized particles. The smallness of the localized fraction validates the truncation of the expansion of the free energy in powers of the order parameter. The smallness of the characteristic inverse square localization length leads to a very simple dependence, via $\sum_{\alpha=0}^{n} |\mathbf{k}^{\alpha}|^2$, on the $n+1$ independent wave vectors of the replica theory, well beyond the permutation invariance demanded by symmetry considerations alone. As a result, near the transition, the amorphous solid state is characterizable in terms of a single universal

function of a single variable, along with the localized fraction.

Although throughout this chapter we have borne in mind the example of RCMSs, the circle of ideas is by no means restricted to such systems. To encompass other systems possessing externally-induced quenched random constraints, such as networks formed by the permanent random covalent bonding of atoms or small molecules (e.g., silica gels), requires essentially no further conceptual ingredients [57, 58, 59].

One may also envisage applications to the glass transition. Although it is generally presumed that externally-induced quenched random variables are not relevant for describing the glass transition, it is tempting to view the freezing-out of some degrees of freedom as the crucial consequence of the temperature-quench, with a form of quenched disorder thereby being developed spontaneously. The approach presented here becomes of relevance to the glass transition if one accepts this view of the temperature-quench, and thus models the nonequilibrium state of the quenched liquid by the equilibrium state of a system in which some fraction of covalent bonds has been rendered permanent (the deeper the quench the larger the fraction) [65]. This strategy, viz., the approximating of pure systems by ones with "self-induced" quenched disorder, has also been invoked in very interesting work on the Bernasconi model for binary sequences of low autocorrelation [66]. Interesting connections are also apparent with recent effective-potential approaches to glassy magnetic systems, in which one retains in the partition function only those configurations that lie close to the equilibrium state reached at the glass transition temperature [67].

Chapter 3

Renormalization-group approach to the vulcanization transition: Basic issues and expansion to order $6 - d$

3.1 Introduction

In Chap. 2 we presented a detailed mean-field description of the amorphous solidification transition by using the Landau approach to continuous phase transitions. In the present chapter and the following one, we investigate this transition beyond the mean-field level. Although most of our results are not specific to any particular system undergoing an amorphous solidification transition, in order to make our presentation concrete we shall from now on discuss the physical content for, and use notation specific to, the case of vulcanization transition for RCMSs. Our goal is to provide a description of the vulcanization transition beyond the mean-field approximation via the application of renormalization-group (RG) ideas to a model that incorporates both the quenched randomness (central to systems undergoing the vulcanization transition) and the thermal fluctuations of the constituents (whose change in character is the fundamental hallmark of the transition). The aim of the present chapter is to shed some light on certain universal properties of the vulcanization transition within the framework of the well-controlled and systematically improvable approximation scheme that the RG provides, viz., an expansion about an upper critical dimension that we shall see takes the value six.

Our approach to the vulcanization transition is based on the Landau-Wilson effective Hamiltonian, Eq. (2.7), that describes the energetics of various order-parameter-field configurations, the

order parameter in question having been crafted to detect and diagnose the vulcanization transition. This order parameter and effective Hamiltonian can be derived (along with specific values for the coefficients of the terms in the effective Hamiltonian) via the application of replica statistical mechanics to a specific semi-microscopic model of RCMSs , viz., the Deam-Edwards model [37]; this procedure is described in detail in Ref. [32]. More generally, the form of the minimal model can be determined from the nature of the order parameter, especially its transformation properties and certain symmetries that the effective Hamiltonian need possess, along with the assumptions of the analyticity of the effective Hamiltonian and the continuity of the transition [51]. This system-nonspecific strategy for determining the minimal model was applied in Chap. 2. There, it was shown that by regarding the effective Hamiltonian as a Landau free energy one could recover from it the mean-field description of both the liquid and emergent amorphous solid states known earlier from the analysis of various semi-microscopic models [31, 32, 55, 56]. The mean-field value of order parameter in the solid state encodes a function rather than a number, and it possesses a certain mean-field "universality," by which we mean that (as the transition is approached from the amorphous solid side) both the exponent governing the vanishing of the fraction of constituents localized (i.e. the gel fraction) and the scaled distribution of localization lengths of the localized constituents turn out to depend not on the coefficients in the Landau free energy but only on its qualitative structure. Support for this mean-field picture of the amorphous solid state, in the form of results for the localized fraction and scaled distribution of localization lengths, has emerged from extensive molecular dynamics computer simulations of three-dimensional, off-lattice, interacting, macromolecular systems, due to Barsky and Plischke [60, 68]. In order to provide a unified theory of the vulcanization transition that encompasses the liquid, critical and random solid states, we shall in the present work be adopting this Landau free energy as the appropriate Landau-Wilson effective Hamiltonian.

We shall be focusing on the liquid and critical states, rather than the amorphous solid state, and shall therefore be concerned with the order-parameter correlator rather than its mean value. Along the way, we shall therefore discuss the physical content of this correlator, why it signals the approaching amorphous solid state, and how it gives rise to an associated susceptibility whose divergence marks the vulcanization transition.

Given the apparent precision of the picture of the amorphous solid state resulting from the mean-field approximation [31, 32, 51, 60, 68], the reader may question the wisdom of our embarking on program that seeks to go beyond the mean-field approximation by incorporating the effects of fluctuations. We therefore now pause to explain what has motivated this program.

(i) Below six spatial dimensions, mean-field theory necessarily breaks down sufficiently close to the vulcanization transition. Although, as we shall also see, the region of crosslink densities within which fluctuations play an important role is narrower for dimensions closer to (but below) six and for longer macromolecules, it is by no means necessary for this region to be narrow for shorter macromolecules and for lower-dimensional systems; thus, systems for which the fluctuation-dominated regime is observably wide certainly exist.

(ii) While there have been many successful treatments of critical phenomena beyond the mean-field approximation in systems with quenched randomness, these have, by and large, been for systems in which the emergent order was not of the essentially random type under consideration here or in the spin glass setting [69]. Instead the emergent order has typically been of the type arising in pure systems, albeit perturbed by the quenched disorder. We are motivated here by the challenge of going beyond mean-field theory in the context of a transition to a structurally random state of matter.

(iii) The vulcanization transition has often been addressed from the perspective of percolation theories [70, 14, 10, 6, 8, 26]. While this perspective can be (and certainly has been) taken beyond the mean-field level, it possesses but a *single* ensemble, and therefore does not incorporate the effects of *both* quenched randomness and thermal fluctuations [71]. Given that an essential aspect of the vulcanization transition is the impact of the quenched random constraints on the thermal motion of the constituents, the *a priori* identification of the vulcanization transition with percolation is thus a nontrivial matter. By contrast with the percolation-type of approaches, the analysis given in this chapter applies directly to the vulcanization transition exhibited by thermally fluctuating systems and driven by quenched random constraints. It should therefore shed some light on the relevance of the percolation-type perspective for the vulcanization transition, as we shall discuss in Sec. 3.4.

This chapter is organized as follows. In Sec. 3.2 we discuss the order-parameter correlator and

susceptibility for the vulcanization transition, and examine their physical content. In Sec. 3.3, we embark on the analysis of the vulcanization transition beyond mean-field theory. We begin by examining the self-consistency of mean-field theory by estimating the impact of fluctuations perturbatively, which results in the construction of a Ginzburg criterion and the identification of six as being the appropriate upper critical dimension. We then apply a momentum-shell RG scheme to the minimal model, thus obtaining certain universal critical exponents in an expansion around six dimensions. Finally, in Sec. 3.4 we give some concluding remarks in which we discuss connections between our approach and those based on percolation, and we examine the role played by thermal fluctuations, especially in lower spatial dimensionalities. In three appendices we provide technical details associated with the derivation of the Ginzburg criterion, we investigate the effects of various fields and vertices omitted from the minimal model, and we present the full derivation of the RG flow equations.

3.2 Order-parameter correlator and susceptibility, and their physical significance

Let us now consider the order-parameter correlator and the associated susceptibility from the perspective of incipient random localization [72]. In the simpler context of, e.g., the ferromagnetic Ising transition, the two-point spin-spin correlator quantifies the idea that the externally-imposed alignment of a particular spin would induce appreciable alignment of most spins within roughly one correlation length of that spin, this distance growing as the transition is approached from the paramagnetic state. How are these ideas borne out in the context of the vulcanization transition? Imagine approaching the transition from the liquid side: then the incipient order involves random localization and so, by analogy with the Ising case, the appropriate correlator is the one that addresses the question: Suppose a monomer is localized to within a region of some size by an external agent: Over what region are other monomers likely to respond by becoming localized, and how localized will they be? We can also consider the order-parameter correlator and the associated susceptibility from the perspective of the formation of (mobile, thermally fluctuating) assemblages of macromolecules, which we refer to as clusters: How do they diagnose the development of larger

and larger clusters of connected macromolecules, as the crosslink density is increased towards the vulcanization transition?

Bearing these remarks in mind, we now go back to the semi-microscopic model of the vulcanization transition, and examine in detail the physical interpretation of the microscopic order-parameter correlator $\langle Q(\hat{k})\, Q(-\hat{k})\rangle^{\rm P}_{n+1}$, which is directly related to the order-parameter field correlator $\langle \Omega(\hat{k})\, \Omega(-\hat{k})\rangle^{S}$ via Eq. (1.26). As we shall see, the correlator $\langle Q(\hat{k})\, Q(-\hat{k})\rangle^{\rm P}_{n+1}$ captures the physics of incipient localization and cluster formation. To see this, consider the construction

$$C_{\mathbf{t}}(\mathbf{r}-\mathbf{r}') \equiv \Big[\frac{V}{N}\sum_{j,j'=1}^{N}\int_0^1 ds\int_0^1 ds' \langle \delta^{(d)}(\mathbf{r}-\mathbf{c}_j(s))\,\delta^{(d)}(\mathbf{r}'-\mathbf{c}_{j'}(s'))\,\rangle \times \langle\, \exp -i\mathbf{t}\cdot(\mathbf{c}_j(s)-\mathbf{r})\, \exp i\mathbf{t}\cdot(\mathbf{c}_{j'(s')}-\mathbf{r}')\rangle\Big], \qquad (3.1)$$

which, in addition to depending on the separation $\mathbf{r}-\mathbf{r}'$, depends on the "probe" wave vector $\mathbf{t}$. The first expectation value in this construction accounts for the likelihood that monomers (j,s) and (j',s') will respectively be found around $\mathbf{r}$ and $\mathbf{r}'$; the second describes the correlation between the respective fluctuations of monomer (j,s) about $\mathbf{r}$ and monomer (j',s') about $\mathbf{r}'$.

Now, the quantity $C_{\mathbf{t}}(\mathbf{r}-\mathbf{r}')$ is closely related to an HRS correlator involving the semi-microscopic order parameter $Q(\hat{k})$, defined in Eq. (1.21). To see this, we introduce Fourier representations of the two delta functions and invoke translational invariance, thus establishing that [73]

$$\begin{aligned} C_{\mathbf{t}}(\mathbf{r}-\mathbf{r}') &= \frac{N}{V}\sum_{\mathbf{k}} \mathrm{e}^{i(\mathbf{k}+\mathbf{t})\cdot(\mathbf{r}-\mathbf{r}')}\Big[\frac{1}{N^2}\sum_{j,j'=1}^{N}\int_0^1 ds\, ds'\, \langle \mathrm{e}^{-i\mathbf{k}\cdot(\mathbf{c}_j(s)-\mathbf{c}_{j'}(s'))}\rangle_\chi \langle \mathrm{e}^{-i\mathbf{t}\cdot(\mathbf{c}_j(s)-\mathbf{c}_{j'}(s'))}\rangle_\chi\Big] \\ &= \frac{N}{V}\sum\nolimits_{\mathbf{k}} \mathrm{e}^{i\mathbf{k}\cdot(\mathbf{r}-\mathbf{r}')}\lim_{n\to 0}\langle Q(\mathbf{0},\mathbf{k}-\mathbf{t},\mathbf{t},\mathbf{0},\ldots,\mathbf{0})^*\, Q(\mathbf{0},\mathbf{k}-\mathbf{t},\mathbf{t},\mathbf{0},\ldots,\mathbf{0})\rangle^{\rm P}_{n+1}. \end{aligned} \qquad (3.2)$$

Having seen that $C_{\mathbf{t}}(\mathbf{r}-\mathbf{r}')$ is closely related to an HRS correlator involving $Q(\hat{k})$] which can be computed using the Ω field theory via Eq. (1.26)], we now explain in more detail how $C_{\mathbf{t}}(\mathbf{r}-\mathbf{r}')$ detects the spatial extent of relative localization. First, let us dispense with the case of $\mathbf{t}=\mathbf{0}$. In this case $C_{\mathbf{t}}(\mathbf{r}-\mathbf{r}')$ is simply (V/N times) the real-space density-density correlation function and, as such, is not of central relevance at the amorphous solidification transition. Next, let us consider the small-$\mathbf{t}$ limit of $C_{\mathbf{t}}(\mathbf{r}-\mathbf{r}')$. This quantity addresses the question: If a monomer at $\mathbf{r}$ is localized

"by hand," what is the likelihood that a monomer at $\mathbf{r}'$ responds by being localized at all, no matter how weakly. It is analogous to the correlation function defined in percolation theory that addresses the connectedness of clusters [21].

To substantiate the claim made in the previous paragraph we examine the contribution, in Eq. (3.1), from each pair of monomers to the quantity $C_{\mathbf{t}}(\mathbf{r}-\mathbf{r}')$. Let us start from the simplest situation, in which no crosslinks have been imposed. We assume that $\mathbf{t}$ is small (i.e. $V^{1/3} \gg |\mathbf{t}|^{-1} \gg R_{\rm g}$, where $R_{\rm g}$ is the radius of gyration for a single macromolecule) and that the macromolecular system has only short-range interactions. For each term in the double summation over monomers there are two cases to consider, depending on whether or not the pair of monomers are on the same macromolecule. For a generic pair of monomers that are on the same macromolecule (i.e. $j = j'$), we expect that $\langle \exp i\mathbf{t}\cdot(\mathbf{c}_j(s)-\mathbf{c}_j(s'))\rangle \sim 1$, and that (for $|\mathbf{r}-\mathbf{r}'| \lesssim R_{\rm g}$) $\langle \delta^{(d)}(\mathbf{r}-\mathbf{c}_j(s))\, \delta^{(d)}(\mathbf{r}'-\mathbf{c}_j(s'))\rangle \sim V^{-1}\, R_{\rm g}^{-d}$. Then the total contribution to $C_{\mathbf{t}}(\mathbf{r}-\mathbf{r}')$ coming from pairs of monomers on the same macromolecule is of order $R_{\rm g}^{-d}$. On the other hand, for a generic pair of monomers that are on different macromolecules (i.e. $j \neq j'$), we expect that $\langle \exp i\mathbf{t}\cdot(\mathbf{c}_j(s)-\mathbf{c}_{j'}(s'))\rangle \sim V^{-1}$, and that $\langle \delta^{(d)}(\mathbf{r}-\mathbf{c}_j(s))\, \delta^{(d)}(\mathbf{r}'-\mathbf{c}_{j'}(s'))\rangle \sim V^{-2}$. Therefore the total contribution to $C_{\mathbf{t}}(\mathbf{r}-\mathbf{r}')$ coming from pairs of monomers on different macromolecules is of order $(N/V)V^{-1}$. Thus, we find that the intra-chain (i.e. $j = j'$) contribution to $C_{\mathbf{t}}(\mathbf{r}-\mathbf{r}')$ dominates over the inter-chain (i.e. $j \neq j'$) contribution in the thermodynamic limit.

Moving on to the physically relevant case, in which crosslinks have been introduced so as to form clusters of macromolecules, we see that what were the intra-chain and inter-chain contributions become intra-cluster and inter-cluster contributions. With the appropriate (slight) changes, the previous analysis holds, which indicates that the intra-cluster contribution dominates $C_{\mathbf{t}}(\mathbf{r}-\mathbf{r}')$ in the thermodynamic limit. In other words, in the small-$\mathbf{t}$ limit a pair of monomers located at $\mathbf{r}$ and $\mathbf{r}'$ contribute unity to $C_{\mathbf{t}}(\mathbf{r}-\mathbf{r}')$ if they are on the same cluster and zero otherwise. This view allows us to identify the small-$\mathbf{t}$ limit of $C_{\mathbf{t}}(\mathbf{r}-\mathbf{r}')$ with the pair-connectedness function defined in (the on-lattice version of) percolation theory [21].

What about $C_{\mathbf{t}}(\mathbf{r}-\mathbf{r}')$ in the case of general $\mathbf{t}$? In this case it addresses the question: If a monomer near $\mathbf{r}$ is localized on the scale t^{-1} (or more strongly), how likely is a monomer near $\mathbf{r}'$ to be localized on the same scale (or more strongly)? This additional domain of physical issues

associated with the strength of localization results from the effects of thermal fluctuations, and is present in the vulcanization picture but not the percolation one.

Let us illustrate the significance of $C_{\mathbf{t}}(\mathbf{r}-\mathbf{r}')$ by computing it in the setting of the Gaussian approximation to the liquid state in three dimensions. To do this, we use Eq. (1.26) to express $C_{\mathbf{t}}(\mathbf{r}-\mathbf{r}')$ in terms of the (Gaussian approximation to the) correlator $\langle \Omega(\hat{k})\, \Omega(\hat{k}') \rangle^{\mathcal{S}}$, which has the Ornstein-Zernicke form given in Eq. (3.8). Thus, we arrive at the real-space Yukawa form

$$|C_{\mathbf{t}}(\mathbf{r}-\mathbf{r}')| \;\propto\; \frac{\exp\left(-|\mathbf{r}-\mathbf{r}'|/\zeta_{\text{eff}}(t)\right)}{|\mathbf{r}-\mathbf{r}'|}, \tag{3.3}$$

$$\frac{1}{\zeta_{\text{eff}}^2(t)} \;\equiv\; \frac{1}{\zeta^2} + bt^2, \tag{3.4}$$

where the correlation length ζ is defined by $\zeta^{-2} \equiv -2a\tau$. Hence, we see the appearance of a probe-wavelength–dependent correlation length $\zeta_{\text{eff}}(t)$. The physical interpretation is as follows: in the $\mathbf{t} \to \mathbf{0}$ limit, $C_{\mathbf{t}}(\mathbf{r}-\mathbf{r}')$ is testing for relative localization, regardless of the strength of that localization and, consequently, the range of the correlator diverges at the vulcanization transition. This reflects the incipience of an infinite cluster, due to which very distant macromolecules can be relatively localized. By contrast, for generic $\mathbf{t}$ it is relative localization on a scale t^{-1} (or smaller) that is being tested for. At sufficiently large separations, even if a pair of macromolecules are relatively localized, this relative localization is so weak that the pair does not contribute to $C_{\mathbf{t}}(\mathbf{r}-\mathbf{r}')$. This picture is reflected by the fact that $\zeta_{\text{eff}}(t)$ remains finite at the transition.

Given that we have identified a correlator that is becoming long-ranged at the transition, it is natural to seek an associated divergent susceptibility $\Theta_{\mathbf{t}}$. To do this, we integrate $C_{\mathbf{t}}(\mathbf{r}-\mathbf{r}')$ over space and obtain

$$\Theta_{\mathbf{t}} \equiv \int \frac{d^d r\, d^d r'}{V}\, C_{\mathbf{t}}(\mathbf{r}-\mathbf{r}') = N \lim_{n\to 0} \langle Q(\mathbf{0},\mathbf{t},-\mathbf{t},\mathbf{0},\ldots,\mathbf{0})^*\, Q(\mathbf{0},\mathbf{t},-\mathbf{t},\mathbf{0},\ldots,\mathbf{0}) \rangle_{n+1}^{\text{P}}\,. \tag{3.5}$$

Passing to the $\mathbf{t} \to \mathbf{0}$ limit, we have

$$\lim_{\mathbf{t}\to\mathbf{0}} \Theta_{\mathbf{t}} \sim (-\tau)^{-\gamma}, \tag{3.6}$$

where the final asymptotic equality is obtained from a computation of the (field-theoretic) correlator $\langle \Omega(\hat{k})\, \Omega(\hat{k}') \rangle^{\mathcal{S}}$ [see Eq. (1.26)]. This quantity is measure of the spatial extent over which pairs of

monomers are relatively localized, no matter how weakly, and thus diverges at the vulcanization transition. At the Gaussian level of approximation, Eq. (3.8), this susceptibility diverges with the classical exponent $\gamma = 1$. By contrast, for generic $\mathbf{t}$ the susceptibility $\Theta_{\mathbf{t}}$ remains finite at the transition, even though an infinite cluster is emerging, due to the suppression of contributions to $\Theta_{\mathbf{t}}$ from pairs of monomers whose relative localization is sufficiently weak (i.e. those that lead to the divergence in the small-$\mathbf{t}$ limit).

3.3 Vulcanization transition beyond mean-field theory

3.3.1 Gaussian correlator: Liquid and critical states

Before embarking on the investigation the critical properties of the vulcanization transition beyond mean-field theory, in the present section, we introduce the Gaussian propagator and prescribe the scaling form for the two-point correlation function near the vulcanization transition. The incipient amorphous solidification, as the vulcanization transition is approached from the liquid side, is marked by strong order-parameter fluctuations, which are diagnosed via the correlator $G(\hat{k})$ defined through

$$N^{-1} \, \delta^{(n+1)d}_{\hat{k}+\hat{k}',\hat{0}} \, G(\hat{k}) \equiv \langle \Omega(\hat{k}) \, \Omega(\hat{k}') \rangle^{\mathcal{S}} \ . \tag{3.7}$$

The unusual factor of $1/N$ is due to our choice of the normalization of $Q(\hat{k})$ in Eq. (1.21). In Sec. 3.2, we have explained the physical content of this correlator and precisely how, via Eq. (1.26), it is able to detect incipient random solidification. The value of the correlator in the mean-field approximation follows from the quadratic terms in Eq. (2.7) and is given by

$$G(\hat{k}) \approx G_0(\hat{k}) \equiv \frac{1}{-2a\tau + b|\hat{k}|^2} \ , \tag{3.8}$$

which below will play the role of the bare propagator. Notice that $G_0(\hat{k})$ obeys the homogeneity relation

$$G(\hat{k}, \tau) \sim |\hat{k}|^{-2+\eta} \, g(|\hat{k}| \, |\tau|^{-\nu}), \tag{3.9}$$

in which $g(x) \sim x^{2-\eta}$ for $x \to +0$, and approaches a constant value for large x. Moreover, the exponents take on the mean-field values $\eta = 0$, $\nu = 1/2$ and $\gamma = \nu(2-\eta) = 1$, this last relationship

guaranteeing that the susceptibility $\lim_{\hat{k}\to\hat{0}} G(\hat{k},\tau)$ diverges as $|\tau|^{-\gamma}$.

3.3.2 Ginzburg criterion for the vulcanization transition

To begin the process of analyzing the vulcanization transition beyond the mean-field (i.e. tree) level, we estimate the width $\delta\tau$ of reduced constraint-densities τ within which the effects of order-parameter fluctuations about the saddle-point value cannot be treated as weak, i.e., we construct the Ginzburg criterion. To do this, we follow the conventional strategy (see, e.g., Ref. [74]) of computing a loop expansion for the two-point vertex function to one-loop order and examining its low-wave-vector limit (i.e. the inverse susceptibility). Note that in the present setting the loop expansion amounts to an expansion in the inverse monomer density. Our starting point is the

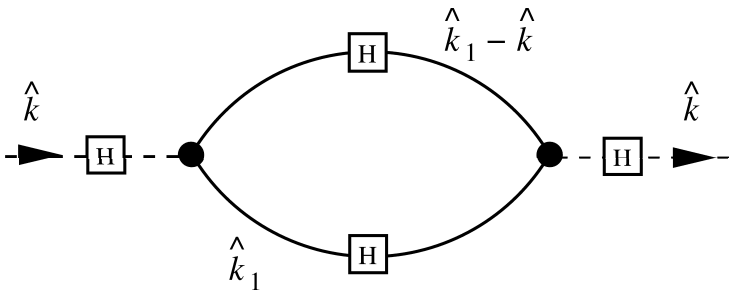

Figure 3.1: One-loop correction to the two-point vertex function. Full lines indicate bare HRS correlators; dashed lines indicate amputated external bare HRS correlators.

minimal model, Eq. (2.7), for which the bare correlator is given by Eq. (3.8). Then the one-loop correction to the two-point vertex function comes from the diagram shown in Fig. 3.1, which is calculated in App. A. We obtain for the inverse susceptibility Ξ^{-1} the result [75]

$$(N\Xi)^{-1} = -2a\tau + 18g^2\frac{V}{N}\int\frac{d^dp}{(-2a\tau + bp^2)^2} \ , \tag{3.10}$$

in which a large wave-vector cut-off at $|\hat{k}| = \Lambda$ is implied. The (one-loop) shifted critical point τ_c marks the vanishing of Ξ^{-1}, i.e., solves

$$0 = -2a\tau_c + 18g^2\frac{V}{N}\int\frac{d^dp}{(-2a\tau_c + bp^2)^2} \ . \tag{3.11}$$

Now, in mean-field theory the transition occurs at $\tau = 0$, with positive (resp. negative) values corresponding to the amorphous solid (resp. liquid) states. From Eq. (3.11) we see that that inclusion of fluctuations enlarges the region of crosslink densities in which liquid state is stable, as one would expect on general physical grounds. However, it is worth noting that without the exclusion of the one-replica sector the converse would occur (i.e. fluctuations would enlarge the region of stability of the amorphous solid state). By subtracting Eq. (3.11) from Eq. (3.10) in the standard way, replacing τ_c by its mean-field value (of zero) in the loop correction, and rescaling the integration variable p^2 according to $bp^2 = -2a\tau k^2$, we arrive at

$$(N\Xi)^{-1} = -2a(\tau - \tau_c)\left(1 - 18g^2(V/N)b^{-d/2}(-2a\tau)^{(d-6)/2}J_d\right), \tag{3.12}$$

where J_d is a dimensionless number dependent on d (and weakly on Λ, at least in regime of interest, i.e., d below 6). Equation (3.12) shows that for $d < 6$ a fluctuation dominated-regime is inevitable for sufficient small τ, and hence that the upper critical dimension for the vulcanization transition is six, in agreement with naïve power-counting arguments applied to the $n \to 0$ limit of the cubic field theory, Eq. (2.7). The Ginzburg criterion amounts to determining the departure of τ from its critical value such that in Eq. (3.12) the one-loop correction is comparable in magnitude to the mean-field level result.

To determine the physical content of the Ginzburg criterion, we invoke the values of the coefficients of the minimal model appropriate for the semi-microscopic model of RCMSs, Eqs. (2.8-2.11), and we exchange the macromolecule density N/V for the volume fraction $\varphi \equiv (N/V)(L/\ell)\ell^d$. Thus we arrive at the following form of the Ginzburg criterion: for $d < 6$, fluctuations cannot be neglected for values of μ^2 satisfying

$$\left|\frac{\mu^2 - \mu_c^2}{\mu_c^2}\right| \lesssim (L/\ell)^{-\frac{d-2}{6-d}}\left(\varphi/g^2\right)^{-\frac{2}{6-d}}, \tag{3.13}$$

from which we see that the fluctuation-dominated regime is narrower for longer macromolecules and higher densities (for $2 < d < 6$). In three dimensions, the width of the critical region goes as $(L/\ell)^{-1/3}$. Such dependence on the degree of polymerization L/ℓ is precisely that argued for long ago by de Gennes on the basis of a percolation-theory picture [50].

Besides the fields and vertices featuring in the minimal model, there are other symmetry-

allowed fields and vertices that are generated by the semi-microscopic theory of RCMSs. Examples are provided by the 1RS field, which describes density fluctuations, along with vertices of cubic, quartic or higher-order that couple the 1RS field to the HRS field. In App. A.2 we investigate the effect of these fields and vertices, which are omitted from the minimal model, and show: (i) that the inclusion of their effects (at the one-loop level) does not change the Ginzburg criterion derived in the present section; and (ii) that the HRS critical fluctuations do not provide any singular contributions to the 1RS density-density correlation function (at least to one-loop order).

3.3.3 Renormalization-group procedure and its subtleties

We now describe the RG procedure that we are using, a schematic depiction of which is given in Fig. 3.2. The main thrust of our approach is the standard "momentum-shell" RG, via which we aim to determine how the parameters of the theory (viz. τ and g) flow under the two RG steps of coarse-graining and rescaling. However, in the present context there are some significant subtleties owing to the need to constrain the fields to lie in the HRS.

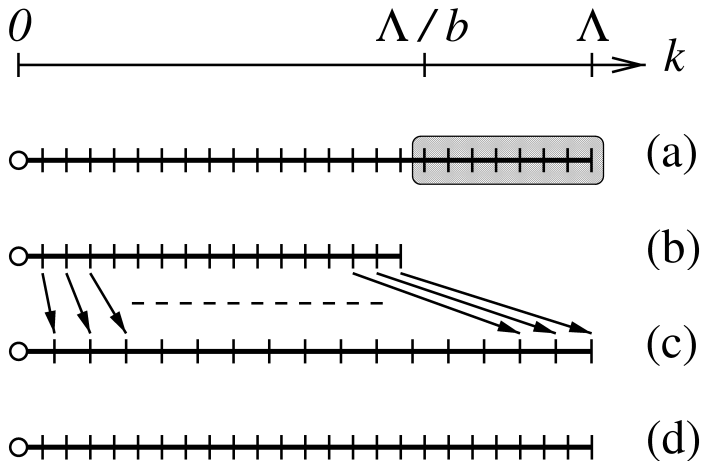

Figure 3.2: Schematic one-dimensional depiction of the basic steps of the RG procedure (the field variables are defined only at the hash marks denoting the quantized wave vectors): from (a) to (b) integrate out the fields at the quantized wave vectors k in the "momentum shell" (shaded); from (b) to (c) rescale lengths to restore the wave-vector cut-off, and rescale the field to restore the gradient term; from (c) to (d) restore the density of the degrees of freedom. (In practice, we employ a momentum shell of infinitesimal width.)

In the coarse-graining step, we integrate out the rapidly-varying components of $\Omega(\hat{k})$ (i.e. those

corresponding to wave vectors satisfying $\Lambda/b < |\hat{k}| < \Lambda$). Here, the constraint that only the HRS field is a critical field demands that one treat the HRS and the 1RS distinctly. We handle this by working with a large but finite (replicated) system contained in a hyper-cubic box of volume V^{n+1} on which periodic boundary conditions are applied. As a consequence, the wave vectors are "quantized," and therefore we can directly make the appropriate subtractions associated with the removal of the zero- and one-replica sectors. Having made the necessary subtractions, we compute the various Feynman diagrams (for the construction of the Ginzburg criterion and the coarse-graining step of the RG) by passing to the continuous wave-vector limit (so that wave-vector summations become integrations).

The replica technique has the following curious feature. In the infinite-volume limit the different sectors are spaces of different dimensionalities, and thus the contributions from the lower replica sectors appear to be sets of measure zero relative to the contributions from the HRS. However, in the replica limit, the contributions from different sectors are comparable and, hence, the lower sectors cannot be neglected.

The coarse-graining step is followed by the rescaling step, in which the aim is to return the theory to its original form. The field- and length-rescaling aspects of this step (to recover the original wave-vector cut-off and form of the gradient term) are standard, but there is a subtlety associated with the fact that the original theory is defined on a finite volume (in order that the wave vectors be quantized and the various replica sectors thereby be readily identifiable). This subtlety is that upon coarse-graining and rescaling one arrives at a theory that is *almost* of the original form, but is defined on a coarser lattice of quantized wave vectors associated with the reduced (real-space) volume. If we wish to return the theory to its truly original form, we are required to increase the density of the coarsened wave-vector lattice. To accomplish this, we choose to make use of the extension to $(n+1)d$ dimensions of the following one-dimensional relation, exact in the thermodynamic (i.e. large real-space size B) limit:

$$\sum_{k \in \{2\pi n b/B\}} f(k) \approx b^{-1} \sum_{k \in \{2\pi n/B\}} f(k). \tag{3.14}$$

One way to understand this is to regard the two sides of Eq. (3.14) as providing different discrete

approximations to the same continuous-wave-vector (i.e. infinite-volume) limit. Thus, we expect the difference between them to be unimportant in the thermodynamic limit. Another way is to regard the right hand side of Eq. (3.14) as pertaining to a system with a larger number of degrees of freedom than the left hand side, but that the factor b^{-1} appropriately diminishes the weight of each degree of freedom. It would be equally satisfactory if we chose, in our RG scheme, *not* to restore the wave-vector lattice spacing, which would amount to our using the left-hand-side of Eq. (3.14).

3.3.4 Expansion around six dimensions

In Secs 3.3.2 and 3.3.3 we have established that the upper critical dimension for the vulcanization transition is six, and we have described an RG procedure capable of elucidating certain universal features of the transition. We now examine the RG flow equations near the upper critical dimension that emerge from this procedure, and discuss the resulting fixed-point structure and universal critical exponents. To streamline the presentation we have relegated the technical details of the derivation of the flow equations to App. B.

Flow equations

As with the mean-field theory and the Ginzburg criterion, our starting point is the replicated cubic field theory, Eq. (2.7). By suitably redefining the scales of $\Omega(\hat{k})$ and $\hat{k}$ we can absorb the coefficients a and b, hence arriving at the Landau-Wilson effective Hamiltonian

$$\mathcal{S}(\{\Omega\}) = N \sum_{\hat{k}\in \mathrm{HRS}} \Big(-\tau + \frac{1}{2}|\hat{k}|^2 \Big) |\Omega(\hat{k})|^2 - Ng \sum_{\hat{k}_1,\hat{k}_2,\hat{k}_3\in \mathrm{HRS}} \Omega(\hat{k}_1)\,\Omega(\hat{k}_2)\,\Omega(\hat{k}_3)\,\delta_{\hat{k}_1+\hat{k}_2+\hat{k}_3,\hat{0}}\,, \quad (3.15)$$

in which all wave-vector summations are cut off beyond replicated wave vectors of large magnitude Λ, from which we can read off the bare correlator

$$G_0(\hat{k}) = \frac{1}{-2\tau + |\hat{k}|^2}\ . \quad (3.16)$$

We shall be working to one-loop order and, correspondingly, the diagrams that contribute to the renormalization of the parameters of the Landau-Wilson effective Hamiltonian are those depicted

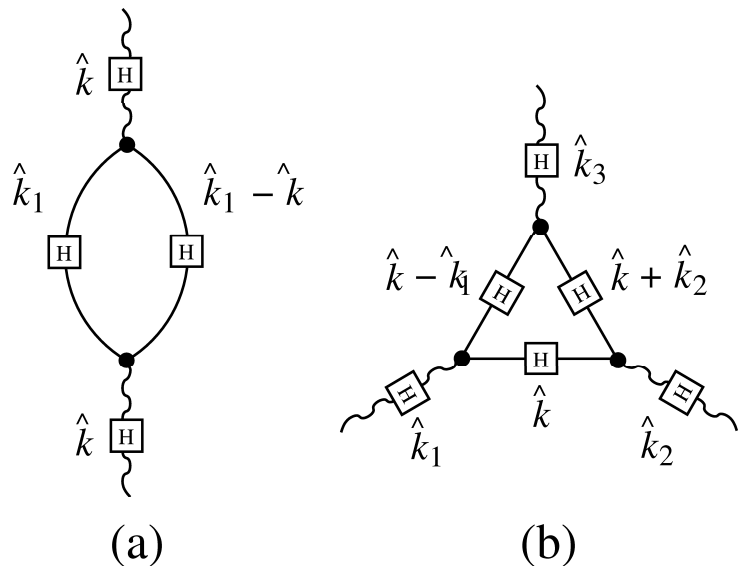

Figure 3.3: Contributing one-loop diagrams. Full lines indicate bare HRS correlators for short-wavelength fields (i.e. fields lying in the momentum shell); wavy lines indicate long-wavelength fields.

in Figs. 3.3 (a) and 3.3 (b). The resulting flow equations are

$$\frac{d\tau}{d\ln b} = 2\,\tau - C_0\,g^2 - C_0'\,\tau\,g^2 - C_1\,\tau\,g^2 + \mathcal{O}(\tau^2 g^2, \tau\varepsilon g^2, \varepsilon g^2, g^4), \tag{3.17}$$

$$\frac{dg}{d\ln b} = g\left(\frac{\varepsilon}{2} - C_3 g^2 - \frac{3}{2}C_1 g^2 + \mathcal{O}(\tau g^2, \varepsilon g^2, g^4)\right), \tag{3.18}$$

$$\frac{dz}{d\ln b} = \frac{1}{2}(d + 2 - C_1 g^2) + \mathcal{O}(\tau g^2, \varepsilon g^2, g^4), \tag{3.19}$$

where $\varepsilon \equiv 6 - d$, b is the length-rescaling factor, z is the field-rescaling factor, and the (constant) coefficients in the flow equations are given by

$$(C_0, C_0', C_1, C_3) = \frac{V}{N}\frac{S_6}{(2\pi)^6}\,(9\Lambda^2, 36, -6, 72), \tag{3.20}$$

in which S_6 is the surface area of a 6-dimensional sphere of unit radius.

Fixed-point analysis and its consequences

We proceed in the standard way by first finding the fixed points (τ_*, g_*) of the flow equations, at which $d(\tau, g)/d\ln b = (0,0)$. We linearize the flow equations about each of the resulting fixed points,

$$\frac{d}{d\ln b}\begin{pmatrix}\tau-\tau_*\\ g-g_*\end{pmatrix} \approx \begin{pmatrix}2-(C_0'+C_1)g_*^2 & -2C_0\,g_*\\ 0 & \frac{1}{2}\varepsilon - 3(C_3+\frac{3}{2}C_1)g_*^2\end{pmatrix}\begin{pmatrix}\tau-\tau_*\\ g-g_*\end{pmatrix}, \tag{3.21}$$

where we have dropped higher-order corrections. We then establish the RG eigenvalues at each fixed point by finding the eigenvalues of the linearized RG transformation matrices. Finally, we solve Eq. (3.21) to obtain the flow near each fixed point.

For ε both negative and positive (i.e. for d both above and below six) we find a *Gaussian* fixed point (GFP): $(\tau_*, g_*) = (0,0)$. Solving Eq. (3.21) about this fixed point gives the flow

$$\begin{pmatrix}\tau(b)\\ g(b)\end{pmatrix} \approx \begin{pmatrix}\tau(1)\,b^{y_1}\\ g(1)\,b^{y_2}\end{pmatrix}, \tag{3.22}$$

with the RG eigenvalues y_1 and y_2 respectively given by $y_\tau = 2$ and $y_g = \varepsilon/2$.

As one can see from Eq. (3.22), above six dimensions (i.e. for $\varepsilon < 0$) the GFP is unstable in the τ direction and stable in the g direction. However, below six dimensions the GFP also becomes unstable in the g direction, and a new fixed point—the Wilson-Fisher fixed point (WFFP)—emerges, located at $(\tau_*, g_*^2) = \big((\Lambda^2/28), (1/126)((2\pi)^6/S_6)(V/N)^{-1}\big)\,\varepsilon$. (Let us mention, in passing, that if we had not correctly implemented the constraint that wave-vector summations exclude contributions for the 1RS then the structure of the flow equations would have been utterly different; e.g., the WFFP would have occurred at a complex value of g.) By solving Eq. (3.21) for the WFFP we find the flow

$$\begin{pmatrix}\tau(b)-\tau_*\\ g(b)-g_*\end{pmatrix} \approx \begin{pmatrix}(\tau(1)-\tau_*)-A(g(1)-g_*)\\ 0\end{pmatrix} b^{y_1} + \begin{pmatrix}A(g(1)-g_*)\\ g(1)-g_*\end{pmatrix} b^{y_2}, \tag{3.23}$$

where $A \equiv (3/\sqrt{14})((V/N)(S_6/(2\pi)^6))^{1/2}(\Lambda^2\varepsilon^{1/2})$ and the RG eigenvalues are given by $y_1 = 2 - (5\varepsilon/21)$ and $y_2 = -\varepsilon$.

We now proceed to obtain the critical exponents for physical quantities from the RG eigenvalues at each fixed point. The homogeneity relation for the correlator $G(\hat{k})$, following from a standard

RG analysis [76], reads

$$G(\hat{k},\tau) = z^2\, b^{-d}\, G(b\hat{k}, b^{y_1}\tau). \tag{3.24}$$

We eliminate b by choosing $b|\hat{k}| = 1$; then comparison with Eq. (3.9) leads to $\nu = 1/y_1$ and $\eta = C_1 g_*^2$. Thus, for the GFP we have

$$\nu^{-1} = 2, \qquad \eta = 0, \tag{3.25}$$

and for the WFFP we have, to first order in ε,

$$\nu^{-1} = 2 - (5\varepsilon/21), \qquad \eta = -\varepsilon/21. \tag{3.26}$$

Both above and below six dimensions, the critical exponents ν and η (and β, to be discussed below) are identical to those governing analogous quantities in percolation theory at first order in ε, as computed via the Potts field theory [77]. We discuss the significance of this result and the relationship between the present approach and percolation/gelation-based approaches in Sec. 3.4.

We have focused on the cubic interaction in the vulcanization field theory. There are, of course, additional symmetry-allowed interactions, such as the quartic interaction. Near to six dimensions, however, the fact that such interactions are irrelevant at the GFP can be shown by naïve power-counting arguments, which hold in the replica limit (and remain uncompromised at the WFFP, owing to its proximity to the GFP).

3.3.5 Scaling for gel fraction and wave-vector-dependent order parameter

In order to relate properties of the amorphous solid state to those computed in the liquid and critical states, we now follow the standard scaling analysis. To do this, we add to the minimal model, Eq. (3.15), a source field that couples linearly to the order parameter: $-N \sum_{\hat{k}\in \mathrm{HRS}} \Omega(\hat{k})\, U(-\hat{k})$. We assume that U contains only long wavelength components, so that it does not couple to any field featuring in any momentum-shell integrations. Then the renormalization of $U(-\hat{k})$ comes only from the rescalings of $\hat{k}$ and $\Omega(\hat{k})$, and thus we have

$$U'(\hat{k}') = z\, b^{-d}\, U(\hat{k}). \tag{3.27}$$

To obtain the exponent β, which describes the scaling of the gel fraction q, the conventional method prescribes the application of a *uniform* source field. In the present theory, the (zero replica sector) field variable $\Omega(\hat{0})$, which would couple to such a uniform source, is excluded, and instead we choose $U(\hat{k}) = h\,\delta_{\hat{k}+\hat{k}_0,\hat{0}}$, where $\hat{k}_0$ lives in the HRS but is otherwise arbitrarily small. (This prescription is consistent with the notion that the gel fraction follows from the long-wavelength limit of the order parameter, the limit being taken via wave vectors in the HRS.) Hence we arrive the recursion relation for h:

$$h' = z\,h = b^{y_h}; \qquad y_h = (d+2-\eta)/2. \tag{3.28}$$

As we are already in possession of η at the GFP and the WFFP, we thus arrive at the scaling dimension y_h of the source field h.

Having obtained y_h, we now use it, together with y_τ, y_g and the singular part of the free energy density f, to determine β, in the following way. According to homogeneity, f has the form

$$f(\tau, g, h) = b^{-d} f(\tau b^{y_\tau}, g b^{y_g}, h b^{y_h}). \tag{3.29}$$

By taking the derivative with respect to h so as to form the order-parameter equation of state, choosing $h = 0$, and passing to the small $\hat{k}_0$ limit, one finds the following scaling behavior of the gel fraction:

$$q(\tau, g, 0) \sim \lim_{\hat{k}_0 \to \hat{0}} \partial f/\partial h|_{h=0} \sim b^{-d+y_h}\, M(\tau b^{y_\tau}, g b^{y_g}, 0) = \tau^{(d-y_h)/y_\tau} M(1, g\tau^{-y_g/y_\tau}, 0). \tag{3.30}$$

Let us first consider the regime $d > 6$, for which the appropriate fixed point is the GFP and, therefore one expects the exponents to take on their classical values. Now, as one can see from the mean-field value for the order parameter $\overline{\Omega}$ (and thus the gel fraction q), Eqs. (2.13) and (2.16), both of which are proportional to g^{-1}, the cubic interaction is dangerously irrelevant at the GFP, and thus one has

$$M(1, g, 0) \sim \frac{1}{g}, \quad \text{for} \quad g \to +0. \tag{3.31}$$

Hence, near the GFP one has

$$q(\tau, g, 0) \sim \tau^{\beta}, \quad \text{for} \quad g \to +0, \tag{3.32}$$

$$\beta = \frac{d - y_h}{y_\tau} + \frac{y_g}{y_\tau} = \frac{d - \frac{d+2}{2} + \frac{6-d}{2}}{2} = 1, \tag{3.33}$$

which is precisely the mean-field value of the exponent β given in Sec. 2.3.

Now let us turn to the regime $d < 6$, for which the exponents are nonclassical. The appropriate fixed point is now the WFFP, at which the cubic interaction is irrelevant but not dangerously so. Thus, in this regime one has the standard scaling relation

$$\beta = \frac{d - y_h}{y_\tau} = 1 - (\varepsilon/7), \tag{3.34}$$

where the second equality holds only to order ε.

In fact, under the (not unreasonable) assumption that there is only one characteristic length-scale in the ordered state (i.e. that the fluctuation correlation length does not provide a length-scale independent from the localization length-scale), we can go beyond the establishing of the scaling of the gel fraction (i.e. the long-wavelength limit of the order parameter) and propose a more general scaling hypothesis, which incorporates the scaling of the (singular part of the) wave-vector-dependent order parameter [78]. This takes the form of the scaling hypothesis:

$$\langle \Omega(\hat{k}) \rangle^{S} \propto \tau^{\beta}\, w(\hat{k}^2 \tau^{-2\nu}). \tag{3.35}$$

The quantity τ^{ν}, which plays the role of the fluctuation correlation length in the liquid state, is here seen to play the role of the characteristic scale for the localization lengths in the ordered state. Presumably, it also governs the scale over which (amplitude-type) fluctuations are correlated in the solid state. Let us note that the mean-field result for the order parameter not only obeys this scaling relation (with $\beta = 2\nu = 1$) but also provides an explicit form for the function w.

3.4 Concluding remarks: Connections with other approaches and the role of thermal fluctuations

Having constructed an RG theory for the liquid and critical states of vulcanized matter, we now examine the results of this RG theory and discuss the relationship between these results and the results of other approaches to the vulcanization transition. As we have seen in Sec. 3.3.4, via an expansion around six spatial dimensions our minimal model for the vulcanization transition yields values for certain critical exponents that characterize the behavior of the system near to and at the transition. These exponents turn out to be numerically equal to those characterizing physically analogous quantities in percolation theory, to first order in the departure ε from six dimensions (see Chap. 4 for further results that is valid to all orders in ε).

This equality between exponents seems reasonable in view of the intimate relationship between percolation theory and the *connectivity* of the system of crosslinked macromolecules, this connectivity pertaining to the *statistics* of systems formed according to the Deam-Edwards distribution of quenched randomness (and hence to the statistical mechanics of the uncrosslinked macromolecular liquid) [79]. Indeed, a connection between the percolation transition and the vulcanization transition already shows up at the level of mean-field theory: the dependence of the gel fraction q on the crosslink-density control parameter μ^2 obtained via the semi-microscopic approach (in the case of RCMSs), viz., that q obeys

$$1 - q = \exp\left(-\mu^2 q\right), \tag{3.36}$$

is identical to the mean-field–percolation dependence of the fraction of sites participating in the infinite cluster, obtained by Erdős and Rényi in their work on random graphs [80], this identity holding not just near the transition, where the dependence of q on $\mu^2 - \mu_c^2$ is linear, but for all crosslink densities. Moreover, the mean-field result emerging from the minimal model of the vulcanization transition yields this linear dependence (but cannot, of course, be applied beyond the transition regime). The relevance of percolation theory to the vulcanization transition also manifests itself beyond the mean-field level in the physical *meaning* of the order-parameter correlator, as we have discussed in Sec. 3.2. This connection has long been realized, and supports the use of percolative approaches as models of certain aspects of the vulcanization transition [70, 14, 10, 6, 8,

26].

In addition to direct applications of percolation theory [70, 14, 10, 6, 8] to the vulcanization transition, mentioned in the preceding paragraph, an approach has been developed by Lubensky and Isaacson [26] in which a correspondence is established between the statistics of branched, polydisperse, macromolecules and a multi-component field theory. This field theory reduces to the one-state limit of the Potts model under circumstances appropriate for the gelation/vulcanization transition.

An essential ingredient of the approaches discussed in the previous paragraph is the Potts model in its one-state limit—a representation of percolation [17, 18]. It is therefore worth considering similarities and differences between the minimal field theory of the vulcanization transition, Eq. (2.7), and the minimal field theory for the Potts model, Eq. (1.9). To facilitate comparison, we write the minimal field theory for the Potts model in a slightly different notation, i.e.,

$$\int_V d^d x \Big(\sum_{\alpha=1}^{n} \Big(\frac{1}{2} r\, \psi_\alpha^2 + \frac{1}{2} |\nabla \psi_\alpha|^2 \Big) - w^{(3)} \sum_{\alpha,\beta,\gamma=1}^{n} \lambda^{(3)}_{\alpha\beta\gamma}\, \psi_\alpha\, \psi_\beta\, \psi_\gamma \Big). \tag{3.37}$$

As discussed Sec. 1.4.3, the percolation transition can be mapped into the $n \to 0$ limit of this cubic n-component field theory.

How does this Potts field theory compare the vulcanization field theory that we have been analyzing in the present chapter? The Potts field theory has, a cubic interaction, as does the vulcanization field theory, and therefore its upper critical dimension is also six. If we examine the RG analysis of the Potts field theory (in an expansion around six dimensions) [23] we see that, at the one-loop level, diagrams identical in form (i.e. those shown in Fig. 3.3) enter the renormalization of the various vertices. (In fact, this is true to all order of loops, see Chap. 4 and App. C for details.) Moreover, in the $n \to 0$ limit the RG flow equations for the two theories turn out to be identical. This striking result is connected to the following observations:

(i) In Potts case, aside from the d-dimensional integrals corresponding to the diagrams, the coefficients in the flow equations are determined by the contractions of Potts-tensor $\lambda^{(3)}_{\alpha\beta\gamma}$ associated with each cubic vertex, these contractions being the origin of the n-dependence of the coefficients in the flow equations.

(ii) In the vulcanization case, the diagrams intrinsically correspond to $(n+1)d$-dimensional integrals but, due to the constraints on the summations over wave vectors, these diagrams produce $(n+1)d$-dimensional integrals (which smoothly reduces to d-dimensional integrals in the $n \to 0$ limit), together with d-dimensional integrals; see Eqs. (A.2,B.17).
(iii) Despite the explicit differences in the forms of the two theories, it turns out that, in the $n \to 0$ limit, the integrals and the combinatorics conspire to produce precisely the same flow equations. In some delicate way, which we do not fully understand, the constraints on the wave-vector summations in the vulcanization theory play a similar role to the field-index contractions in the Potts theory.

Having discussed the similarities of the Potts and vulcanization approaches, let us now catalogue the many distinctions between them:
(i) The Potts field theory has a multiplet of n real fields on d-dimensional space; the vulcanization field theory has a real singlet field living on $(n+1)$-fold replicated d-dimensional space.
(ii) The Potts field theory represents a setting involving a *single* ensemble [71], the ensemble of percolation configurations, whereas the vulcanization field theory describes a physical problem in which *two* distinct ensembles (thermal and disorder) play essential roles. As such, the vulcanization field theory is capable of providing a unified theory not only of the transition but also of the structure, correlations and (e.g. elastic) response of the emerging amorphous solid state. This is already manifested at the mean-field level, inasmuch as the vulcanization field theory presents an order parameter that is far richer in its physical content that the one presented by the Potts model.
(iii) The entire symmetry structures possessed by the percolation and vulcanization field theories are quite different. The Potts field theory has translational and rotational invariance (in unreplicated space), along with the discrete symmetry of $(n+1)$-fold permutations of the field components. The vulcanization field theory has the symmetries of the independent translations and rotations of the $(n+1)$ replicas of space, along with the discrete symmetry of $(n+1)$-fold permutations amongst the replicas.
(iv) The nature of the spontaneous symmetry breaking at the percolation and vulcanization phase transitions is distinct. The percolation transition (in its Potts representation) involves the spontaneous breaking of the ($n \to 0$ limit) of a *discrete* $(n+1)$-fold permutation symmetry. By contrast,

the vulcanization transition involves the spontaneous breaking of the ($n \to 0$ limit of the) *continuous* symmetry of relative translations and rotations of the $n+1$ replicas; the permutation symmetry remains intact in the amorphous solid state, as does the symmetry of common translations and rotations of replicated space. Thus, the vulcanization transition is associated with the appearance of low-energy, long-wavelength, Goldstone-type excitations [49], which we expect to lead to the restoration of the broken continuous symmetry in and below a lower critical dimension of two. By contrast, fluctuations destroy the percolation transition only at and below the lower critical dimension of unity.

While there are these apparent distinctions between the percolation and vulcanization approaches, especially in low dimensions, there is also evidence in favor of some sort of sharp correspondence between the physics of percolation and vulcanization coming from the computation of critical exponents near the upper critical dimension. This apparent dichotomy can, however, be reconciled if we carefully delineate between three logically distinct physical properties pertaining to RCMSs and other randomly constrained systems:

(i) Macroscopic network formation (by which we mean that constraints are present in sufficient density to connect a nonzero fraction of the constituents into a giant random molecule);

(ii) Random localization (by which we mean the change in thermal motion of a nonzero fraction of the constituents from wandering throughout the container to fluctuating only over finite distances from their random mean positions); and

(iii) The acquisition of rigidity (by which we mean the emergence of a nonzero static shear modulus).

Within mean-field theory (and hence above six spatial dimensions), these three properties go hand in hand, emerging simultaneously at the phase transition. At and below six dimensions they appear to continue to go hand in hand (although, strictly speaking, we have not yet investigated the issue of the acquisition of rigidity beyond mean-field theory) until one reaches two dimensions where we believe this broad picture will change (as we shall discuss shortly). Thus, it appears that, within the limited sphere of issues concerning amorphous solidification that percolation-based approaches are capable of addressing, such approaches do not lead one astray. In other words, the superposition of thermal fluctuations on the positions of the constituents of the macroscopic network that emerges

as the constraint density is increased towards the phase transition does not lead to any changes in the critical exponents governing percolation-type quantities: disorder fluctuations appear to play a more important role than do thermal fluctuations, as far as the percolative aspects of the critical phenomenon are concerned.

This brings up the interesting issue of the nature of the vulcanization transition and its relationship with the percolation transition as the dimensionality of space is reduced to the neighborhood of two spatial dimensions, two being the lower critical dimension of the vulcanization transition. (The ideas reported in this paragraph result from an ongoing collaboration with H. E. Castillo [82].) Indeed, the case of two dimensions is especially fascinating in view of the fact that there is a conventional percolation transition in two dimensions, whereas the thermal fluctuations are expected to be sufficiently prominent to destabilize the amorphous solid phase, in which case the macroscopic network formation no longer occurs simultaneously with the random localization of constituents of the network. It is tempting to speculate [82] that in two dimensions an anomalous type of vulcanization transition (not accompanied by true localization) continues to happen simultaneously with percolation transition. As the constraint density is tuned from below to above criticality, the amorphous solidification order parameter would remain zero, whereas the order-parameter correlations would change from decaying exponentially to decaying algebraically with distance. One might say that (constraint-density controlled) cluster fragmentation (rather than the thermal excitation of lattice defects, as in regular two-dimensional melting) would be mediating the melting transition. If this scenario should happen to be borne out then, at sufficiently high crosslink densities one would have a quasi-amorphous solid state—the random analogue of a two-dimensional solid [83]—exhibiting quasi-long-range positional order but of a random rather than regular type.

Chapter 4

Connecting the vulcanization transition to percolation: Renormalization-group analysis to all orders in $6 - d$

4.1 Introduction and overview

In Chap. 3 we employed the momentum-shell RG scheme to investigate the critical properties of the vulcanization transition to the first order in $6 - d$ [52], and found the critical exponents, at this order, to be the same as those governing physically analogous quantities in the percolation transition. In addition, we discussed the intimate relationship (which has long been anticipated on physical grounds [84, 8, 26]) between the vulcanization transition and the percolation transition, via a discussion of mean-field results, a detailed analysis of the physical significance of the vulcanization order-parameter correlator and a comparison of the field-theoretic formulations of the vulcanization transition and the percolation transition. The next step, naturally, is to go beyond first order in ε, and to seek a definite conclusion as to whether the vulcanization transition and the percolation transition belong to the same universality class. The present chapter aims to answer this question. In doing so, we first carry on the RG analysis of the vulcanization transition to second order in ε, by using a field-theoretic RG method instead of the momentum-shell method; the latter would become very awkward if used beyond first-order RG analysis. As shown in App. C, we find that the critical exponents turn out to be the same as those of percolation transition, not just to order ε, but also

to order ε^2. Then, motivated by the ε^2 RG results, we develop an all-orders perturbative approach, which, in essence, constructs a mapping between the relevant operators in the vulcanization field theory and those in the percolation field theory, to relate the critical properties of the vulcanization transition and the percolation transition. We shall focus on this all-orders approach in the present chapter, and relegate the second-order RG calculation to App. C.

The central result of this chapter is the explicit reduction of certain basic critical properties of the vulcanization transition to equivalent basic critical properties of the percolation transition. As we shall see, this reduction can be accomplished via an exact diagrammatic analysis of the complete perturbative expansion of the appropriate vertex functions of the vulcanization transition. These are shown to furnish, in the replica limit, precisely the field-theoretic formulation of the percolation transition due to Houghton, Reeve and Wallace [25]. Hence, we establish that the critical properties of the vulcanization transition and the percolation transition are identical, not just to first order but to all orders in the departure of the spatial dimension d from the upper critical dimension.

It is worth observing that the vulcanization transition and the percolation transition do, nevertheless, represent distinct physical phenomena. This is exemplified, e.g., by the amorphous solid state that emerges at the vulcanization transition, which does not have an evident counterpart in percolation transition. Another point of distinction is revealed by the role of fluctuations in low-dimensional systems, which are expected to have qualitatively different impacts on the states emerging at the vulcanization transition and the percolation transition [85]. Yet another point of distinction concerns the nature of the degrees of freedom involved in the description of the vulcanization transition and the percolation transition. The former arises in systems having both quenched and equilibrating randomness, whereas the latter takes place in systems involving just one type of randomness (typically taken to be the quenched randomness); see Ref. [85].

We note that Janssen and Stenull [62] have arrived at, inter alia, essentially the same results as those contained in the present chapter via a related approach, conducted independently of and simultaneously with the present work.

4.2 Demonstrating the equivalence of the critical properties of the vulcanization and percolation transitions

Our analysis is based upon the minimal model of the vulcanization transition, Eq. (4.1), introduced in Chap. 3

$$\mathcal{S}(\Omega) = \frac{1}{V^{n+1}} \frac{1}{2} \sum_{\hat{k} \in \mathrm{HRS}} \left(r_0 + |\hat{k}|^2 \right) |\Omega(\hat{k})|^2 + \frac{1}{V^{2(n+1)}} \frac{g}{3!} \sum_{\hat{k}_1, \hat{k}_2, \hat{k}_3 \in \mathrm{HRS}} \Omega(\hat{k}_1)\, \Omega(\hat{k}_2)\, \Omega(\hat{k}_3)\, \delta_{\hat{k}_1 + \hat{k}_2 + \hat{k}_3, \hat{0}} \ , \tag{4.1}$$

To ease comparison with the HRW field theory of the percolation transition, the coefficients and fields featuring in $\mathcal{S}$ are not defined exactly as they have been in the preceding chapters [86].

4.2.1 Overall strategy

We now explain the strategy that we shall use to relate the vulcanization transition and the percolation transition. We shall focus on the replica limit of the long-wave-length behavior of the two- and three-point vertex functions, $\Gamma_n^{(2)}(\hat{k})$ and $\Gamma_n^{(3)}(\hat{k}_1, \hat{k}_2)$ in the vulcanization field theory. The physical significance $\Gamma_n^{(2)}(\hat{k})$ as a probe of connectedness has been elucidated in Sec. 3.2 [52]. Now, the symmetry of the vulcanization field theory dictates that the only suitably invariant term quadratic in the wave vector $\hat{k}$ is $\hat{k} \cdot \hat{k}$ (recall that $\hat{k} \cdot \hat{k} \equiv \hat{k}^2 \equiv \mathbf{k}^0 \cdot \mathbf{k}^0 + \mathbf{k}^1 \cdot \mathbf{k}^1 + \cdots + \mathbf{k}^n \cdot \mathbf{k}^n$). Thus, in a long-wave-length expansion for $\Gamma_n^{(2)}(\hat{k})$, we have

$$\Gamma_n^{(2)}(\hat{k}) = \Gamma_n^{(2)}(\hat{0}) + \frac{1}{(n+1)d} \sum_{\alpha=0}^{n} \left(\frac{\partial}{\partial \mathbf{k}^\alpha} \cdot \frac{\partial}{\partial \mathbf{k}^\alpha} \right) \Gamma_n^{(2)}(\hat{k}) \Big|_{\hat{k}=\hat{0}} \hat{k} \cdot \hat{k} + \cdots \tag{4.2}$$

$$= A_n + B_n \hat{k} \cdot \hat{k} + \cdots \ . \tag{4.3}$$

As the upper critical dimension for the vulcanization transition is six, and this is the dimension about which one may imagine expanding, general renormalizability considerations demand that just these two vertex functions ($\Gamma_n^{(2)}$ and $\Gamma_n^{(3)}$) contain the primitive divergences, and do so via the constants A_n, B_n and $C_n \equiv \Gamma_n^{(3)}(\hat{0}, \hat{0})$ (see Ref. [87]).

Having identified the quantities central to a renormalization-group analysis of the vulcanization

transition, we shall establish that these quantities are identical, in the replica limit, to the corresponding quantities in percolation theory, more specifically, the one-state ($Q \to 1$) limit of Potts field theory, the Hamiltonian of which is shown in EQ. (1.9). To do this we shall make use of a convenient representation of the critical properties of percolation theory, viz., the HRW field theory representation [25]. So that we know what we need to make contact with, we write down the HRW Landau-Wilson Hamiltonian, Eq. (1.11), again,

$$\mathcal{H} = \int d^d x \left\{ \frac{1}{2}(\nabla\phi)^2 - \frac{1}{2}(\nabla\psi)^2 + \frac{1}{2} r_0(\phi^2 - \psi^2) + \frac{g}{3!}(\phi + \psi)^3 \right\} . \tag{4.4}$$

Here ϕ is an ordinary field but ψ is a ghost field, both of which residing in d-dimensional space. As HRW [25] have shown, provided one enforces the rule that *only graphs that are connected by ϕ-lines are included* (an example of this rule is given in Sec. 1.4.3, Fig. 1.6) , the two- and three-point ϕ vertex functions are identical (order by order in perturbation theory in the coupling constant g) to those of the one-state (i.e. percolation) limit of the Potts model.

Our strategy for demonstrating the equivalence of the critical properties of the vulcanization and percolation transitions is as follows. Consider the standard Feynman diagram expansion for the two- and three-point vertex functions of the vulcanization field theory in powers of the coupling constant g in the Hamiltonian (4.1).

(i) To deal with the constraint that the internal wave vectors in the resulting diagrams reside in the HRS, we relax this constraint on summations over internal wave vectors but compensate for this by making appropriate subtractions of terms.

(ii) Next, we observe that all diagrams for the two- and three-point vertex functions can be organized into two categories: those in which there is at least one route between every pair of external points via propagators having unconstrained wave vectors (which we call *freely-connected diagrams*); and the remaining diagrams, in which there is at least one pair of external points between which no paths exist consisting solely of propagators having unconstrained wave vectors (which we call *freely-unconnected diagrams*). Having made this categorization, we show that the appropriate version of wave-vector conservation renders the freely-unconnected diagrams negligible in the thermodynamic limit, leaving us with a representation that is already reminiscent of the HRW approach.

(iii) At this stage we have reduced the construction of the two- and three-point vertex functions

to the computation of freely-connected diagrams only. Next, via a straightforward combinatorial analysis, we show that, in the replica limit, only a small class of diagrams survive.
(iv) Finally, we explain how, again in the replica limit, the values of the remaining diagrams are precisely those occurring in the HRW prescription for percolation.
We now set about implementing this strategy.

4.2.2 Relaxing the constraint to higher replica sector wave vectors

In the vulcanization field theory the internal wave vectors occurring in the Feynman diagrams are constrained to lie in the HRS. In order to perform summations over these wave vectors, it is convenient to work with the continuum of wave vectors (i.e. to take the thermodynamic limit) rather than the discrete lattice of them. In order to be able to take this limit, we re-express summations over HRS wave vectors in terms of unconstrained summations over $(n+1)d$-dimensional wave vectors, together with further unconstrained summations over d-dimensional wave vectors (and certain trivial additional terms). In what follows, we use $\{\hat{e}^\alpha\}_{\alpha=0}^n$ as the collection of unit vectors in replicated wave-vector space, so that, e.g., a generic vector $\hat{p}$ can be expressed as $\sum_{\alpha=0}^n \mathbf{p}^\alpha \hat{e}^\alpha$. We note that for a generic function $F(\hat{k})$ we have

$$\begin{aligned}
\sum_{\hat{k}\in\mathrm{HRS}} F(\hat{k}) &= \sum_{\hat{k}} \left(1 - \Big(\sum_{\alpha=0}^{n}\sum_{\mathbf{q}\neq\mathbf{0}} \delta_{\hat{k},\mathbf{q}\hat{e}^\alpha}\Big) - \delta_{\hat{k},\hat{0}}\right) F(\hat{k}) && (4.5)\\
&= \sum_{\hat{k}} \left(1 - \Big(\sum_{\alpha=0}^{n}\sum_{\mathbf{q}} \delta_{\hat{k},\mathbf{q}\hat{e}^\alpha}\Big) + n\delta_{\hat{k},\hat{0}}\right) F(\hat{k}) && (4.6)\\
&= \sum_{\hat{k}} F(\hat{k}) - \sum_{\alpha=0}^{n}\sum_{\mathbf{q}^\alpha} F(\mathbf{0},\ldots,\mathbf{0},\mathbf{q}^\alpha,\mathbf{0},\ldots) + nF(\hat{0}), && (4.7)
\end{aligned}$$

which effects the re-expression of the summations just described. Note that, as it always comes with the factor n, the $\delta_{\hat{k},\hat{0}}$ term will vanish in the replica limit, and can therefore be safely ignored. We shall refer to the wave vectors included in the term $\sum_\alpha \sum_{\mathbf{q}}$ as *lower replica sector* (LRS) wave vectors. Via these steps one can relax a constrained summation over HRS wave vectors, instead freely summing over all replicated wave vectors, provided one compensates by augmenting the

summand with the factor

$$1 - \sum_{\alpha=0}^{n} \sum_{\mathbf{q}} \delta_{\hat{k},\mathbf{q}\hat{e}^{\alpha}} \ . \tag{4.8}$$

How does this constraint relaxation manifest itself in the setting of Feynman diagram computations? One simply augments every internal propagator $V^{n+1}G_0(\hat{k})$ with a factor (4.8):

$$G_0(\hat{k}) \equiv \frac{1}{r_0 + |\hat{k}|^2} \quad \longrightarrow \quad \frac{1 - \sum_{\alpha} \sum_{\mathbf{q}} \delta_{\hat{k},\mathbf{q}\hat{e}^{\alpha}}}{r_0 + |\hat{k}|^2} \tag{4.9}$$

$$= \quad \frac{1}{r_0 + |\hat{k}|^2} - \frac{1}{r_0 + |\hat{k}|^2} \sum_{\alpha=0}^{n} \sum_{\mathbf{q}} \delta_{\hat{k},\mathbf{q}\hat{e}^{\alpha}} . \tag{4.10}$$

How this decomposition is expressed diagrammatically is shown in Fig. 4.1.

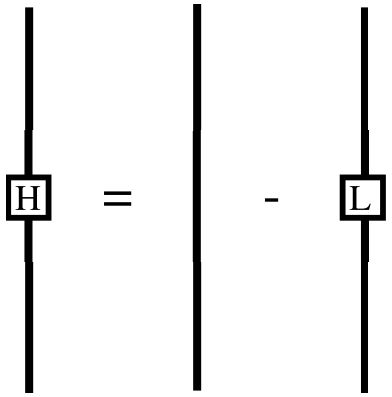

Figure 4.1: Decomposition of an HRS propagator (indicated by H) into an unconstrained propagator (the unadorned line), less an LRS propagator (indicated by L).

In this manner, each HRS internal line in an original Feynman diagram can be decomposed into an unconstrained internal line, less an LRS internal line. Thus, the various vertex functions can be expressed in terms of Feynman diagrams composed of unconstrained lines together with LRS internal lines. Note, for future reference, that physically meaningful vertex functions have external wave vectors in the HRS.

We illustrate this decomposition for the case of a simple diagram in Fig. 4.2. More generally, we arrive at the following modified Feynman rules for the vulcanization field theory:

(i) Write down all diagrams arising from the original theory. In these diagrams all wave vectors are constrained to the HRS.

(ii) Replace each diagram with the collection of diagrams obtained by allowing each internal line to carry either an unconstrained replicated wave vector or a LRS wave vector. (Thus, an original diagram with L internal lines spawns a total of 2^L diagrams.) Identically-valued diagrams can be represented by a single diagram, together with a suitable combinatorial factor (see, e.g., the factor of 2 in Fig 4.2).

(iii) Provide a factor of -1 for each LRS internal line.

From now on, when we say Feynman diagrams we mean those composed of unconstrained inner lines together with LRS internal lines. At this stage we observe that the combinatorics of our diagrammatic expansion coincides with those of the HRW expansion, provided one identifies the internal unconstrained and LRS lines of the vulcanization theory with, respectively, the corresponding internal ϕ- and ψ-lines of the HRW representation.

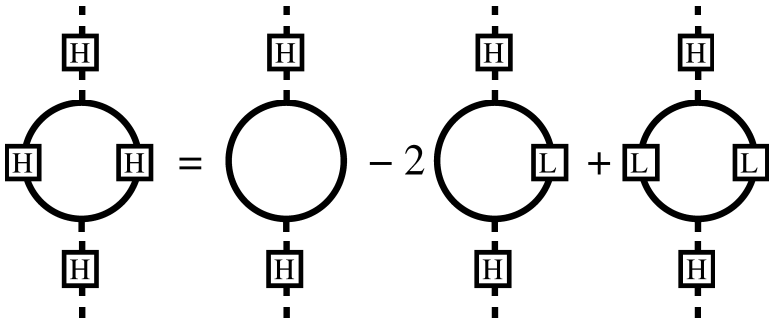

Figure 4.2: Decomposition of the one-loop diagram for the two-point vertex function. On the right-hand side of this equation, the first and second diagrams are freely-connected diagrams, and the third is a freely-unconnected diagram. Dashed lines denote amputated external HRS bare propagators.

We have, however, yet to show that the diagrams removed by hand in HRW can be safely omitted from the vulcanization field theory, and that the numerical values of the (replica limits of) the vulcanization diagrams are identical to those of the HRW diagrams. We shall establish these facts in the following subsections.

4.2.3 Elimination of freely-unconnected diagrams

We remind the reader that in the HRW theory for the two- and three-point ϕ-field (i.e. the physical) vertex functions, one is instructed to remove, by hand, those diagrams in which there is at least one

pair of external points between which no paths exist consisting solely of ϕ-field propagators. The corresponding diagrams in the vulcanization theory are those in which there is at least one pair of external points between which no paths exist consisting solely of propagators having unconstrained wave vectors, i.e., freely-unconnected diagrams. We now show that these freely-unconnected diagrams of the vulcanization theory automatically vanish in the thermodynamic limit.

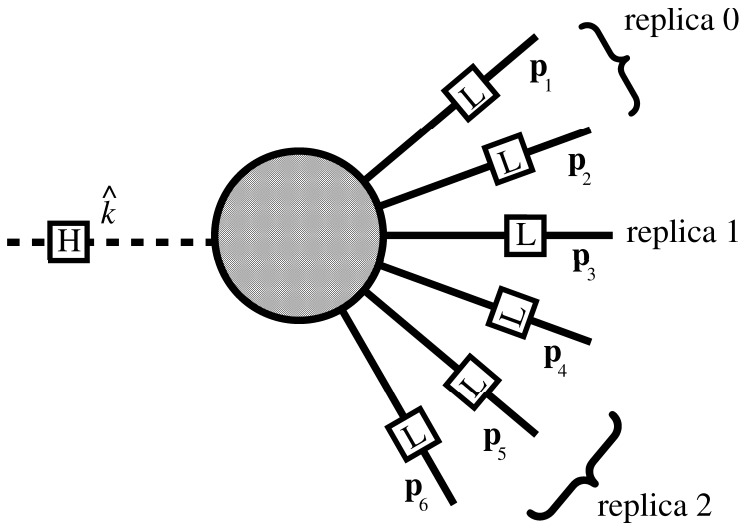

Figure 4.3: Schematic illustration of a piece of a diagram in the vulcanization field theory obtained by cutting LRS lines in a freely-unconnected diagram. Note that the wave vector $\hat{k}$ flowing through the external point lies in the HRS. The shaded circle represents any way to connect the exhibited lines using the cubic interaction vertex, unconstrained propagators and LRS propagators.

To do this, consider a generic vulcanization theory diagram for the two- or three-point vertex functions. Observe that freely-unconnected diagrams have the following property: as there exists a pair of external points not connected by a path of unconstrained internal lines, there must exist at least one scheme of cutting solely LRS internal lines that causes the diagram to separate into disconnected pieces with the external points shared amongst the pieces. As we are considering only two- and three-point vertex functions, at least one of these pieces involves only a single HRS external point, along with a number of cut LRS lines. A schematic illustration of such a piece is shown in Fig. 4.3.

Let us examine the consequences of applying wave-vector conservation to this piece, noting that the wave vector $\hat{k}$ flowing in through the external point must lie in the HRS, whereas the wave

vectors flowing out through the remaining (i.e. cut) lines lie in the LRS. Now, according to the vulcanization field theory, wave-vector conservation requires that the incoming HRS wave vector $\hat{k}$ be equal, replica by replica, to the sum of the outgoing ($m = 2, 3, \ldots$) LRS wave vectors flowing in a given replica, i.e., that

$$\mathbf{k}^{\alpha} = \sum_{j=1}^{m} \delta^{\alpha,\alpha_j} \mathbf{p}_j \ , \quad (\text{for } \alpha = 0, 1, 2, \ldots, n) \tag{4.11}$$

where $\alpha_1, \alpha_2, \ldots$ indicate the replicas through which wave vectors $\mathbf{p}_1, \mathbf{p}_2, \ldots$ flow. As a consequence, because the incoming wave vector lies in the HRS, the outgoing LRS wave vectors must flow out through more than one replica. This is the key observation, as the following example, depicted in Fig. 4.3 reveals. Here, there are six outgoing LRS lines, two with wave vectors flowing in replica 0, one with wave vector flowing in replica 1, and three with wave vectors flowing in replica 2. For replica 0, wave-vector conservation reads $\mathbf{k}^0 = \mathbf{p}_1 + \mathbf{p}_2$, so that, e.g., $\mathbf{p}_1$ determines $\mathbf{p}_2$. Similarly, for replica 1, wave-vector conservation reads $\mathbf{k}^1 = \mathbf{p}_3$, so that $\mathbf{p}_3$ is determined. More generally, as this special case exemplifies, the number of independent outgoing LRS wave vectors is reduced by at least *two* (rather than the *one* that total wave-vector conservation demands) simply because of the fact that the outgoing LRS wave vectors must flow out through more than one replica. This, in turn, means that in the uncut diagram there are fewer independent wave vectors to be summed over than the number of loop wave vectors suggested by simple topological counting. As a result, additional denominators of V^{n+1} remain, even after the summation over independent wave vectors in the uncut diagram are replaced by their thermodynamic-limit integrals, which renders the corresponding freely-unconnected diagram negligible.

As a concrete example of the foregoing argument, we compute the third diagram on the right-hand side of the equation depicted in Fig. 4.2. In this diagram, both of the internal lines lie in the LRS, and the diagram does not (by simple wave-vector conservation) contribute unless the external wave vector $\hat{k}$ has nonzero d-vector components in precisely in two replicas (e.g. replicas one and two). In this case, the diagram makes the contribution

$$2V^{n+1}\, G_0(\mathbf{k}^1)\, V^{n+1} G_0(\mathbf{k}^2)\, \left(g\, V^{-2(n+1)}\right)^2 = 2g^2\, V^{-2(n+1)}\, G_0(\mathbf{k}^1)\, G_0(\mathbf{k}^2) \ . \tag{4.12}$$

The coefficient 2 comes from the two ways of distributing the external wave vector on the two internal lines. On the right-hand side, one denominator of V^{n+1} will combine with the Kronecker δ-function to maintain overall wave-vector conservation (via a Dirac δ-function in the thermodynamic limit); the other V^{n+1} denominator (which, in usual cases, would combine with the summation over a loop wave vector to produce an integral) makes this diagram vanish. This special case exemplifies the general emergence, in the setting of the vulcanization transition, of the central aspect of the HRW formulation, viz., the removal of the ϕ-unconnected diagrams.

4.2.4 Replica sums and their decomposition in the replica limit

Now that we have demonstrated that only the freely-connected vulcanization field theory diagrams contribute, we make a closer examination of these diagrams for the relevant cases of the two- and three-point vertex functions. We begin by noting that each diagram exhibits the full symmetry of the vulcanization field theory, viz., invariance under separate d-dimensional rotations in each replica and permutations of the replicas. Therefore, the small-wave-vector expansion of $\Gamma_n^{(2)}(\hat{k})$ given in Eq. (4.3) remains valid, diagram by diagram.

Now, the computation of any contributing diagram involves summations over a number of independent LRS (but otherwise unconstrained) wave vectors, as well as summations over the replicas through which these wave vectors flow. These latter summations over replicas can be decomposed as follows:

$$\sum_{\alpha_1,\alpha_2,\ldots,\alpha_l} F_{\alpha_1,\alpha_2,\ldots,\alpha_l} = \left(\sum_{\substack{\alpha_1,\alpha_2,\ldots,\alpha_l \\ \text{all equal}}} + \sum_{\substack{\alpha_1,\alpha_2,\ldots,\alpha_l \\ \text{two distinct}}} + \sum_{\substack{\alpha_1,\alpha_2,\ldots,\alpha_l \\ \text{three distinct}}} + \cdots \sum_{\substack{\alpha_1,\alpha_2,\ldots,\alpha_l \\ \text{all distinct}}} \right) F_{\alpha_1,\alpha_2,\ldots,\alpha_l}, \qquad (4.13)$$

where $F_{\alpha_1,\alpha_2,\ldots,\alpha_l}$ is a generic function of the l replica indices. Said equivalently, the summation can be decomposed into: terms in which all wave vectors flow through a common replica; those in which the wave vectors flow through two distinct replicas; etc.

Now let us make use of this decomposition. For A_n and C_n in Eq. (4.3) the external wave vector is zero [87], and therefore the summand $F_{\alpha_1,\alpha_2,\ldots,\alpha_l}$ is invariant under permutations of the replicas [88]. Thus, in the first term of the decomposition, F is constant [i.e. independent of the (common) value of the replica arguments], and hence this term contributes $(n+1)F_{0,0,\ldots,0}$. In

the replica limit, this becomes $F_{0,0,\ldots,0}$. As for the second term, let us further decompose it into partitionings of the set of replica indices into two subsets, the replica indices in each subset having a common value. In each such partitioning F is constant, and thus each partitioning contributes $(n+1)nF$, which vanishes in the replica limit. By continuing with this decomposition tactic via tri-partitioning, tetra-partitioning, etc., we establish that all of the terms on the right-hand side of Eq. (4.13) except the first vanish in the replica limit.

We next consider the coefficient B_n. As mentioned above, symmetry considerations dictate that each diagram contributing to the two-point vertex function has the small-wave-vector expansion

$$A_n^{(\mathrm{dia})} + B_n^{(\mathrm{dia})} \hat{k} \cdot \hat{k} + \cdots , \tag{4.14}$$

where $A_n^{(\mathrm{dia})}$ and $B_n^{(\mathrm{dia})}$ are the contributions to A_n and B_n from the diagram in question. We exploit the (larger than mandated) $(n+1)d$-dimensional rotational invariance of the terms retained in this small-wave-vector expansion by choosing $\hat{k}$ to be rotated into a single replica: $\{\mathbf{k}, \mathbf{0}, \ldots, \mathbf{0}\}$. (Although it has, until this stage, been vital to ensure that $\hat{k}$ lies in the HRS, e.g., in order to eliminate the freely-unconnected diagrams, one is now at liberty to ignore this requirement.) Repeating the tactic just used for the analysis of A_n and C_n, with the slight elaboration needed to accommodate the fact that the (suitably rotated) external wave vector $\{\mathbf{k}, \mathbf{0}, \ldots, \mathbf{0}\}$ breaks the permutation symmetry group from $\mathcal{P}_{n+1}$ down to $\mathcal{P}_n$. In this way, we see that the only contributions that survive the replica limit are from the *all-equal* partition and, furthermore, from the case in which all of the independent LRS wave vectors lie in replica zero.

Let us look at the diagram shown in Fig. 4.4 to exemplify the arguments above. Its contribution to the two-point vertex function is

$$V^{-3(n+1)} \sum_{\alpha,\beta} \sum_{\mathbf{p},\mathbf{q}} G_0(\mathbf{p})\, G_0(\mathbf{q})\, G_0(\mathbf{p}\hat{e}^\alpha + \mathbf{q}\hat{e}^\beta)^2\, G_0(\hat{k} + \mathbf{p}\hat{e}^\alpha + \mathbf{q}\hat{e}^\beta) \ . \tag{4.15}$$

For this diagram,

$$V^{3(n+1)} A_n \quad = \quad \sum_{\alpha,\beta} \sum_{\mathbf{p},\mathbf{q}} G_0(\mathbf{p})\, G_0(\mathbf{q})\, G_0(\mathbf{p}\hat{e}^\alpha + \mathbf{q}\hat{e}^\beta)^3$$

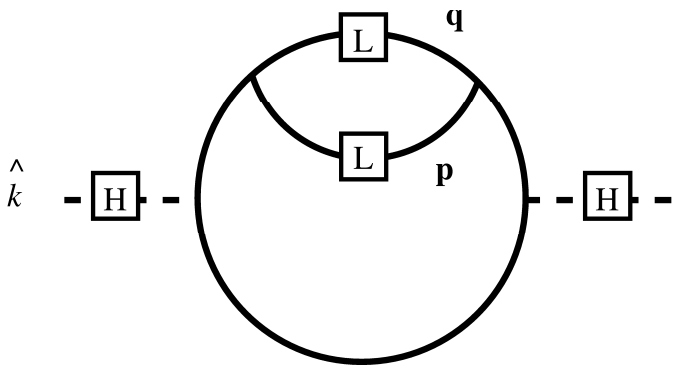

Figure 4.4: A two-loop diagram for the exemplification of replica decomposition. This diagram that has two internal LRS lines.

$$
\begin{aligned}
&= \sum_{\mathbf{p},\mathbf{q}} G_0(\mathbf{p})\, G_0(\mathbf{q}) \left(\sum_{\alpha} G_0(\mathbf{p}\hat{e}^{\alpha} + \mathbf{q}\hat{e}^{\alpha})^3 + \sum_{\substack{\alpha,\beta \\ (\alpha\neq\beta)}} G_0(\mathbf{p}\hat{e}^{\alpha} + \mathbf{q}\hat{e}^{\beta})^3 \right) \\
&= \sum_{\mathbf{p},\mathbf{q}} G_0(\mathbf{p})\, G_0(\mathbf{q}) \Big((n+1) G_0(\mathbf{p}\hat{e}^{0} + \mathbf{q}\hat{e}^{0})^3 + (n+1) n G_0(\mathbf{p}\hat{e}^{0} + \mathbf{q}\hat{e}^{1})^3 \Big) \\
&\xrightarrow{n\to 0} \sum_{\mathbf{p},\mathbf{q}} G_0(\mathbf{p})\, G_0(\mathbf{q})\, G_0(\mathbf{p}\hat{e}^{0} + \mathbf{q}\hat{e}^{0})^3 \ . \qquad (4.16)
\end{aligned}
$$

On the other hand, the contribution from this diagram to B_n is the coeffcient of the quadratic term of an expansion in $\hat{k}$ of Eq. (4.15). As we have argued on symmetry grounds, rotating the external wave vector $\hat{k}$ does not affect the extraction of this coefficient. By choosing $\hat{k} = \mathbf{k}\hat{e}^{0}$, Expression (4.15) becomes,

$$
\begin{aligned}
& V^{-3(n+1)} \sum_{\mathbf{p},\mathbf{q}} \sum_{\alpha,\beta} G_0(\mathbf{p})\, G_0(\mathbf{q})\, G_0(\mathbf{p}\hat{e}^{\alpha} + \mathbf{q}\hat{e}^{\beta})^2\, G_0(\mathbf{k}\hat{e}^{0} + \mathbf{p}\hat{e}^{\alpha} + \mathbf{q}\hat{e}^{\beta}) \\
&\quad = V^{-3(n+1)} \sum_{\mathbf{p},\mathbf{q}} G_0(\mathbf{p})\, G_0(\mathbf{q}) \Big(G_0(\mathbf{p}\hat{e}^{0} + \mathbf{q}\hat{e}^{0})^2\, G_0(\mathbf{k}\hat{e}^{0} + \mathbf{p}\hat{e}^{0} + \mathbf{q}\hat{e}^{0}) \\
&\qquad\quad + \sum_{\alpha(\neq 0)} G_0(\mathbf{p}\hat{e}^{\alpha} + \mathbf{q}\hat{e}^{\alpha})^2\, G_0(\mathbf{k}\hat{e}^{0} + \mathbf{p}\hat{e}^{\alpha} + \mathbf{q}\hat{e}^{\alpha}) \\
&\qquad\quad + 2 \sum_{\substack{\alpha \\ (\alpha\neq\beta,\beta=0)}} G_0(\mathbf{p}\hat{e}^{\alpha} + \mathbf{q}\hat{e}^{0})^2\, G_0(\mathbf{k}\hat{e}^{0} + \mathbf{p}\hat{e}^{\alpha} + \mathbf{q}\hat{e}^{0}) \\
&\qquad\quad + \sum_{\substack{\alpha,\beta \\ (\alpha\neq\beta,\alpha\neq 0,\beta\neq 0)}} G_0(\mathbf{p}\hat{e}^{\alpha} + \mathbf{q}\hat{e}^{\beta})^2\, G_0(\mathbf{k}\hat{e}^{0} + \mathbf{p}\hat{e}^{\alpha} + \mathbf{q}\hat{e}^{\beta}) \Big) \\
&\quad = V^{-3(n+1)} \sum_{\mathbf{p},\mathbf{q}} G_0(\mathbf{p})\, G_0(\mathbf{q}) \Big(G_0(\mathbf{p}\hat{e}^{0} + \mathbf{q}\hat{e}^{0})^2\, G_0(\mathbf{k}\hat{e}^{0} + \mathbf{p}\hat{e}^{0} + \mathbf{q}\hat{e}^{0})
\end{aligned}
$$

$$
\begin{aligned}
&+ nG_0(\mathbf{p}\hat{e}^{\alpha} + \mathbf{q}\hat{e}^{\alpha})^2\, G_0(\mathbf{k}\hat{e}^0 + \mathbf{p}\hat{e}^1 + \mathbf{q}\hat{e}^1) \\
&+ 2nG_0(\mathbf{p}\hat{e}^1 + \mathbf{q}\hat{e}^0)^2\, G_0(\mathbf{k}\hat{e}^0 + \mathbf{p}\hat{e}^1 + \mathbf{q}\hat{e}^0) \\
&+ n(n-1)G_0(\mathbf{p}\hat{e}^1 + \mathbf{q}\hat{e}^2)^2\, G_0(\mathbf{k}\hat{e}^0 + \mathbf{p}\hat{e}^1 + \mathbf{q}\hat{e}^2)\Big) \\
\stackrel{n\to 0}{\longrightarrow}\; & V^{-3} \sum_{\mathbf{p},\mathbf{q}} G_0(\mathbf{p})\, G_0(\mathbf{q})\, G_0(\mathbf{p}\hat{\mathbf{e}}^{\mathbf{0}} + \mathbf{q}\hat{e}^0)^2\, G_0(\mathbf{k}\hat{e}^0 + \mathbf{p}\hat{e}^0 + \mathbf{q}\hat{e}^0)\ . \qquad (4.17)
\end{aligned}
$$

The result exhibited in Eq. (4.17) demonstrates the arguments given above for B_n, the last line showing that the contribution from this diagram to B_n can be extracted from the term in which all of the independent LRS wave vectors lie in replica zero.

4.2.5 Feynman integrals and their reduction to HRW integrals in the replica limit

Having shown that the topology and combinatorics of the vulcanization field theory diagrams for A_n, B_n and C_n coincide with those of the HRW field theory diagrams, the task that remains is to show that, for every diagram contributing to these coefficients, the actual *value* of the corresponding Feynman integral reduces, in the replica limit, to the appropriate HRW value. That this is so can most straightforwardly be seen by employing the Schwinger representation [89] of the powers of the propagator, viz.,

$$
\frac{(s-1)!}{(r_0 + |\hat{k}|^2)^s} = \int_{\sigma} \sigma^{s-1}\, \mathrm{e}^{-\sigma(r_0 + |\hat{k}|^2)} = \int_{\sigma} \sigma^{s-1} \mathrm{e}^{-\sigma r_0} \prod_{\alpha=0}^{n} \mathrm{e}^{-\sigma \mathbf{k}^{\alpha}\cdot\mathbf{k}^{\alpha}} \qquad (\text{for } s = 1, 2, \ldots), \qquad (4.18)
$$

where the Schwinger parameter σ ranges between 0 and ∞. Observe that Eq. (4.18) presents the propagator in a form that is very conveniently factorized on the replica index.

Let us begin with a concrete example. In the thermodynamic limit, the diagram depicted in Fig. 4.5 contributes to A_n a term proportional to

$$
\begin{aligned}
& g^4 \int d^{(n+1)d}k\; d^d p\; G_0(\hat{k})^2\, G_0(\mathbf{p})^2\, G_0(\hat{k} + \mathbf{p})^2 \\
&\quad = g^4 \int d^d k^0\; d^d p \int_{\sigma_1\sigma_2\sigma_3} \sigma_1\sigma_2\sigma_3\, \mathrm{e}^{-(\sigma_1+\sigma_2+\sigma_3)r_0} \mathrm{e}^{-(\sigma_1+\sigma_3)\mathbf{k}^0\cdot\mathbf{k}^0}\, \mathrm{e}^{-(\sigma_2+\sigma_3)\mathbf{p}\cdot\mathbf{p}}\, \mathrm{e}^{-2\sigma_3\mathbf{k}^0\cdot\mathbf{p}} \\
&\qquad\qquad \times \prod_{\alpha=1}^{n} \int d^d k^{\alpha}\, \mathrm{e}^{-(\sigma_1+\sigma_3)\mathbf{k}^{\alpha}\cdot\mathbf{k}^{\alpha}}
\end{aligned}
$$

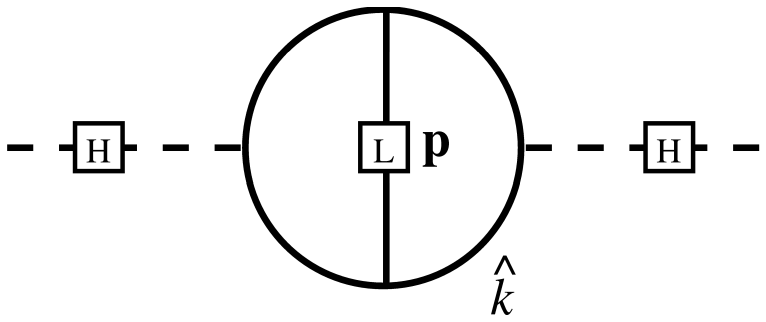

Figure 4.5: A two-loop diagram used to exemplify the decoupling of the replicas furnished by the Schwinger representation.

$$
\begin{aligned}
&= g^4 \int d^d k^0 \; d^d p \int_{\sigma_1\sigma_2\sigma_3} \sigma_1\sigma_2\sigma_3 \, \mathrm{e}^{-(\sigma_1+\sigma_2+\sigma_3) r_0} \mathrm{e}^{-(\sigma_1+\sigma_3)\mathbf{k}^0\cdot\mathbf{k}^0} \, \mathrm{e}^{-(\sigma_2+\sigma_3)\mathbf{p}\cdot\mathbf{p}} \, \mathrm{e}^{-2\sigma_3\mathbf{k}^0\cdot\mathbf{p}} \\
&\qquad \times \left(\int d^d k \, \mathrm{e}^{-(\sigma_1+\sigma_3)\mathbf{k}\cdot\mathbf{k}} \right)^n \\
&\stackrel{n\to 0}{\longrightarrow} g^4 \int d^d k \, d^d p \int_{\sigma_1\sigma_2\sigma_3} \sigma_1\sigma_2\sigma_3 \, \mathrm{e}^{-(\sigma_1+\sigma_2+\sigma_3) r_0} \mathrm{e}^{-(\sigma_1+\sigma_3)\mathbf{k}\cdot\mathbf{k}} \, \mathrm{e}^{-(\sigma_2+\sigma_3)\mathbf{p}\cdot\mathbf{p}} \, \mathrm{e}^{-2\sigma_3\mathbf{k}\cdot\mathbf{p}} \\
&= g^4 \int d^d k \; d^d p \; G_0(\mathbf{k})^2 \, G_0(\mathbf{p})^2 \, G_0(\mathbf{k}+\mathbf{p})^2 . \qquad (4.19)
\end{aligned}
$$

This limiting value is *precisely* that occurring for the corresponding diagram in the HRW field theory for the percolation transition.

The tactic that we have just employed, viz., the use of the Schwinger representation to decouple the replicas from one another, provides easy and explicit access to the replica limit and, hence, to the precise correspondence with the HRW prescription. It can straightforwardly be invoked not only for all diagrams that contribute to the coefficients A_n and (by the same procedure) C_n, but also for the coefficient B_n.

When considering diagrams contributing to A_n and C_n, we saw that what survived were terms in which all internal LRS wave vectors flowed in a common (but otherwise arbitrary) replica. Now, as we consider B_n, there is a slight complication arising from the presence of an external wave vector, which spoils the full $\mathcal{P}_{n+1}$ permutation symmetry. However, this external wave vector has been chosen to lie in replica zero and, as we have shown above, the only surviving contribution is the one in which all internal LRS wave vectors also flow in replica zero (see Fig. 4.4 and Eq. (4.17 for an example). Then, via the Schwinger representation of the propagators, and via factorization

on the replica indices, we see that the Feynman integral, in the replica limit, is identical to that in the HRW approach. Hence, the vulcanization transition presents not only the same coefficients A_0 and C_0 of the two- and three-point vertex functions as does the HRW representation, but also the same coefficient B_0.

4.3 Concluding remarks

Let us summarize what we have presented in this chapter. We have addressed the vulcanization transition via a minimal field-theoretic model. This model is built from an order parameter whose argument is the $(n+1)$-fold replication of ordinary d-dimensional space. [The structure of this theory should be contrasted with that of more familiar replica field theories, in which it is the (internal) *components* of the field that are replicated rather than the (external) *argument*.] We have considered appropriate long-wave-length aspects of the two- and three-point vertex functions for this model, to all orders in perturbation theory in the cubic nonlinearity. Via a detailed analysis of the diagrammatic expansion for these quantities, we have found that, in the replica limit, these vulcanization-theory vertex functions precisely coincide with the corresponding vertex functions of a certain field-theoretic representation (due to Houghton, Reeve and Wallace) of the percolation transition. Hence, percolation theory correctly captures the critical phenomenology the liquid and critical states of vulcanized matter, just as has long been conjectured.

Chapter 5

Density-correlator signatures of the vulcanization transition

5.1 Introduction and basic ingredients

In the present chapter, we investigate the properties of correlators that solely involve the local monomer density. We are motivated to explore the properties of these density correlators in the context of the vulcanization transition for the following reasons. First, from the theoretical perspective, the natural collective coordinate from which to view the vulcanization transition is *not* the local density; rather it is the amorphous solid order parameter [see (1.12)], which becomes nonzero as the amorphous solid state is entered and whose correlator-decay properties directly mark the onset of amorphous solidification. However, as we shall discuss further below, from the perspective of experiment, the amorphous solid order parameter is rather more elusive than one would like, the most direct way to measure it being via incoherent quasi-elastic neutron scattering, whereas probes that couple to the density are more plentiful. Second, density correlators closely related to the ones we shall be considering also feature in the diagnostics of "non-ergodic media" studied by Pusey, Van Megen and collaborators in their work on amorphous states of colloidal and gel systems [90], as well as in certain recent approaches to structural glasses [91]. It would be interesting to compare the behaviors of these density correlators in different physical situations. For these reasons, we wish to examine these density correlators in the vicinity of the vulcanization transition, and the extent to which they can provide access to both the structure of the amorphous solid state and the long-ranged amorphous solid order-parameter correlations that develop near the vulcanization

transition. Along the way, we shall explore the relationship of these density correlators to various experimental probes, and the connections of these density correlators with related studies by other researchers.

Let us now turn to the issue of the order parameter for the vulcanization transition, Eq. (1.12). We remind the reader that it is the following function of A wavevectors $\{\mathbf{k}^1, \mathbf{k}^2, \cdots, \mathbf{k}^A\}$:

$$\Big[\frac{1}{N} \sum_{j=1}^{N} \int_0^1 ds \, \langle \exp i\mathbf{k}^1 \cdot \mathbf{c}_j(s) \rangle_\chi \langle \exp i\mathbf{k}^2 \cdot \mathbf{c}_j(s) \rangle_\chi \cdots \langle \exp i\mathbf{k}^A \cdot \mathbf{c}_j(s) \rangle_\chi \Big]. \tag{5.1}$$

Why is the amorphous solid order parameter measurable in neutron scattering experiments? In quasi-elastic neutron scattering the *incoherent* contribution of the scattering cross-section is proportional to

$$\left\langle \sum_{j=1}^{N} \int_0^1 ds \exp\Big(i\mathbf{q} \cdot \mathbf{c}_j(s,0) \Big) \, \exp\Big(-i\mathbf{q} \cdot \mathbf{c}_j(s,t) \Big) \right\rangle_\chi , \tag{5.2}$$

where $\mathbf{c}_j(s,t)$ is the position of the monomer s at time t, the $t \to \infty$ limit of the correlator being proportional (up to disorder averaging) to a special case of Eq. (1.12), viz.,

$$\frac{1}{N} \sum_{j=1}^{N} \int_0^1 ds \left\langle \exp i\mathbf{q} \cdot \mathbf{c}_j(s) \right\rangle_\chi \left\langle \exp -i\mathbf{q} \cdot \mathbf{c}_j(s) \right\rangle_\chi . \tag{5.3}$$

On the other hand, in several other experimental techniques, such as those to be discussed below, it is certain form of correlator involving the local monomer density $\rho(\mathbf{r}, t)$, which is defined via

$$\rho(\mathbf{r}, t) \equiv \sum_{j=1}^{N} \int_0^1 ds \, \delta(\mathbf{r} - \mathbf{c}_j(s,t)) \tag{5.4}$$

that is probed. One frequently-measured correlator is the auto-correlation function of the local density $\langle \rho(\mathbf{x}, 0) \, \rho(\mathbf{y}, t) \rangle_\chi$, or equivalently $\langle \rho(\mathbf{q}, 0) \rho(-\mathbf{q}, t) \rangle_\chi$, where $\rho(\mathbf{q})$ is the Fourier transform of $\rho(\mathbf{x})$, i.e., $\rho(\mathbf{q}) = \int d^d x \, \rho(\mathbf{x}) \exp(-i\mathbf{q} \cdot \mathbf{x})$ [92]. For example, in neutron scattering experiments this quantity is proportional to the *coherent* part of the quasi-elastic neutron scattering cross-section (see, e.g., Ref. [32], Sec. IIIE), and in dynamical light scattering experiments, such as those performed on "non-ergodic" media by Pusey and van Megen [90], this quantity is proportional to the intermediate scattering function (also known as the dynamical structure factor) $F(k, t)$.

(The average over quenched disorder $[\cdots]$ in the present work essentially plays the role of the ensemble average $\langle\cdots\rangle_{\mathrm{E}}$ of Ref. [90].) The present theoretical framework is a static equilibrium framework and, as such, is not suitable for computing dynamical correlators. However, by using the cluster property (i.e. the fact that the connected correlators vanish for $t \to \infty$) we see that the long-time limit of the density-density auto-correlation function is built from the equilibrium entity $\langle\rho(\mathbf{x})\rangle_\chi \langle\rho(\mathbf{y})\rangle_\chi$ or, equivalently, its Fourier transform $\langle\rho(\mathbf{q})\rangle_\chi \langle\rho(-\mathbf{q})\rangle_\chi$, an entity that is calculable (up to disorder averaging) within our static equilibrium framework. In fact, our approach to the vulcanization transition is capable of calculating precisely this kind of quantity and, therefore, of providing contact with experiments.

As our results for density correlators are relatively straightforward, we first report the results, deferring the construction and operation of the necessary theoretical machinery to subsequent sections. Specifically, we find that:

(i) The usual (i.e. disorder-averaged) density-density correlator $[\langle\rho(\mathbf{q})\rho(-\mathbf{q})\rangle_\chi]$ is insensitive to the vulcanization transition, depending only analytically (i.e. smoothly) on the constraint density, both at the level of mean-field theory and beyond (i.e. to one-loop order).

(ii) The density-density correlator involving two thermal averages, $[\langle\rho(\mathbf{q})\rangle_\chi\langle\rho(-\mathbf{q})\rangle_\chi]$, is zero in the liquid phase but becomes nonzero, continuously, as the system enters the amorphous solid phase. This behavior is a manifestation of the freezing-in of random density fluctuations, which is the hallmark of the amorphous solid state. This correlator turns out to be proportional to the order parameter (at least for weak coupling between the density and the order parameter fluctuations). As the order parameter encodes the fraction of localized particles and the distribution of localization lengths, this result indicates that these physical diagnostics are accessible via this density-density correlator.

(iii) The four-density correlator involving two thermal averages, $[\langle\rho(\mathbf{k})\rho(-\mathbf{k})\rangle_\chi\langle\rho(\mathbf{q})\rho(-\mathbf{q})\rangle_\chi]$, realizable as $\lim_{t\to\infty}[\langle\rho(\mathbf{k},0)\,\rho(-\mathbf{k},0)\,\rho(\mathbf{q},t)\,\rho(-\mathbf{q},t)\rangle_\chi]$, becomes long-ranged as the vulcanization transition is approached from the liquid side. We exhibit this phenomenon at the level of mean-field theory.

(iv) The two density-chanel signatures of the vulcanization transition given in (ii) and (iii) also provide a means for identifying certain critical exponents at the vulcanization transition, such as the

gel-fraction exponent β, and the correlation-length exponent ν. Therefore, these density signatures provide another avenue for accessing experimentally the critical exponents of the vulcanization transition.

5.2 Field-theoretic formulation: Minimal model and coupling to density field

The approach that we shall adopt to study these density correlators is based upon the minimal model, Eq. (2.7). We now extend the effective free energy, Eq. (2.7), by including the field R that is associated with spatial monomer density fluctuations, i.e., $R = \sum_{j=1}^{N} \int_0^1 ds \, \exp i\mathbf{k} \cdot \mathbf{c}_j(s)$ [93]. The field R takes as its argument 1RS replicated wavevectors $\mathbf{k}\hat{e}^\alpha$. (We remind the reader that $\{\hat{e}^\alpha\}_{\alpha=0}^n$ is the collection of unit vectors in replicated space, so that, e.g., a generic replicated vector $\hat{p}$ can be expressed as $\sum_{\alpha=0}^n \mathbf{p}^\alpha \hat{e}^\alpha$.) We incorporate the energetics of the 1RS fields $R(\mathbf{k}\hat{e}^\alpha)$ [94], and add the significant symmetry-allowed cubic term that couples the order-parameter and density fields, thus arriving at

$$\mathcal{F}_n(\Omega, R) = \mathcal{S}(\Omega) + \mathcal{F}_n^{\rm 1RS}(R) - \frac{h}{N} \sum_{\substack{\hat{k}_3 \in {\rm HRS} \\ \hat{k}_1, \hat{k}_2 \in {\rm 1RS}}} R(\hat{k}_1)\, R(\hat{k}_2)\, \Omega(\hat{k}_3)\, \delta_{\hat{k}_1 + \hat{k}_2 + \hat{k}_3, \hat{0}} \,, \tag{5.5}$$

$$\mathcal{F}_n^{\rm 1RS}(R) = \frac{1}{N} \sum_{\hat{k} \in {\rm 1RS}} \Big(r^{-2} + \frac{c}{2} |\hat{k}|^2 \Big) |R(\hat{k})|^2 + \cdots \,. \tag{5.6}$$

The term $\mathcal{F}_n^{\rm 1RS}(R)$ is the effective free energy for the density fluctuations; in principle, it also includes nonlinear couplings between the R fields. This effective free energy term already incorporates the effects of the short-range repulsion between macromolecules. The parameter r is the correlation length for density fluctuations. (In the context of a dense melt, it is simply determined by the monomer density and the effective excluded-volume interaction strength [5].) The correlation length r remains large and varies analytically (with the constraint density) across the vulcanization transition, and the R field remains a non-ordered field. This is representative of the fact the *disorder-averaged* physical monomer-density is homogeneous in both the liquid state and the amorphous solid state.

In addition to the coupling presented in Eq. (5.5), there is one further term at cubic order that couples the R and Ω fields, i.e., the vertex $\Omega\Omega R$ consisting of two HRS fields and one 1RS field. It can readily be shown by dimensional analysis that both this cubic vertex and that given in Eq. (5.5) are irrelevant with respect to the fixed points of HRS Ω theory near $d = 6$ and, therefore, the critical properties of the vulcanization transition (i.e. the fixed point structure, the flow equation and the critical exponents) are not affected by the coupling to density fluctuations (at least near $d = 6$). Based on the effective free energy (5.5), our approach is to explore the correlators of the 1RS fields (and hence the density correlators), taking into account the effects of the vulcanization transition in the HRS fields by treating what happens in the HRS as "input" to be added to the effective free energy of the 1RS theory, and working perturbatively (i.e. effectively we assume that the coupling h is small).

The reason why we ignore the cubic coupling $\Omega\Omega R$, besides its irrelevance in the RG sense, is that it does not contribute to the density correlators that we are interested in (at least to one-loop order). There are two points to make in this regard. First, at the mean-field level, the HRS field can be viewed as an external source for the 1RS field in the cubic coupling $\Omega\Omega R$. Due to translational invariance, $\langle \Omega(\hat{k}_1)\Omega(\hat{k}_2)\rangle^{\mathcal{S}} = 0$. Therefore, on average, the term $\Omega\Omega R$ will not generate a non-zero $\langle R\rangle$. [$\langle\cdots\rangle$ denotes an average weighted by the replicated effective free energy presented in Eq. (5.5).] Second, at the one-loop level (and beyond), this term will renormalize the coefficient r^{-2} (in a singular way) but, as has already been shown in App. A.2.2, at least to the one-loop level, there is (in the replica limit) no contribution to the density-density correlator coming from HRS critical fluctuations via this kind of vertex.

In order to help make the physical content of the results that we shall present clear, we pause to give the relationship between the physical density correlators and the R correlators:

$$\lim_{n\to 0} \left\langle R(\mathbf{k}\hat{e}^{\alpha})\, R(-\mathbf{k}\hat{e}^{\beta}) \right\rangle_{\mathrm{c}} = \begin{cases} \left[\langle \rho(\mathbf{k})\, \rho(-\mathbf{k}) \rangle_{\chi} \right]; & \text{for } \alpha = \beta, \\ \left[\langle \rho(\mathbf{k}) \rangle_{\chi}\, \langle \rho(-\mathbf{k}) \rangle_{\chi} \right]; & \text{for } \alpha \neq \beta, \end{cases} \tag{5.7}$$

where c denotes that a correlator is connected. (Such relationships can be established by following the replica technique used in Appendix A of Ref. [32].) On the right hand side of Eq. (5.7), the correlators differ in the locations of the thermal averages; on the left hand side they differ in their

replica indices, the former being diagonal and the latter being off-diagonal in replica space.

5.3 Freezing-in of density fluctuations

Now that we have constructed an extended model containing not only the critical order parameter (i.e. HRS) fields but also the noncritical replicated density (i.e. 1RS) fields, we proceed to study the effect of critical HRS phenomena on the density fields, treating the latter at the tree level. The basic mechanism at work is that the order parameter field, which is capable of ordering spontaneously, couples to the density fluctuations via a cubic vertex that is replica-off-diagonal as far as the density fields are concerned. A non-zero value of $\overline{\Omega} \equiv \langle \Omega \rangle^{\mathcal{S}}$, as occurs in the amorphous solid state due to spontaneous symmetry breaking in the HRS, contributes replica-off-diagonal terms to the "mass matrix" of the R-field and, hence, leads to the existence of nonzero replica-off-diagonal density-field correlators.

In order to see this more clearly, we replace Ω by its expectation value plus fluctuations, i.e., we write $\Omega = \overline{\Omega} + \delta\Omega$ and, hence, arrive at the effective free energy

$$\begin{aligned}
\mathcal{F}_n(R,\Omega) &= \mathcal{S}(\Omega) + \tilde{\mathcal{F}}_n^{\mathrm{1RS}}(R,\overline{\Omega}) - \frac{h}{N} \sum_{\substack{\hat{k}_3 \in \mathrm{HRS} \\ \hat{k}_1, \hat{k}_2 \in \mathrm{1RS}}} R(\hat{k}_1)\, R(\hat{k}_2)\, \delta\Omega(\hat{k}_3)\, \delta_{\hat{k}_1+\hat{k}_2+\hat{k}_3,\hat{0}}\,, \\
\tilde{\mathcal{F}}_n^{\mathrm{1RS}}(R,\overline{\Omega}) &= \frac{1}{N} \sum_{\mathbf{k}\neq\mathbf{0}} \sum_{\alpha,\beta=0}^{n} \Big((r^{-2} + \frac{c}{2}k^2)\delta^{\alpha,\beta} - h\,\overline{\Omega}(-\mathbf{k}\hat{e}^1 + \mathbf{k}\hat{e}^2)(1-\delta^{\alpha,\beta}) \Big)\, R(\mathbf{k}\hat{e}^\alpha) R(-\mathbf{k}\hat{e}^\beta) \\
&\qquad + \cdots . \qquad (5.8)
\end{aligned}$$

To arrive at this result, we have taken advantage of the facts that both $\mathcal{F}_n$ and $\overline{\Omega}$ are replica (i.e. permutation) symmetric, and that $\overline{\Omega}(-\mathbf{k}_1\hat{e}^\alpha - \mathbf{k}_2\hat{e}^\beta)$ is macroscopically translational invariant (i.e. it contains a factor of $\delta_{\mathbf{k}_1+\mathbf{k}_2,\mathbf{0}}$) [51].

We now aim to compute the correlator $\left\langle R(\mathbf{k}\hat{e}^\alpha)\, R(-\mathbf{k}\hat{e}^\beta) \right\rangle$. By treating h as a small quantity and expanding perturbatively, a direct calculation yields

$$\left\langle R(\mathbf{k}\hat{e}^\alpha)\, R(-\mathbf{k}\hat{e}^\beta) \right\rangle = \left\langle R(\mathbf{k}\hat{e}^\alpha)\, R(-\mathbf{k}\hat{e}^\beta) \right\rangle^{\tilde{\mathcal{F}}_n^{\mathrm{1RS}}} + O(h^2). \qquad (5.9)$$

To obtain the correlator at the tree (in R) level, we neglect the nonlinear self-couplings of R and

then invert the coefficient matrix of the quadratic term in Eq. (5.8). Thus, in the $n \to 0$ limit we arrive at

$$\lim_{n\to 0} \left\langle R(\mathbf{k}\hat{e}^{\alpha})\, R(-\mathbf{k}\hat{e}^{\beta}) \right\rangle = \begin{cases} \dfrac{N/2}{r^{-2} + \frac{1}{2}ck^2}, & \text{for } \alpha = \beta; \\ \dfrac{Nh\overline{\Omega}/2(-\mathbf{k}\hat{e}^1 + \mathbf{k}\hat{e}^2)}{(r^{-2} + \frac{1}{2}ck^2)((r^{-2} + \frac{1}{2}ck^2) + h\overline{\Omega}(-\mathbf{k}\hat{e}^1 + \mathbf{k}\hat{e}^2))}, & \text{for } \alpha \neq \beta. \end{cases} \tag{5.10}$$

In the liquid state we have $\overline{\Omega} = 0$, and therefore $\langle R(\mathbf{k}\hat{e}^{\alpha})\, R(-\mathbf{k}\hat{e}^{\beta})\rangle = 0$ (for $\alpha \neq \beta$). However, in the amorphous solid state, according to Eqs. (2.20) and (2.21),

$$\overline{\Omega}(\mathbf{k}_1\hat{e}^1 + \mathbf{k}_2\hat{e}^2) = q\delta_{\mathbf{k}_1+\mathbf{k}_2,\mathbf{0}}\, \omega(\sqrt{\frac{2b}{a\tau}(k_1^2 + k_2^2)}) \neq 0 \ , \tag{5.11}$$

and therefore $\langle R(\mathbf{k}\hat{e}^{\alpha})\, R(-\mathbf{k}\hat{e}^{\beta})\rangle \neq 0$ (for $\alpha \neq \beta$). Here, the number q is the gel fraction and the function $\omega(|\hat{k}|)$, which decays rapidly with increasing wavevector magnitude on the characteristic wavevector scale τ^{ν} [52], encodes the distribution of localization lengths. The simplest setting for the density-density correlator emerges near the vulcanization transition, where q is small and $\omega(|\hat{k}|)$ is negligible unless $|\hat{k}| \lesssim \tau^{\nu}$. In this regime, by making use of Eq. (5.7) we find that

$$\Big[\, \langle\rho(\mathbf{k})\rangle_{\chi}\, \langle\rho(-\mathbf{k})\rangle_{\chi} \,\Big] = \begin{cases} 0, & \text{liquid;} \\ (Nhr^4/2)\overline{\Omega}(-\mathbf{k}\hat{e}^1 + \mathbf{k}\hat{e}^2) = (Nhr^4/2)\tau^{\beta}\, \omega(|\hat{k}|\tau^{-\nu}), & \text{amorphous solid.} \end{cases} \tag{5.12}$$

On the other hand, the diagonal correlator $[\, \langle\rho(\mathbf{k})\rho(-\mathbf{k})\rangle_{\chi}\,]$ does not vary with τ (and hence varies smoothly with the physical constraint density).

Deeper into the amorphous solid state, the order parameter $\overline{\Omega}$ does not decay so rapidly with k, and hence the quantity $[\, \langle\rho(\mathbf{k})\rangle_{\chi}\, \langle\rho(-\mathbf{k})\rangle_{\chi}\,]$ should remain appreciable (and thus experimentally accessible) over a wider range of k. Now, we expect Eq. (5.10) to remain valid, provided the coupling h is small and both the wavevector dependence of h and the finer wavevector dependence of 1RS bare correlator are incorporated. (We have omitted the wavevector dependence of h so as to simplify our presentation.) Under these circumstances, the wavevector dependence of the replica-off-diagonal correlator has the possibility of exhibiting additional features, representative of the ordinary density-density correlator $[\langle\rho(\mathbf{k})\rho(-\mathbf{k})\rangle_{\chi}]$, superposed on the decaying trend due to the factor w (i.e. due to random monomer localization) [96].

5.4 Inherited criticality of density correlators

In the HRS field theory, the vulcanization transition is signaled in two ways: (i) via the emergence of a nonzero order parameter, and (ii) via the divergence of the correlation length of order-parameter fluctuations. We have already studied the replica-off-diagonal density correlator, which is closely related to the order parameter and becomes nonzero upon entering the amorphous solid state. We now examine the four-field density correlator $[\langle\rho(\mathbf{k})\,\rho(-\mathbf{k})\rangle_\chi\,\langle\rho(\mathbf{p})\,\rho(-\mathbf{p})\rangle_\chi]$, which has the property that it becomes long-ranged at the vulcanization transition.

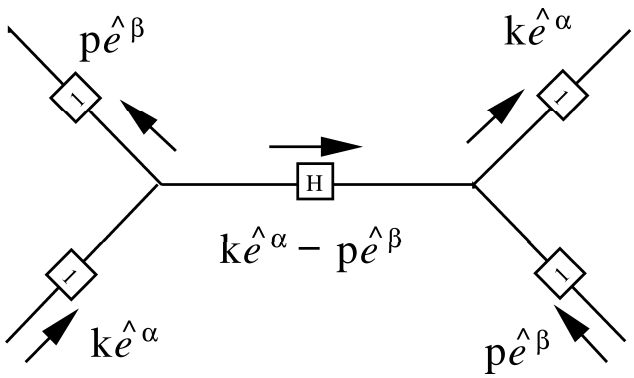

Figure 5.1: Divergent 4-field tree level density correlator. The solid line labeled with "H" indicates the bare HRS correlator; The solid lines labeled with "1" indicate bare 1RS correlators.

We calculate the correlator mentioned in the previous sentence at the tree level (with respect to h vertices) in the liquid state and at the vulcanization transition itself: at the tree level the Feynman diagram shown on Fig. 5.1 is the only contribution, and gives

$$\begin{aligned}[\langle\rho(\mathbf{k})\,\rho(-\mathbf{k})\rangle_\chi\,\langle\rho(\mathbf{p})\,\rho(-\mathbf{p})\rangle_\chi] &= \lim_{n\to 0}\langle R(\mathbf{k}\hat{e}^\alpha)R(-\mathbf{p}\hat{e}^\beta)R(-\mathbf{k}\hat{e}^\alpha)R(\mathbf{p}\hat{e}^\beta)\rangle \\ &\propto (h/N)^2\Big\{\langle R(\mathbf{k}\hat{e}^\alpha)R(-\mathbf{k}\hat{e}^\alpha)\rangle^{\mathcal{F}_n^{\rm 1RS}}\Big\}^2\Big\{\langle R(\mathbf{p}\hat{e}^\beta)R(-\mathbf{p}\hat{e}^\beta)\rangle^{\mathcal{F}_n^{\rm 1RS}}\Big\}^2 \\ &\quad\times\langle\Omega(\mathbf{k}\hat{e}^\alpha-\mathbf{p}\hat{e}^\beta)\Omega(-\mathbf{k}\hat{e}^\alpha+\mathbf{p}\hat{e}^\beta)\rangle^{\mathcal{S}}. \end{aligned} \tag{5.13}$$

As anticipated, this density correlator becomes long-ranged at the vulcanization transition, due to the factor of the HRS order-parameter correlator $\langle\Omega\Omega\rangle^{\mathcal{S}}$ which itself becomes long-ranged at the vulcanization transition.

5.5 Discussion and conclusions

We have studied density-sector correlators that furnish analogs of the two principal order-parameter signatures of the vulcanization transition: the off-diagonal density correlator $[\langle\rho(\mathbf{q})\rangle_\chi \langle\rho(-\mathbf{q})\rangle_\chi]$, which becomes nonzero as the amorphous solid state is entered; and the four-field correlator $[\langle\rho(\mathbf{k})\,\rho(-\mathbf{k})\rangle_\chi \langle\rho(\mathbf{p})\,\rho(-\mathbf{p})\rangle_\chi]$, which becomes long-ranged at the vulcanization transition. We have shown that these density correlators provide useful information about both the emergent amorphous solid state and the critical properties of the transition itself. They provide schemes for accessing experimentally the kinds of quantities that have been found useful in theoretical investigations of the liquid, critical and amorphous solid states, e.g., of vulcanized matter. We are not aware of any explorations of such signatures in the density correlators via percolation/gelation approaches to the vulcanization transition.

Although, as we have seen, the off-diagonal density correlator $[\langle\rho(\mathbf{q})\rangle_\chi \langle\rho(-\mathbf{q})\rangle_\chi]$ is closely related to the order parameter of the vulcanization transition, its non-zero value being induced by a non-zero order parameter, the off-diagonal density correlator can be used to diagnose a more general class of systems. By looking at the microscopic definition of the order parameter for the vulcanization transition, Eq. (1.12) (especially for the special case in which only two thermal averages are involved), we see that it involves only a *single* summation over monomers and, therefore, the order parameter cannot be expressed in terms of local monomer densities. In essence, the order parameter signals the amorphous solid phase via its detection of all individual monomers that are localized (and, owing to the explicit crosslinks, distinguishable). On the other hand, the off-diagonal density correlator $[\langle\rho(\mathbf{q})\rangle_\chi \langle\rho(-\mathbf{q})\rangle_\chi]$ signals the amorphous solid state via the detection of the frozen structure of the local density fluctuations. In RCMSs, the localization of monomers invariably induces the freezing of this structure, so these two quantities are equivalent. However in systems such as glasses, the (local density) structure is, presumably, frozen but each individual particle is able to wander throughout the system, given enough time, and therefore all particles retain their indistinguishability [95]. A quantity essentially identical to the off-diagonal correlator considered here has been employed by Mézard and Parisi [91] in the context of their theoretical approach to glassy systems. A similar quantity is employed in the diagnosis of the freezing-in of structure in colloidal glassy systems and gel systems in the dynamical light scattering experiments

of Pusey and Van Megen and collaborators [90, 97]

Vulcanized matter certainly is different from glassy systems, inasmuch as it possesses explicit quenched disorder in the form of permanent random crosslinks. Because of this, it affords a framework in which the off-diagonal density correlator and other density correlators are directly calculable in a well controlled way, both near the transition and in the amorphous solid state. Despite the difference with glassy systems, we hope that results such as those presented here in the setting of vulcanized matter will not only be useful but also shed some light on the more difficult problem of glassy systems.

Appendix A

Derivation of the Ginzburg criterion

A.1 Inverse susceptibility

In this Appendix we calculate the one-loop correction to the two-point vertex function $\Gamma^{(2)}(\hat{k})$, using the Hamiltonian (2.7). To do this, we first calculate the self-energy $\Sigma_n(\hat{k})$ (i.e. the sum of all two-point one-particle-irreducible amputated diagrams), in terms of which $\Gamma^{(2)}(\hat{k})$ is given by $\Gamma^{(2)}(\hat{k}) \equiv G_0(\hat{k})^{-1} - \Sigma_n(\hat{k})|_{n\to 0}$. To one-loop order, $\Sigma_n(\hat{k})$ is given by the amputated diagram shown in Fig. 3.1, i.e.,

$$\Sigma_n(\hat{k}) = 18g^2 \sum_{\substack{\hat{k}_1\in \mathrm{HRS} \\ (\hat{k}-\hat{k}_1\in \mathrm{HRS})}} G_0(\hat{k}_1)\, G_0(\hat{k}_1 - \hat{k}). \tag{A.1}$$

Let us emphasize the meaning of the notation: one is directed to sum over all replicated wave vectors $\hat{k}_1 \in$ HRS subject to the constraint that $\hat{k} - \hat{k}_1 \in$ HRS; one should also bear in mind the fact that the external wave vector $\hat{k}$ lies in the HRS. This constrained summation can be expressed in terms of several unconstrained summations (for cases in which $\hat{k}$ has nonzero entries in at least three replicas, i.e., lies in the 3^+RS) as

$$\begin{aligned}\sum_{\substack{\hat{k}_1\in \mathrm{HRS} \\ (\hat{k}-\hat{k}_1\in \mathrm{HRS})}} O(\hat{k}_1) \;=\; & \sum_{\hat{k}_1} O(\hat{k}_1) - \sum_{\alpha=0}^{n}\sum_{\mathbf{p}} O(\hat{k}_1)\Big|_{\hat{k}_1=\mathbf{p}\hat{e}^\alpha} + nO(\hat{k}_1)\Big|_{\hat{k}_1=\hat{0}} \\ & - \sum_{\alpha=0}^{n}\sum_{\mathbf{p}} O(\hat{k}_1)\Big|_{\hat{k}_1=\mathbf{p}\hat{e}^\alpha+\hat{k}} + nO(\hat{k}_1)\Big|_{\hat{k}_1=\hat{k}}\,,\end{aligned} \tag{A.2}$$

for any $O(\hat{k}_1)$. When $\hat{k}$ belongs to the 2RS [e.g. $\hat{k} = (\mathbf{0}, \mathbf{l}^1, \mathbf{l}^2, \mathbf{0}, \ldots, \mathbf{0})$, $\mathbf{l}^1 \neq \mathbf{0}$ and $\mathbf{l}^2 \neq \mathbf{0}$] there is a slight modification of Eq. (A.2) and, instead, we have

$$\begin{aligned}\sum_{\substack{\hat{k}_1 \in \mathrm{HRS} \\ (\hat{k}-\hat{k}_1 \in \mathrm{HRS})}} O(\hat{k}_1) &= \sum_{\hat{k}_1} O(\hat{k}_1) - \sum_{\alpha=0}^{n} \sum_{\mathbf{p}} O(\hat{k}_1)\Big|_{\hat{k}_1 = \mathbf{p}\hat{e}^\alpha} + nO(\hat{k}_1)\Big|_{\hat{k}_1=\hat{0}} - \sum_{\alpha=0}^{n} \sum_{\mathbf{p}} O(\hat{k}_1)\Big|_{\hat{k}_1 = \mathbf{p}\hat{e}^\alpha + \hat{k}} \\ &\quad + nO(\hat{k}_1)\Big|_{\hat{k}_1=\hat{k}} + O(\hat{k}_1)\Big|_{\hat{k}_1=\mathbf{l}^1\hat{e}^1} + O(\hat{k}_1)\Big|_{\hat{k}_1=\mathbf{l}^2\hat{e}^2} . \qquad \text{(A.3)}\end{aligned}$$

For the moment, let us focus on the case of $\hat{k} \in 3^+\mathrm{RS}$. By making use of Eq. (A.2), and subsequently transforming each unconstrained summation into an integral, we obtain

$$\begin{aligned}\Sigma_n(\hat{k}) &= 18g^2\Big(V^{n+1} \int d^{(n+1)d}k_1 \, G_0(\hat{k}_1)\, G_0(\hat{k}_1 - \hat{k}) \\ &\quad -2\sum_{\alpha=0}^{n} V \int d^d p \, G_0(\mathbf{p}\hat{e}^\alpha)\, G_0(\mathbf{p}\hat{e}^\alpha - \hat{k}) + 2n\, G_0(\hat{0})\, G_0(\hat{k})\Big). \qquad \text{(A.4)}\end{aligned}$$

The limit of the validity of the Landau theory (i.e. the tree-level approximation) can be ascertained by enquiring when the loop corrections to the inverse susceptibility become comparable its tree-level value. Thus we take the long-wavelength limit of the correction (A.1) via a sequence of wave vectors $\hat{k}$ lying in the HRS, obtaining

$$\Sigma_n(\hat{k})|_{\hat{k}\to\hat{0}} = 18g^2\Big(V^{n+1} \int d^{(n+1)d}k_1 \, G_0(\hat{k}_1)^2 - 2(n+1)V \int d^d p \, G_0(\mathbf{p})^2 + 2nG_0(\hat{0})^2\Big). \qquad \text{(A.5)}$$

At this stage, the $n \to 0$ limit may be taken [the reason for this is discussed in Sec. 2.2, shortly after Eq. (2.7)]. In addition, the integral over the $(n+1)$-fold replicated space goes smoothly into an integral over the ordinary (i.e. unreplicated) space. Thus, we arrive at

$$\Sigma(\hat{k})|_{\hat{k}\to\hat{0}} \equiv \lim_{n\to 0} \Sigma_n(\hat{k})|_{\hat{k}\to\hat{0}} = 18g^2\Big(V \int d^d p \, G_0(\mathbf{p})^2 - 2V \int d^d p \, G_0(\mathbf{p})^2\Big). \qquad \text{(A.6)}$$

From this expression, we see an example of what turns out to be a typical effect of the exclusion of the 1RS, viz., that it reverses the sign relative to the unconstrained version. By collecting this loop correction together with the tree-level inverse susceptibility, we arrive at the result that we

shall use to establish the Ginzburg criterion:

$$(N\Xi)^{-1} \equiv N^{-1}\Gamma^{(2)}(\hat{k})|_{\hat{k}\to\hat{0}} = G_0(\hat{0})^{-1} - N^{-1}\Sigma(\hat{k})|_{\hat{k}\to\hat{0}} = -2a\tau + 18g^2\frac{V}{N}\int \frac{d^dp}{(-2a\tau + bp^2)^2} \ . \quad \text{(A.7)}$$

We mention that when $\hat{k}$ lies in the 2RS, we need to use Eq. (A.3) instead of Eq. (A.2) in evaluating the constrained summation. The resulting two extra terms in Ξ^{-1} turn out to be nonextensive and non-divergent at the transition, and hence vanish in the expression for $(N\Xi)^{-1}$ (in the thermodynamic limit) and do not change the result for the Ginzburg criterion. [The appearance of non-extensive terms may seem strange; it is related to the way we define our fields, i.e. Eq. (1.21). If we rescale the fields and coefficients appropriately, as we do in Eq. (4.1) of Chap. 4, then those terms disappear in the thermodynamic limit, as shown in Eq. (4.12).]

A.2 Subleading elements: Additional semi-microscopically generated fields and vertices

The inspiration for the minimal model, Eq. (2.7), discussed in Sec. 2.2, comes from experience with detailed statistical-mechanical investigations of various semi-microscopic models of RCMSs and related systems [31, 32, 55, 56]. The field theories obtained in these investigations contain additional fields and vertices beyond those featuring in the minimal model. Among them are: the 1RS field [variously denoted as $\Omega(\mathbf{k}\hat{e}^\alpha)$ or $\Omega^\alpha(\mathbf{k})$], which describes density fluctuations; various vertices that couple the 1RS field to itself and to the HRS field; and quartic or higher-order HRS vertices. In the present section we discuss the role of these additional fields and vertices. We shall confine our attention to effects that show up at the one-loop level. To avoid confusion we shall, in this section, denote the bare HRS and 1RS correlators respectively by $G_0^{\rm HRS}$ and $G_0^{\rm 1RS}$.

A.2.1 Subleading influences on the higher replica sector

We begin by considering the possible corrections to the HRS self-energy $\Sigma_n(\hat{k})|_{\hat{k}\to\hat{0}}$ arising from the additional fields and vertices. At the one-loop level, the only contributions arising from an omitted vertex are those associated with the quartic vertex, for which there are two situations to consider, depending on whether the loop wave vector lies in the 1RS or the HRS. Figure A.1 shows

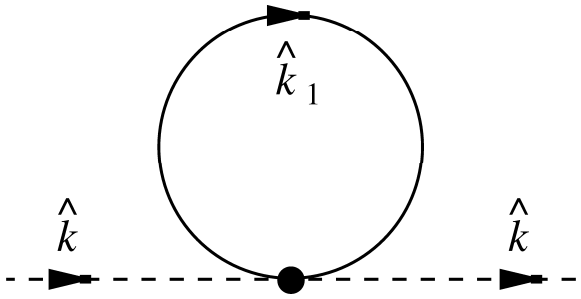

Figure A.1: Example of a one-loop correction to the self-energy due to a vertex omitted from the minimal model.

the relevant diagram.

Let us first look at the contribution of this diagram when the loop wave vector lies in the HRS. In this case, evaluating the diagram involves the constrained summation:

$$\begin{aligned}\sum_{\hat{k}\in\mathrm{HRS}} G_0^{\mathrm{HRS}}(\hat{k}) &= \sum_{\hat{k}} G_0^{\mathrm{HRS}}(\hat{k}) - \sum_{\alpha=0}^{n}\sum_{\mathbf{k}} G_0^{\mathrm{HRS}}(\mathbf{k}\hat{e}^{\alpha}) + nG_0^{\mathrm{HRS}}(\hat{0}) \\ &= \sum_{\hat{k}} G_0^{\mathrm{HRS}}(\hat{k}) - (n+1)\sum_{\mathbf{k}} G_0^{\mathrm{HRS}}(\mathbf{k}) + nG_0^{\mathrm{HRS}}(\hat{0}), \end{aligned} \tag{A.8}$$

which vanishes in the $n \to 0$ limit.

Let us now look at the contribution of this diagram when the loop wave vector lies in the 1RS. In this case, no critical bare correlators feature, so that the resulting contribution to $\Sigma_n(\hat{k})|_{\hat{k}\to\hat{0}}$ is finite. There are also contributions to $\Sigma_n(\hat{k})|_{\hat{k}\to\hat{0}}$ arising from one-loop diagrams involving two cubic vertices, in which either one or both loop-wave-vectors lie in the 1RS. None of these contributions alters the Ginzburg criterion established in Sec. 3.3.2.

A.2.2 Absence of feedback of critical fluctuations on the density-density correlator

As we have discussed in Sec. 1.6, the 1RS field $\Omega(\mathbf{k}\hat{e}^{\alpha})$, which describes density fluctuations, remains "massive" at the vulcanization transition (i.e. the coefficient of the term quadratic in this field remains positive at the transition), and the corresponding bare correlator is nonsingular at the vulcanization transition. We now examine the effects of HRS critical fluctuations on the correlator

of the 1RS field. We approach this issue by studying those one-loop diagrams for the 1RS self-energy in which at least one internal wave vector lies in the HRS; there are three types of contribution to consider:

(i) There is the contribution associated with the diagram shown in Fig. A.1 but with the external wave vectors now lying in the 1RS. By the same reasoning that we applied to Eq. (A.8), this contribution vanishes in the $n \to 0$ limit.

(ii) There are the two contributions associated with the type of diagram shown in Fig. 3.1. When one of the internal wave vectors lies in the 1RS and the other lies in the HRS, the contribution involves a constrained summation over $\hat{k}$ with $\hat{k} \in$ HRS and $(\mathbf{p}\hat{e}^{\alpha} - \hat{k}) \in$ 1RS (where $\hat{k}$ is the loop wave vector and $\mathbf{p}\hat{e}^{\alpha}$ is the external wave vector). In this case, the constraints on the summation require that $\hat{k} \in$ 2RS and $\hat{k} = \mathbf{p}\hat{e}^{\alpha} + \mathbf{l}\hat{e}^{\beta}$, where $\beta \neq \alpha$ and $\mathbf{l} \neq \mathbf{0}$. Then, the contribution to the 1RS self-energy reads

$$\begin{aligned}
\sum_{\substack{\hat{k}\in\mathrm{HRS} \\ (\mathbf{p}\hat{e}^{\alpha}-\hat{k}\in\mathrm{1RS})}} G_0^{\mathrm{HRS}}(\hat{k})\, G_0^{\mathrm{1RS}}(\mathbf{p}\hat{e}^{\alpha} - \hat{k}) &= \sum_{\beta(\neq\alpha)} \sum_{\mathbf{l}\neq\mathbf{0}} G_0^{\mathrm{HRS}}(\mathbf{p}\hat{e}^{\alpha} + \mathbf{l}\hat{e}^{\beta})\, G_0^{\mathrm{1RS}}(-\mathbf{l}\hat{e}^{\beta}) \\
&= n \sum_{\mathbf{l}\neq\mathbf{0}} G_0^{\mathrm{HRS}}(\mathbf{p}\hat{e}^{\alpha} + \mathbf{l}\hat{e}^{\beta})\, G_0^{\mathrm{1RS}}(-\mathbf{l}\hat{e}^{\beta})\Big|_{\beta\neq\alpha} , \qquad \text{(A.9)}
\end{aligned}$$

which evidently vanishes in the $n \to 0$ limit. On the other hand, when both internal wave vectors lie in the HRS, the contribution involves the constrained summation over $\hat{k}$ with $\hat{k} \in$ HRS and $(\mathbf{p}\hat{e}^{\alpha} - \hat{k}) \in$ HRS. In this case, the contribution to the 1RS self-energy reads

$$\begin{aligned}
&\sum_{\substack{\hat{k}\in\mathrm{HRS} \\ (\mathbf{p}\hat{e}^{\alpha}-\hat{k}\in\mathrm{HRS})}} G_0^{\mathrm{HRS}}(\hat{k})\, G_0^{\mathrm{HRS}}(\mathbf{p}\hat{e}^{\alpha} - \hat{k}) \\
&\qquad = \sum_{\hat{k}\in\mathrm{HRS}} G_0^{\mathrm{HRS}}(\hat{k})\, G_0^{\mathrm{HRS}}(\mathbf{p}\hat{e}^{\alpha} - \hat{k}) - \sum_{\substack{\hat{k}\in\mathrm{HRS} \\ (\mathbf{p}\hat{e}^{\alpha}-\hat{k}\in\mathrm{1RS})}} G_0^{\mathrm{HRS}}(\hat{k})\, G_0^{\mathrm{HRS}}(\mathbf{p}\hat{e}^{\alpha} - \hat{k}) \\
&\qquad \propto n\,, \qquad \text{(A.10)}
\end{aligned}$$

which also evidently vanishes in the $n \to 0$ limit. [In the last step we have used Eq. (A.9), as well the strategy for handling constrained summations employed in Eq. (A.8).]

We conclude that, to one-loop order, the 1RS self-energy does not acquire any singular contributions due to critical fluctuations in the HRS. In this sense, the two sectors are separated in the

neighborhood of the vulcanization transition.

Appendix B

Derivation of flow equations within the epsilon expansion

B.1 Implementation of the momentum-shell RG

The first step in the momentum-shell RG approach that we are adopting is to integrate out Fourier components of the field $\Omega(\hat{k})$ having wave vectors in the shell $\Lambda/b < |\hat{k}| < \Lambda$. To do this, we define $\Omega^<$ and $\Omega^>$, respectively the long and short wavelength components of $\Omega(\hat{k})$, by

$$\Omega^<(\hat{k}) = \begin{cases} 0, & \text{for } \Lambda/b < |\hat{k}| < \Lambda; \\ \Omega(\hat{k}), & \text{for } 0 < |\hat{k}| < \Lambda/b; \end{cases} \tag{B.1}$$

$$\Omega^>(\hat{k}) = \begin{cases} \Omega(\hat{k}), & \text{for } \Lambda/b < |\hat{k}| < \Lambda; \\ 0, & \text{for } 0 < |\hat{k}| < \Lambda/b. \end{cases} \tag{B.2}$$

Then, by exchanging $\Omega(\hat{k})$ for $\Omega^>(\hat{k})$ and $\Omega^<(\hat{k})$ in Eq. (3.15) we can re-express the effective Hamiltonian as

$$\mathcal{S}(\{\Omega\}) = \mathcal{S}(\{\Omega^<\}) + N \sum_{\hat{k}\in \mathrm{HRS}} \Big(-\tau + \frac{1}{2}|\hat{k}|^2 \Big) |\Omega^>(\hat{k})|^2 - V(\{\Omega\}) \ , \tag{B.3}$$

$$\begin{aligned} V(\{\Omega\}) \equiv\ & Ng \sum_{\hat{k}_1,\hat{k}_2,\hat{k}_3\in \mathrm{HRS}} \delta_{\hat{k}_1+\hat{k}_2+\hat{k}_3,\hat{0}} \Big(\Omega^>(\hat{k}_1)\, \Omega^>(\hat{k}_2)\, \Omega^>(\hat{k}_3) \\ & + 3\, \Omega^<(\hat{k}_1)\, \Omega^>(\hat{k}_2)\, \Omega^>(\hat{k}_3) + 3\, \Omega^<(\hat{k}_1)\, \Omega^<(\hat{k}_2)\, \Omega^>(\hat{k}_3) \Big) \ . \end{aligned} \tag{B.4}$$

Now, focusing on the partition function, we integrate out the aforementioned short-wavelength field components $\Omega^{>}$ in the context of a cumulant expansion in V. Thus, Eq. (2.5) becomes

$$[Z^n] \propto \int \overline{\mathcal{D}}^{\dagger}\Omega^{<} \exp\big(-\mathcal{S}^{<,\mathrm{eff}}\big), \tag{B.5}$$

$$\mathcal{S}^{<,\mathrm{eff}}(\{\Omega^{<}\}) \equiv \mathcal{S}(\{\Omega^{<}\}) - \ln\langle \exp V\rangle_{>}, \tag{B.6}$$

$$\begin{aligned}\ln\langle \exp V\rangle_{>} &\equiv \ln\left\{\frac{\displaystyle\int \overline{\mathcal{D}}^{\dagger}\Omega^{>} \exp\Big(-N\sum\nolimits_{\hat{k}\in\mathrm{HRS}}\big(-\tau+\frac{1}{2}|\hat{k}|^2\big)|\Omega^{>}(\hat{k})|^2\Big)\exp V}{\displaystyle\int \overline{\mathcal{D}}^{\dagger}\Omega^{>} \exp\Big(-N\sum\nolimits_{\hat{k}\in\mathrm{HRS}}\big(-\tau+\frac{1}{2}|\hat{k}|^2\big)|\Omega^{>}(\hat{k})|^2\Big)}\right\}\\ &\approx \langle V\rangle_{>} + \frac{1}{2!}\Big(\langle V^2\rangle_{>} - \langle V\rangle_{>}^2\Big) + \frac{1}{3!}\Big(\langle V^3\rangle_{>} - 3\langle V\rangle_{>}\langle V^2\rangle_{>} + 2\langle V\rangle_{>}^3\Big) + \mathcal{O}(V^4).\end{aligned} \tag{B.7}$$

Note that we have not explicitly given the factor associated with Gaussian fluctuations in the wavevector shell because it is nonsingular and, therefore, does not contribute to the quantities that we are focusing on, viz., the RG flow equations.

Next, we calculate $\mathcal{S}^{<,\mathrm{eff}}$ to the one-loop level by computing the cumulant expansion to $\mathcal{O}(V^3)$ and discarding operators that are irrelevant in the vicinity of $d = 6$. This amounts to retaining only terms of the form of those present in the original minimal model, and thus we are in a position to begin the task of recasting the resulting theory in its original form. The terms that must be considered correspond to the diagrams shown in Fig. 3.3, and are computed in Sec. B.2. When included, they produce the following intermediate form for the effective coarse-grained Hamiltonian:

$$\mathcal{S}^{<,\mathrm{eff}} = \mathcal{S}^{<} - \sum_{\hat{k}\in\mathrm{HRS}} f_2(\hat{k})\,|\Omega^{<}(\hat{k})|^2 - \sum_{\hat{k}_1,\hat{k}_2,\hat{k}_3\in\mathrm{HRS}} f_3(\hat{k}_1,\hat{k}_2,\hat{k}_3)\,\Omega^{<}(\hat{k}_1)\,\Omega^{<}(\hat{k}_2)\,\Omega^{<}(\hat{k}_3)\,\delta_{\hat{k}_1+\hat{k}_2+\hat{k}_3,\hat{0}}\,, \tag{B.8}$$

where the functions f_2 and f_3 can be found in Sec. B.2. In fact, only their long-wavelength parts are needed, i.e., we shall only need the constants $f_2^{(0)}$, $f_2^{(1)}$ and $f_3^{(0)}$ in the Taylor expansions

$$f_2(\hat{k}) \approx f_2^{(0)} + \frac{1}{2}f_2^{(1)}|\hat{k}|^2 + \mathcal{O}(\hat{k}^4)\,, \tag{B.9}$$

$$f_3(\hat{k}_1,\hat{k}_2,\hat{k}_3) \approx f_3^{(0)} + \mathcal{O}(\hat{k}_1^2,\hat{k}_2^2,\hat{k}_3^2,\hat{k}_1\cdot\hat{k}_2,\hat{k}_1\cdot\hat{k}_3,\hat{k}_2\cdot\hat{k}_3)\,. \tag{B.10}$$

The next step is to rescale $\Omega^<$ and $\hat{k}$ via

$$\Omega^<(\hat{k}) = z\,\Omega'(\hat{k}')\,, \tag{B.11}$$

$$\hat{k}' = b\,\hat{k}\,. \tag{B.12}$$

The recasting of the theory in its original form also involves the restoration of the wave-vector lattice, as discussed in Sec. 3.3.3. Having made this restoration, we arrive at recursion relations for τ and g, along with the condition that the coefficient of the gradient term be restored to its original value:

$$\tau' = (\tau + f_2^{(0)}/N) z^2 b^{-(n+1)d}\,, \tag{B.13}$$

$$g' = (g + f_3^{(0)}/N) z^3 b^{-2(n+1)d}\,, \tag{B.14}$$

$$1 = (1 - f_2^{(1)}/N) z^2 b^{-(n+1)d-2}\,. \tag{B.15}$$

The computation of the coefficients in the recursion relations simplifies under the convenient choice of $b = 1+x$ with x positive and very small, because it allows the approximation of the shell integrals by the product of end-point values of the integrands and the shell volumes. Thus, we arrive at the differential RG recursion relations (i.e. flow equations) given in the main text in Eqs. (3.17) and (3.18), along with the coefficients (3.20).

B.2 Evaluation of two diagrams

The renormalizations of τ and the gradient term acquire a nontrivial contribution associated with diagram (a) of Fig. 3.3, which determines $f_2(\hat{k})$ in Eq. (B.8). Thus, including the symmetry factor of the diagram, we need to evaluate

$$f_2(\hat{k}) = 9g^2 \sum_{\substack{\hat{k}_1 \in \mathrm{HRS} \\ (\hat{k}_1 - \hat{k} \in \mathrm{HRS})}} G_0(\hat{k_1})\, G_0(\hat{k}_1 - \hat{k}). \tag{B.16}$$

We have encountered this kind of constrained summation in App. A, and we use the recipe given there, together with the facts that the external wave vector satisfies $|\hat{k}| \in (0, \Lambda/b)$ whereas the

internal wave vectors satisfy $|\hat{k}_1| \in (\Lambda/b, \Lambda)$ and $|\hat{k}_1 - \hat{k}| \in (\Lambda/b, \Lambda)$. In practice, we are concerned with the small-$\hat{k}$ behavior of $f_2(\hat{k})$, in which case the latter two constraints are equivalent (the difference in their effects being sub-dominant). Thus, by invoking Eq. (A.2) we arrive at

$$f_2(\hat{k}) = 9g^2 \left(\frac{V^{n+1}}{(2\pi)^{(n+1)d}} \int\limits_{\Lambda/b<|\hat{k}|<\Lambda} d^{(n+1)d}k_1 \, G_0(\hat{k_1}) \, G_0(\hat{k}_1 - \hat{k}) \right.$$
$$\left. -2\sum_{\alpha=0}^{n} \frac{V}{(2\pi)^d} \int\limits_{\Lambda/b<|\mathbf{p}|<\Lambda} d^d p \, G_0(\mathbf{p}\hat{e}^\alpha) \, G_0(\mathbf{p}\hat{e}^\alpha - \hat{k}) \right). \qquad \text{(B.17)}$$

Then, by expanding for small $\hat{k}$ and taking the $n \to 0$ limit, we obtain

$$f_2^{(0)} = -\frac{9}{4} g^2 V \frac{S_d}{(2\pi)^d} \int_{\Lambda/b}^{\Lambda} \frac{k^{d-1} dk}{(-\tau + k^2/2)^2} + \mathcal{O}(g^4), \qquad \text{(B.18)}$$

$$f_2^{(1)} = -\frac{9}{4} g^2 V \frac{S_d}{(2\pi)^d} \left(-\int_{\Lambda/b}^{\Lambda} \frac{k^{d-1} dk}{(-\tau + k^2/2)^3} + \frac{2}{d} \int_{\Lambda/b}^{\Lambda} \frac{k^{d+1} dk}{(-\tau + k^2/2)^4} \right) + \mathcal{O}(g^4), \qquad \text{(B.19)}$$

where S_d is the surface area of a d-dimensional sphere of unit radius.

The renormalization of g acquires a nontrivial contribution associated with diagram (b) of Fig. 3.3, which determines $f_3(\hat{k}_1, \hat{k}_2, \hat{k}_3)$ in Eq. (B.8). Thus, including the symmetry factor of the diagram, we need to evaluate

$$f_3(\hat{k}_1, \hat{k}_2, \hat{k}_3) = \frac{8}{3!}(3g)^3 \sum_{\substack{\hat{k} \in \text{HRS} \\ (\hat{k}+\hat{k}_2 \in \text{HRS}) \\ (\hat{k}-\hat{k}_1 \in \text{HRS})}} G_0(\hat{k}) \, G_0(\hat{k} + \hat{k}_2) \, G_0(\hat{k} - \hat{k}_1). \qquad \text{(B.20)}$$

This constrained sum is similar to the one analyzed in the context of Eq. (A.2), but is more lengthy, yielding

$$f_3(\hat{k}_1, \hat{k}_2, \hat{k}_3) = 36g^3 \left(\frac{V^{n+1}}{(2\pi)^{(n+1)d}} \int\limits_{\Lambda/b<|\hat{k}|<\Lambda} d^{(n+1)d}k \, G_0(\hat{k}) \, G_0(\hat{k} + \hat{k}_2) \, G_0(\hat{k} - \hat{k}_1) \right.$$
$$\left. -\sum_{\alpha=0}^{n} \frac{V}{(2\pi)^d} \int\limits_{\Lambda/b<|\mathbf{p}|<\Lambda} d^d p \, G_0(\mathbf{p}) \, G_0(\mathbf{p}\hat{e}^\alpha + \hat{k}_2) \, G_0(\mathbf{p}\hat{e}^\alpha - \hat{k}_1) \right.$$

$$-\sum_{\alpha=0}^{n}\frac{V}{(2\pi)^d}\int\limits_{\Lambda/b<|\mathbf{p}|<\Lambda} d^dp\, G_0(\mathbf{p}\hat{e}^\alpha-\hat{k}_2)\, G_0(\mathbf{p})\, G_0(\mathbf{p}\hat{e}^\alpha-\hat{k}_2-\hat{k}_1)$$
$$-\sum_{\alpha=0}^{n}\frac{V}{(2\pi)^d}\int\limits_{\Lambda/b<|\mathbf{p}|<\Lambda} d^dp\, G_0(\mathbf{p}\hat{e}^\alpha+\hat{k}_1)\, G_0(\mathbf{p}\hat{e}^\alpha+\hat{k}_1+\hat{k}_2)\, G_0(\mathbf{p}\hat{e}^\alpha)\Bigg). \quad \text{(B.21)}$$

In fact, what we need is the $n \to 0$ limit of $f_3(\hat{0},\hat{0},\hat{0})$, which is given by

$$f_3^{(0)} = -9g^3V\frac{S_d}{(2\pi)^d}\int_{\Lambda/b}^{\Lambda}\frac{k^{d-1}dk}{(-\tau+k^2/2)^3}+\mathcal{O}(g^5). \quad \text{(B.22)}$$

It is worth emphasizing that, once again, the essential consequence of the exclusion of the 1RS from the theory. Without it, even signs of all three coefficients, $f_2^{(0)}$, $f_2^{(1)}$ and f_3, would be reversed, and the fixed-point structure of theory would be completely changed.

Appendix C

Evaluation of two-loop diagrams contributing to the renormalization-group analysis

Motivated by our results of the RG analysis of the vulcanization transition to the first order in ε, we proceed to calculate the second order contributions. The momentum-shell method is not well suited for this purpose because the complexity associated with computing diagrams having loop momentums in the momentum-shell increase dramatically as the number of loops in the diagrams increases, even from one to two. Instead, we follow closely the field-theoretic RG method that was used in Bonfim et al. [24], where they calculated the critical exponents of the percolation transition to ε^3 on the basis of the field-theoretic Potts model, Eq. (3.37). As with the vulcanization field theory, the non-linear term in the Potts field theory is cubic, the Potts field theory and the vulcanization field theory have the same two-loop diagrams (in the sense of the topology of the diagrams). The replica limit of the diagrams in the vulcanization field theory can be relatively easily found by via the decomposition scheme discussed in Chap. 4, and the resulting expressions is a combinatorial factor times a d-dimensional integral, with exactly the same d-dimensional integrals appearing in the work of Bonfim et al. [24]. As a result, once we find out the combinatorial factor for each vulcanization diagram, we can borrow the results from Bonfim et al. [24] to obtain the critical exponents.

Below, we list all the two-loop diagrams that contribute to the two- and three-point vertex function, as well as their values in the replica limit. After detailed calculation, we find that the combinatorial factor for each diagram is exactly the same as that of (the percolation limit of) Potts

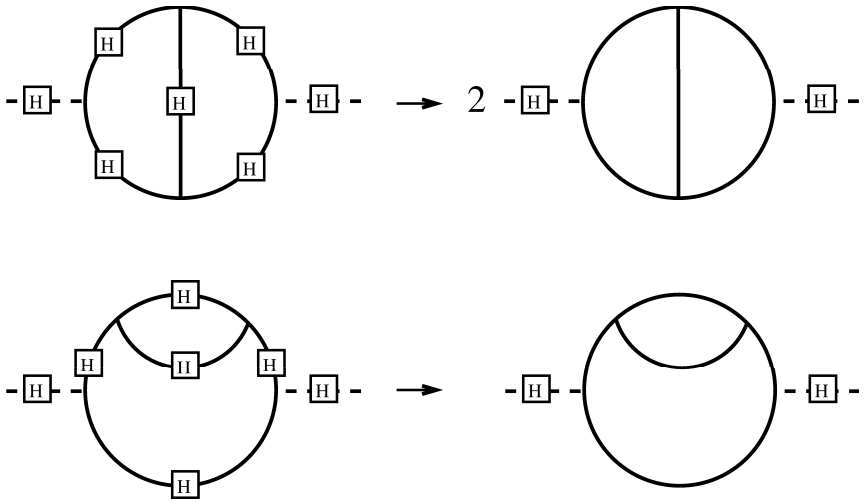

Figure C.1: The one-part-irreducible two-loop diagrams that contribute to the two-point vertex function. On the left-hand side are the vulcanization diagrams; on the right-hand side are their corresponding values in the replica limit. The number in the front are the combinatorial factors, the diagrams represent values taken by the diagram provided that the all the internal wave vectors reside in the same d-dimensional space.

field theory for the diagram that is topologically the same. (In the language of Bonfim et al., in the order of the diagrams shown in Figs. C.1 and C.2, they are: $\alpha\beta = 2$; $\alpha^2 = 1$; $\beta^2 = 4$; $\beta\alpha = 2$ and $\gamma = 5$.) Therefore, we find that even at the two-loop level, the critical exponents are the same as those of the percolation transition.

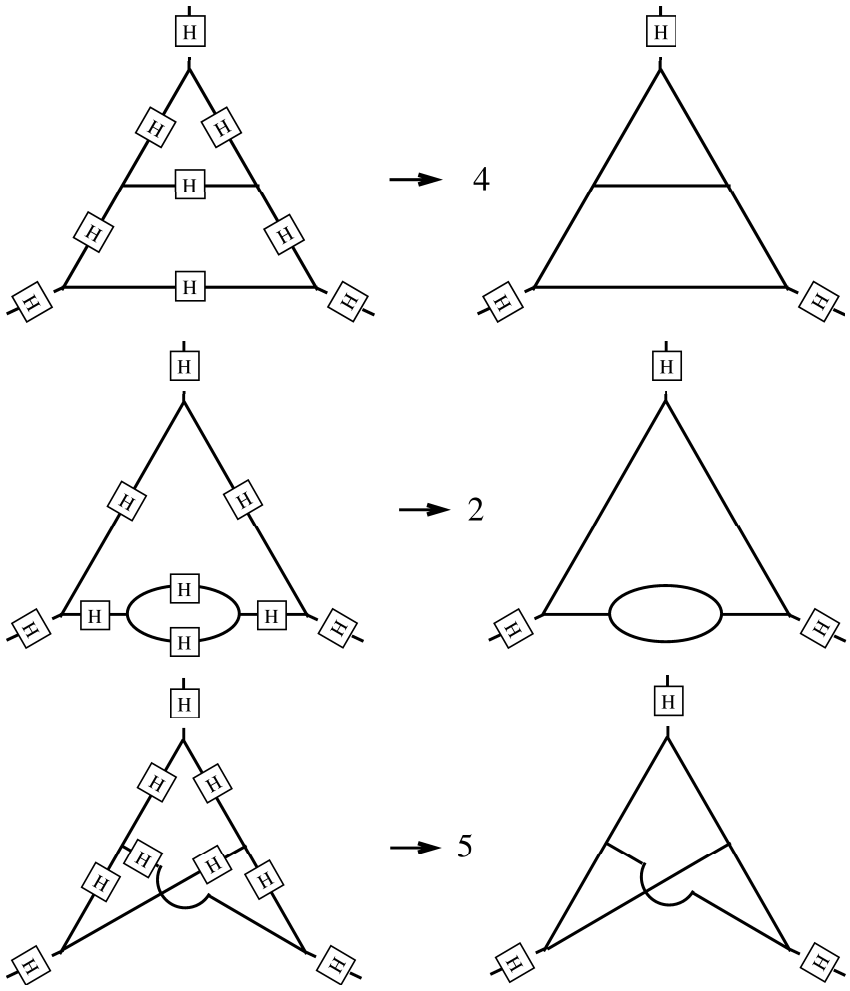

Figure C.2: The one-part-irreducible two-loop diagrams that contribute to the three-point vertex function. On the left-hand side are the vulcanization diagrams; on the right-hand side are their corresponding values in the replica limit. The numbers in the front are the combinatorial factors, and the diagrams represent values taken by the diagrams provided that the all the internal wave vectors reside in the same d-dimensional space.

References

[1] For a general and elementary account of polymer science, see, e.g., L. R. G. Treloar, *Introduction to Polymer Science* (Taylor & Francis, London, 1982). For a more thorough introduction, see, e.g., L. H. Sperling, *Introduction to Physical Polymer Science* (John Wiley & Sons, New York, 1986) and also Ref. [6].

[2] see, also, H. E. Castillo, Ph.D. thesis, University of Illinois at Urbana Champaign (unpublished, 1999).

[3] R. E. A. C. Paley and N. Wiener, Am. Math. Soc. Colloquium Publ. **19** (1934).

[4] S. F. Edwards, Proc. Phys. Soc. (London) **85**, 613 (1965).

[5] See, e.g., M. Doi and S. F. Edwards, *The Theory of Polymer Dynamics* (Oxford University Press, New York, 1986).

[6] P.-G. de Gennes, *Scaling Concepts in Polymer Physics* (Cornell University Press, Ithaca, 1979).

[7] J. W. Nicholson, *The Chemistry of Polymers* (The Royal Society of Chemistry, Cambridge, 1991).

[8] See, e.g., D. Stauffer, A. Coniglio, and M. Adam, Adv. in Polym. Sci. **44**, 103 (1982).

[9] See, also, A. Bunde and S, Havlin (Eds.), *Fractals and Disordered Systems*, Second Edition (Springer, Berlin, 1996).

[10] For a review, see, e.g., D. Stauffer and A. Aharony, *Introduction to Percolation Theory*, Second Edition (Taylor and Francis, Philadelphia, 1991).

[11] P. J. Flory, J. Am. Chem. Soc. **63**, 3083; ibid. 3091; ibid. 3906 (1941).

[12] W. H. Stockmayer, J. Chem. Phys. **11**, 45 (1943).

[13] P.-G. de Gennes, J. Phys. (Paris) **36**, 1049 (1976); ibid. **37**, L1 1976.

[14] D. Stauffer, J. Chem. Soc. Faraday Trans. II **72**, 1354 (1976).

[15] R. B. Potts, Proc. Camb. Phil. Soc. **48**, 106 (1952).

[16] For a general review of the equilibrium properties of the Potts model, see, e.g., F. Y. Wu, Rev. Mod. Phys. **54**, 235 (1982).

[17] P. W. Kastelyn and C. M. Fortuin, J. Phys. Soc. Jpn. Suppl. **16**, 11 (1969); C. M. Fortuin and P. W. Kastelyn, Physica **57**, 536 (1972).

[18] See, e.g., Ref. [19], especially Chap. 8.

[19] See, e.g., J. Cardy, *Scaling and Renormalization in Statistical Physics* (Cambridge University Press, 1996).

[20] R. K. P. Zia and D. J. Wallace, J. Phys. A. **8**, 1495 (1975).

[21] For a review, see, e.g., T. C. Lubensky, pp. 405-475, in *Ill-Condensed Matter* (Les Houches XXXI, 1978), edited by R. Balian, R. Maynard and G. Toulouse (North Holland: Amsterdam, 1979).

[22] R. G. Priest and T. C. Lubensky, Phys. Rev. B. **13**, 4159 (1976).

[23] D. J. Amit, J. Phys. A. **9**, 1441 (1976).

[24] O. F. de Alcantara Bonfim, J. E. Kirkham and A. J. McKane, J. Phys. A. **13**, L247 (1980); J. Phys. A. **14**, 2391 (1981).

[25] A. Houghton, J. S. Reeve and D. J. Wallace, Phys. Rev. B **17**, 2956 (1978).

[26] T. C. Lubensky and J. Isaacson, Phys. Rev. Lett. **41**, 829 (1978); Phys. Rev. Lett. **42**, 410 (1979) (E); Phys. Rev. A **20**, 2130 (1979); J. Physique **42**, 175 (1981); see also the paper cited in Ref. [21].

[27] P. G. de Gennes, Phys. Lett. **38A**, 339 (1972); see also Ref. [6].

[28] J. des Cloizeaux, J. Phys. (Paris) **36**, 281 (1975).

[29] P. M. Goldbart and N.Goldenfeld, Phys. Rev. Lett. **58**, 2676 (1987); Macromol. **22** (1989) 948; Phys. Rev. A **39** (1989) 1402; ibid., **39** (1989) 1412.

[30] P. M. Goldbart and A. Zippelius, Phys. Rev. Lett. **71**, 2256 (1993).

[31] H. E. Castillo, P. M. Goldbart and A. Zippelius, Europhys. Lett. **28**, 519 (1994).

[32] P. M. Goldbart, H. E. Castillo and A. Zippelius, Adv. Phys. **45**, 393 (1996).

[33] A. Zippelius and P. M. Goldbart, pp. 357-389, in Ref. [34].

[34] *Spin Glasses and Random Fields*, edited by A. P. Young (World Scientific, Singapore, 1998).

[35] P. M. Goldbart, in *Rigidity Theory and Applications*, pp. 95-124, edited by M. F. Thorpe and P. M. Duxbury (New York: Kluwer Academic/Plenum Publishers, 1999).

[36] P. M. Goldbart, J. Phys. Cond. Matt. **12**, 6585 (2000).

[37] R. T. Deam and S. F. Edwards, Phil. Trans. R. Soc. **280A**, 317 (1976).

[38] R. C. Ball and S. F. Edwards, Macromol. **13**, 748 (1980); R. C. Ball, Ph.D. Thesis, Cambridge University (1980).

[39] S. F. Edwards and P. W. Anderson, J. Phys. F **5**, 965 (1975).

[40] See, e.g., M. Mézard, G. Parisi and M. A. Virasoro, *Spin Glass Theory and Beyond*, (World Scientific, Singapore, 1987); K. Binder, A. P. Young, Rev. Mod. Phys. **58**, 801 (1986).

[41] For convenience, the dimensionful position vector $\mathbf{R}$ and arclength σ that feature in (1.2) has been exchanged for the dimensionless versions $\mathbf{c}$ and s via the transformation: $\mathbf{R}_i(\sigma) \equiv \sqrt{\ell L/d}\ \mathbf{c}_i(s)$ and $\sigma \equiv L\, s$. The excluded-volume parameter u_0 is exchanged for λ^2 accordingly, i.e. $u_0 = (\ell L/d)^{d/2}\,(\ell/L)^2\,\lambda^2$ [32].

[42] The measure $\overline{\mathcal{D}}^{\dagger}\Omega$ indicates that we integrate $\Omega(\hat{k})$ with $\hat{k} \in$ HRS and with $\hat{k}$ restricted to a half-space via an additional condition $\hat{k}\cdot\hat{m} > 0$ for some suitable unit $(n+1)d$-vector $\hat{m}$. This is due to the fact that $Q(-\hat{k}) = Q(\hat{k})^*$ (i.e. its Fourier transform is real). Similarly, $\mathcal{D}_n^{\dagger}\Omega$

indicates that we integrate the 1RS version of $\Omega(\hat{k})$ for $\hat{k} \in$ 1RS (similarly constrained by reality to a suitable half-space).

[43] see, e.g., Eqs. (4.17) and (5.15a) of Ref. [32].

[44] See, e.g., J. Zinn-Justin, *Quantum Field Theory and Critical Phenomena* (Clarendon Press, Oxford, 1989), especially Chap. 21.

[45] See, e.g., R. C. Ball, M. Doi, S. F. Edwards and M. Warner, Polymer **22**, 1010 (1981).

[46] S. V. Panyukov, Pis'ma Zh. Eksp. Teor. Fiz. **55**, 584 (1992) [JETP Lett. **55**, 608 (1992)]; Zh. Eksp. Teor. Fiz. **103**, 1644 (1993) [Sov. Phys. JETP **76**, 808 (1993)]. See, also Ref. [47].

[47] S. Panyukov and Y. Rabin, Phys. Rep. **269**, 1 (1996).

[48] H. E. Castillo and P. M. Goldbart, Phys. Rev. E **58**, R24 (1998); ibid., E **62**, 8159 (2000).

[49] H. E. Castillo, P. M. Goldbart and A. Zippelius, Phys. Rev. B **60**, 14702 (1999).

[50] P. G. de Gennes, J. Physique Lett. **38**, L355 (1977); see also Ref. [6].

[51] W. Peng, H. E. Castillo, P. M. Goldbart and A. Zippelius Phys. Rev. B **57**, 839 (1998).

[52] W. Peng and P. M. Goldbart, Phys. Rev. E **61**, 3339 (2000).

[53] W. Peng, P. M. Goldbart and A. J. McKane, submitted to Phys. Rev. E., (2001).

[54] W. Peng and P. M. Goldbart, Euro. Phys. J. B **19**, 461 (2001).

[55] M. Huthmann, M. Rehkopf, A. Zippelius and P. M. Goldbart, Phys. Rev. E **54**, 3943 (1996).

[56] C. Roos, A. Zippelius and P. M. Goldbart, J. Phys. A **30**, 1967 (1997).

[57] P. M. Goldbart and A. Zippelius, Europhys. Lett. **27**, 599 (1994); O. Thiessen, A. Zippelius and P. M. Goldbart, Int. J. Mod. Phys. B **11**, 1945 (1996).

[58] K. A. Shakhnovich and P.M. Goldbart, Phys. Rev. B **60**, 3862 (1999).

[59] K.A. Shakhnovich, Ph.D. thesis, University of Illinois at Urbana Champaign (unpublished, 2001);

[60] S. J. Barsky and M. Plischke, Phys. Rev. E **53**, 871 (1996); S. J. Barsky, Ph.D. thesis, Simon Fraser University, Canada (unpublished, 1996); S. J. Barsky and M. Plischke (unpublished, 1997).

[61] In principle, one can construct a minimal model directly in terms of $Q(\hat{k})$ by following the same general considerations that lead to the minimal model for $\Omega(\hat{k})$. The minimal model for $Q(\hat{k})$ is equivalent in physical content to the minimal model for $\Omega(\hat{k})$; the difference would only lie in the values of the phenomenological parameters a, b and g. In order to make contact with the strategy used in Ref. [32], we choose $\Omega(\hat{k})$ as the central quantity in our minimal model.

[62] H.-K. Janssen and O. Stenull, *On the relevance of percolation theory to the vulcanization transition*, cond-mat/0103583.

[63] See, e.g., S.-K. Ma, *Modern Theory of Critical Phenomena* (Benjamin, Reading, MA, 1971).

[64] A. Zippelius, P. M. Goldbart and N. Goldenfeld, Europhys. Lett. **23**, 451 (1993).

[65] This strategy has been discussed in greater depth in [36]; see also Refs. [57] and [34].

[66] E. Marinari, G. Parisi and F. Ritort, J. Phys. A **27**, 7615 (1994); ibid. 7647; J.-P. Bouchaud and M. Mézard, J. Phys. I (France) **4**, 1109 (1994).

[67] S. Franz and G. Parisi, J. Phys. I (France) **5**, 1401 (1995).

[68] S. J. Barsky and M. Plischke kindly allowed us to report results from their simulations in Ref. [51].

[69] For a discussion of spin glass theory beyond the mean-field level see, e.g., K. H. Fischer and J. A. Hertz, *Spin Glasses* (Cambridge University Press, 1991), especially Sec. 8.3; and C. De Dominicis, I. Kondor and T. Temesvári, pp. 119-160, in Ref. [34].

[70] P. J. Flory, *Principles of Polymer Chemistry* (Cornell University Press, 1953).

[71] The single ensemble must be identified either with the equilibrium configurations of a system without quenched randomness or with the realizations of a quenched-disordered system that is not fluctuating thermally. Which identification is made depends on the physical setting that

the ensemble is intended to describe. If, e.g., the intended setting involves *weak* (*reversible* , i.e. bond formation is reversible on the timescale of the experiment) then the elements of the ensemble correspond to the distinct configurations of the system that are accessible in thermal equilibrium. If, on the other hand, the intended setting is *strong* (*irreversible*) gelation (i.e. bond formation is irreversible on the timescale of the experiment) then the elements of the ensemble correspond to distinct realizations of the permanent bonding, and fluctuations from one element to another correspond not to thermal fluctuations but to variations from sample to sample. The various percolative approaches, as well as the Lubensky & Isaacson approach, identify the single ensemble with the statistics of the bond formation, i.e., they apply only to *strong* gelation.

[72] Some initial considerations of these issues were given in Ref. [33].

[73] To obtain the relationship (3.1) between $C_{\mathbf{t}}(\mathbf{r}-\mathbf{r}')$ and the order parameter correlator requires an application of the replica technique that we do not give explicitly here; see App. A of Ref. [32].

[74] D. J. Amit, *Field Theory, the Renormalization Group, and Critical Phenomena* (World Scientific, Singapore, 1989).

[75] The result for the inverse susceptibility Ξ depends on the route through wavevector space through which the $\hat{k} \to \hat{0}$ limit is taken. Specifically, one gets distinct results for the inverse susceptibility depending on whether or not the limit is taken via HRS wavevectors $\hat{k}$ that are in the two-replica sector or not. However, the difference goes away in the thermadynamic limit, and both routes lead to the same Ginzburg criterion; see App. A.

[76] See, e.g., Ref. [19], especially Chap. 3.

[77] A. B. Harris, T. C. Lubensky, W. K. Holcomb and C. Dasgupta, Phys. Rev. Lett. **35**, 327 (1975); and **35**, 1397 (E).

[78] The very possibility that the ordered state is characterized by a *function* rather than a number (or discrete set of numbers), and thus the possibility of a wavevector-dependent scaling form for the order parameter itself, is a natural feature of the vulcanization transition. It arises

from the impossibility of restoring stability by "condensation" into a homogeneous state, this impossibility being due to the absence of the homogeneous sector from the theory.

[79] The relevance of percolation theory to the *thermal* motion (i.e. the statistical *mechanics*) of the resulting crosslinked macromolecular system is less clear.

[80] P. Erdős and A. Rényi, Magyar Tud. Akad. Mat. Kut. Int. Közl. **5**, 17 (1960), especially Theorem 9b; reprinted in Ref. [81], Chap. 14, article [324]. For an informal discussion, see P. Erdős and A. Rényi, Bull. Inst. Internat. Statist. **38**, 343 (1961); reprinted in Ref. [81], Chap. 14, article [v].

[81] *Paul Erdős: The Art of Counting*, edited by J. Spencer (MIT Press, 1973).

[82] H. E. Castillo, P. M. Goldbart and W. Peng, work in progress (2001).

[83] For a review of quasi-long-range order in two-dimensional systems without quenched disorder, see D. R. Nelson, *Defect-mediated phase transitions*, pp. 1-99, in *Phase Transitions and Critical Phenomena*, vol. 7, edited by C. Domb and J. L. Leibowitz (London: Academic Press, 1983).

[84] See, e.g., References [6, 70, 14].

[85] See Sec. VI of Ref. [52] and Ref. [36] for further remarks on this issue. We thank H. E. Castillo for discussions on this subject.

[86] The precise correspondence, determined by comparing Eq. (4.1) of the present chapter with Eq. (2.7) of Chap. 3 is: the current Ω is equivqlent to the previous $(NV^{n+1})^{1/2}\Omega$, r_0 is equivalent to -2τ and the current g is equivalent to the previous $-3!(V^{n+1}/N)^{1/2}g$.

[87] Strictly speaking, as the wave vector in question is required to be in the HRS, it can not be exactly $\hat{0}$. Instead, one should conceive of the value at $\hat{0}$ as being the limiting value as $\hat{k} \to \hat{0}$ via a path in the HRS.

[88] By this we mean $F_{\alpha_1,\alpha_2,\ldots,\alpha_l} = F_{\pi(\alpha_1),\pi(\alpha_2),\ldots,\pi(\alpha_l)}$, where $\pi(\alpha)$ is an arbitrary permutation of the replicas.

[89] See, e.g., M. Le Bellac, *Quantum and Statistical Field Theory* (Oxford University Press, 1991), Sec. 5.5.3.

[90] P. N. Pusey and W. van Megen, Physica A **157**, 705 (1989).

[91] M. Mézard and G. Parisi, J. Phys. A **29**, 6515 (1996).

[92] Unless noted otherwise, the wavevector $\mathbf{q}$ is assumed to be non-zero.

[93] We are departing from the convention of our previous works in order to avoid some unnecessary complications. Let us pause to clarify the relationship between these conventions. Here, we employ $R(\mathbf{k}\hat{e}^{\alpha})$ as our 1RS field variable, rather than the $\Omega(\mathbf{k}\hat{e}^{\alpha})$ used in Refs. [32, 52]. R is closely related to the variable Q that is microscopically defined in Refs. [32, 52]. In fact, $R(\mathbf{k}\hat{e}^{\alpha}) = NQ(\mathbf{k}\hat{e}^{\alpha}) = \sum_{j=1}^{N} \int_0^1 ds \, \exp i\mathbf{k} \cdot \mathbf{c}_j(s)$ [32]. The reason we choose $R(\mathbf{k}\hat{e}^{\alpha})$ instead of $\Omega(\mathbf{k}\hat{e}^{\alpha})$ is that the RR correlator is simply the density correlator as exhibited in Eq. (5.7), whereas the $\Omega\Omega$ correlator has a more complicated (and model-dependent) relationship with the physical density correlator because $\Omega(\mathbf{k}\hat{e}^{\alpha})$ is a conjugate variable resulting from a Hubbard-Stratonovich transformation of $Q(\mathbf{k}\hat{e}^{\alpha})$. In order to avoid this unnecessary complication, we adopt the $R(\mathbf{k}\hat{e}^{\alpha})$ as our field variable. In principle, one can construct such a minimal model by following the general symmetry considerations that lead to the minimal model for $\Omega(\hat{k})$.

[94] Functional integration over 1RS fields is implied.

[95] M. Mézard (private communication).

[96] Such additional features have been observed in amorphous colloidal systems; see Ref. [97].

[97] W. van Megen and P. N. Pusey, Phys. Rev. A **43**, 5429 (1991).

Vita

Weiqun Peng was born in Beijing, P. R. China, on July 29, 1969. He received his Bachelor of Science in Physics in 1992, and Master of Science in Physics in 1995, Both from Peking Univeristy.